AD-A096 506 DAVID W TAYLOR NAVAL SHIP RESEARCH AND DEVELOPMENT CE--ETC F/G 13/10
EXPERIMENTAL INVESTIGATION OF HYDROFOIL FORCE RESPONSE IN REGUL--ETC(U
FEB 81 G KARAFIATH
UNCLASSIFIED DTNSRDC/SPD-0956-01 NL

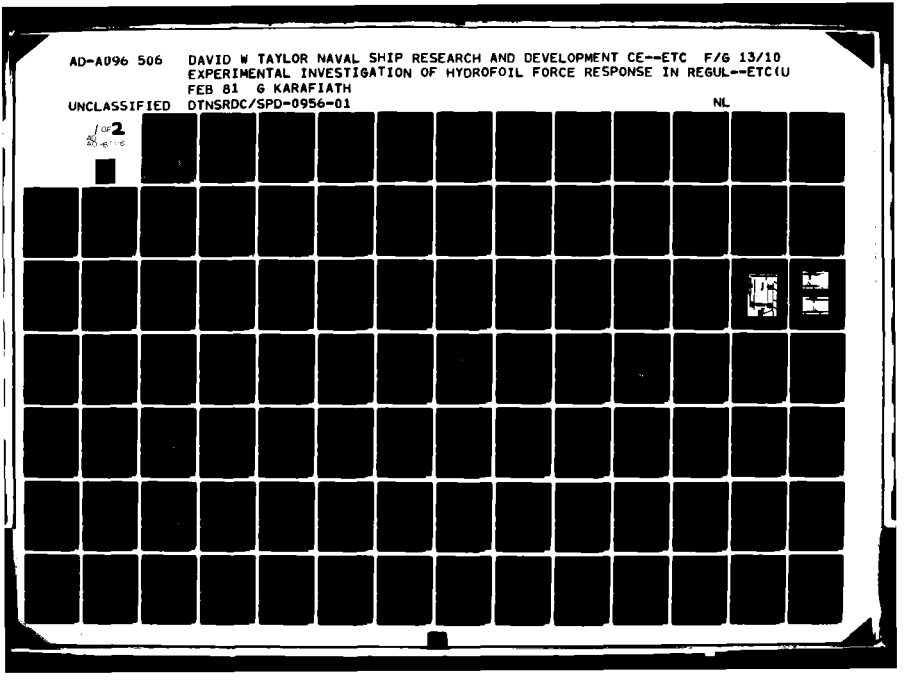

SPD-0956-01

DAVID W. TAYLOR NAVAL SHIP RESEARCH AND DEVELOPMENT CENTER

Bethesda, Maryland 20084

AD A096506

EXPERIMENTAL INVESTIGATION OF HYDROFOIL FORCE RESPONSE IN REGULAR SEAS AT LOW CHORD FROUDE NUMBERS

by

Gabor Karafiath

APPROVED FOR PUBLIC RELEASE: DISTRIBUTION UNLIMITED

SHIP PERFORMANCE DEPARTMENT
DEPARTMENTAL REPORT

FEBRUARY 1981

DTNSRDC/SPD-0956-01

MAJOR DTNSRDC ORGANIZATIONAL COMPONENTS

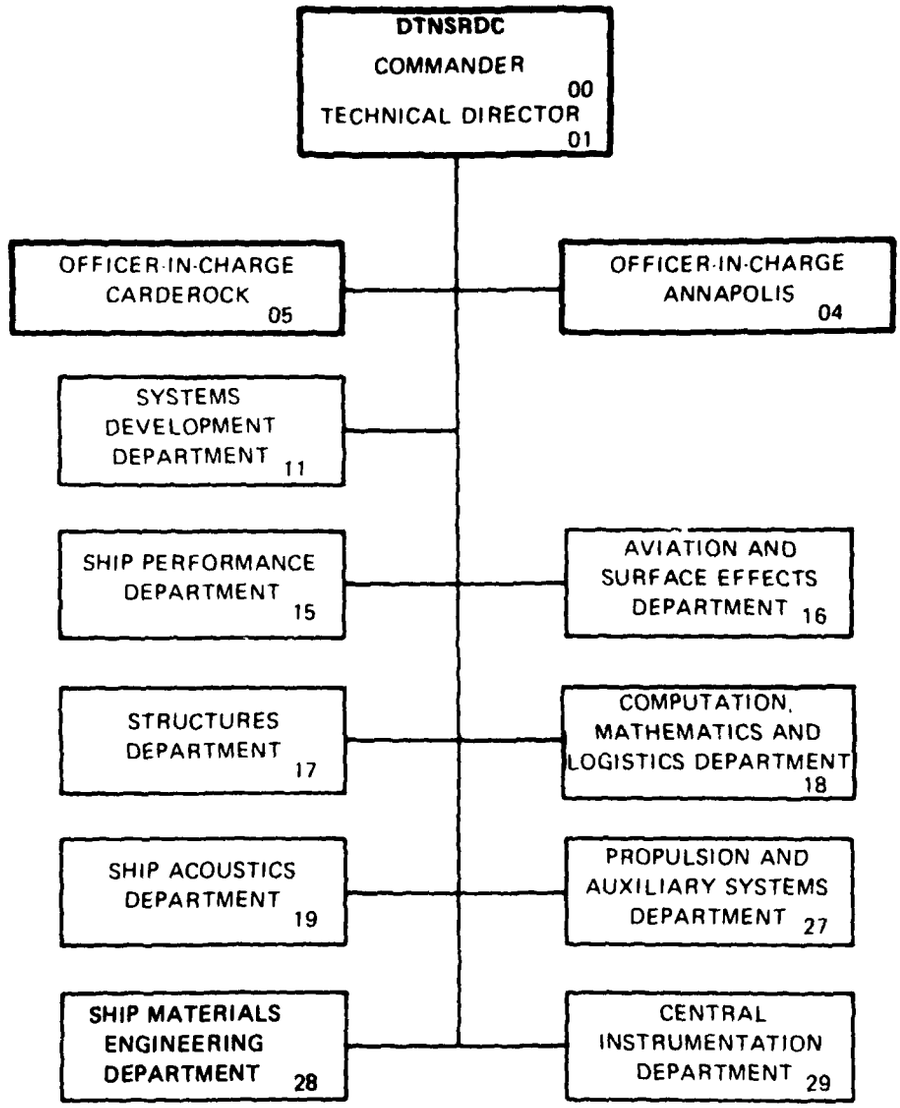

UNCLASSIFIED

SECURITY CLASSIFICATION OF THIS PAGE (When Date Entered)

REPORT DOCUMENTATION PAGE	READ INSTRUCTIONS BEFORE COMPLETING FORM
1. REPORT NUMBER: SPD-0956-01	2. GOVT ACCESSION NO. / 3. RECIPIENT'S CATALOG NUMBER
4. TITLE (and Subtitle): EXPERIMENTAL INVESTIGATION OF HYDROFOIL FORCE RESPONSE IN REGULAR SEAS AT LOW CHORD FROUDE NUMBERS.	5. TYPE OF REPORT & PERIOD COVERED / 6. PERFORMING ORG. REPORT NUMBER
7. AUTHOR(s): Gabor Karafiath	8. CONTRACT OR GRANT NUMBER(s)
9. PERFORMING ORGANIZATION NAME AND ADDRESS: David W. Taylor Naval Ship R&D Center, Bethesda, Maryland 20084	10. PROGRAM ELEMENT, PROJECT, TASK AREA & WORK UNIT NUMBERS: Task Area ZF43-421-001, Work Unit 1-1500-104-69.
11. CONTROLLING OFFICE NAME AND ADDRESS	12. REPORT DATE / 13. NUMBER OF PAGES
14. MONITORING AGENCY NAME & ADDRESS (if different from Controlling Office)	15. SECURITY CLASS. (of this report) / 15a. DECLASSIFICATION/DOWNGRADING SCHEDULE

16. DISTRIBUTION STATEMENT (of this Report)

APPROVED FOR PUBLIC RELEASE: DISTRIBUTION UNLIMITED

17. DISTRIBUTION STATEMENT (of the abstract entered in Block 20, if different from Report)

18. SUPPLEMENTARY NOTES

19. KEY WORDS (Continue on reverse side if necessary and identify by block number)

Hydrofoil Response
Lift
Low Froude Number
Drag
Regular Waves

20. ABSTRACT (Continue on reverse side if necessary and identify by block number)

The dynamic lift and drag response of a large 8 ft (2.43 m) span, aspect ratio 6 hydrofoil operating in regular waves was experimentally determined for a range of chord Froude numbers varying from 1.22 to 3.66. The amplitude of the fundamental frequency lift response was found to increase significantly with decreasing chord Froude number, while the second harmonic lift response was zero. The amplitude of the first and second harmonic drag response also varied with chord Froude number. The first harmonic drag response was a

DD FORM 1 JAN 73 1473 EDITION OF 1 NOV 65 IS OBSOLETE
S/N 0102-LF-014-6601

UNCLASSIFIED

SECURITY CLASSIFICATION OF THIS PAGE (When Date Entered)

maximum at the lowest chord Froude number of 1.22, and the shallowest depth chord ratio of 0.5. Several theoretical predictions of the lift amplitude response are compared with the experimental results.

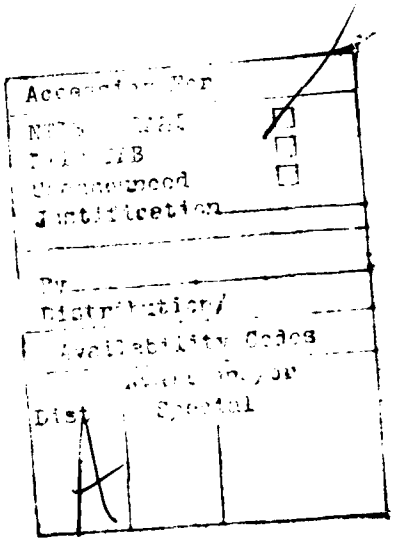

TABLE OF CONTENTS

LIST OF FIGURES

Page

Page

LIST OF TABLES

NOTATION

		Dimensions*
A_p	Projected planform area of hydrofoil	L^2
AR	Aspect ratio AR = $\bar{c}/b$	---
b	Hydrofoil span	L
c	Wave celerity c = $\frac{g}{\omega}$	L/T
$\bar{c}$	Mean chord	L
d	Depth to semi chord ratio d = $h/(\bar{c}/2)$	---
C(k)	Theodoresen's function C(k) = F + i G	---
C_D	Drag coefficient $C_D = \frac{D}{\frac{1}{2}\rho V^2 A_p}$	---
$\bar{C}_D$	Mean drag coefficient in waves $\bar{C}_D = \frac{\bar{D}}{\frac{1}{2}\rho V^2 A_p}$	---
C_{D1}	Fundamental frequency drag response coefficient; $C_{D1} = \frac{D_1}{\frac{1}{2}\rho V^2 A_p}$	---
C_{D2}	Second harmonic drag response coefficient; $C_{D2} = \frac{D_2}{\frac{1}{2}\rho V^2 A_p}$	---
C_L	Lift coefficient	---
$\bar{C}_L$	Mean lift coefficient in waves; $\bar{C}_L = \frac{\bar{L}}{\frac{1}{2}\rho V^2 A_p}$	---

*M = Mass; L = Length; T = Time.

C_{L1}	Fundamental frequency lift response coefficient; $C_{L1} = \frac{L_1}{\frac{1}{2}\rho V^2 A_p}$	---
C_{L2}	Second harmonic lift response coefficient; $C_{l.2} = \frac{L_2}{\frac{1}{2}\rho V^2 A_p}$	---
D	Drag	ML/T^2
$\overline{D}$	Mean or average drag in waves	ML/T^2
D_1	Amplitude of the drag response at the fundamental encounter frequency	ML/T^2
D_2	Amplitude of the drag response at the second harmonic	ML/T^2
F	Real part of Theodorsen's function	---
f_E	Encounter frequency, hertz; $f_E = \omega_E/2\pi$	1/T
F_{nc}	Chord Froude number; $F_{nc} = \frac{V}{\sqrt{g\,\overline{c}}}$	---
F_{nh}	Depth Froude number; $F_{nh} = \frac{V}{\sqrt{gh}}$	---
g	Acceleration due to gravity	L/T^2
G	Imaginary part of Theodoresen's function	---

h	Foil depth (measured from the mean free surface to the ½ chord position on the nose-tail line)	L
i	Imaginary unit; $\sqrt{-1}$	---
K	Dimensionless wave number; $K = \frac{2\pi}{\lambda} (\frac{\bar{c}}{2})$	---
k	Reduced frequency; $k = \frac{\omega b}{V}$	---
k_e	Reduced frequency of encounter; $k_e = \frac{\omega b}{V} (1.0 + \frac{\omega V}{g})$	---
L	Lift force	ML/T^2
L'	Amplitude of the lift response per unit span	M/T^2
$\bar{L}$	Mean lift in waves	ML/T^2
L_1	Amplitude of the lift response at the fundamental encounter frequency	ML/T^2
L_2	Amplitude of the lift response at the second harmonic	ML/T^2
L_{hi}; L_{hr}; $L_{\alpha i}$; $L_{\alpha r}$	Aerodynamic nondimensional response coefficients (imaginary and real parts)	---
L_w; λ	Wave length; $L_w = \frac{2\pi g}{\omega^2}$	L
r	Wave amplitude to semi chord ratio; $r = 2\zeta_a/\bar{c}$	---
$v(x,y,t)$	Vertical velocity distribution in the wave	L/T
V	Velocity of hydrofoil in the horizontal direction	L/T
ω	Circular wave frequency	rad/T
ω_E; ω_e	Circular frequency of encounter	rad/T

α	Foil incidence angle	degrees
Φ_{D1}	Phase angle of the fundamental frequency drag response	radians or degrees
Φ_{D2}	Phase angle of the second harmonic drag response	radians or degrees
Φ_{L1}	Phase angle of the fundamental frequency lift response	radians or degrees
Φ_{L2}	Phase angle of the second haromine lift response	radians or degrees
ϕ_1	Phase angle of pitch motion relative to heave motion	radians
$\zeta(x,t)$	Free surface elevation	L
ζ_a	Wave amplitude (½ trough to crest distance)	L
ρ	Water density	M/L^3
σ	Reisner's 3 dimensional correction to Theodorsen's function	---
τ_o	Wave Period	T

ABSTRACT

The dynamic lift and drag response of a large 8 ft (2.43 m) span, aspect ratio 6 hydrofoil operating in regular waves was experimentally determined for a range of chord Froude numbers varying from 1.22 to 3.66. The amplitude of the fundamental frequency lift response was found to increase significantly with decreasing chord Froude number, while the second harmonic lift response was zero. The amplitude of the first and second harmonic drag response also varied with chord Froude number. The first harmonic drag response was a maximum at the lowest chord Froude number of 1.22, and the shallowest depth chord ratio of 0.5. Several theoretical predictions of the lift amplitude response are compared with the experimental results.

ADMINISTRATIVE INFORMATION

The work reported herein was carried out for the Ship Performance and Hydromechanics Block Program, funded by the Naval Material Command (08T23), Task Area ZF43-421-001, Work Unit 1-1500-104-69.

INTRODUCTION

This report describes and presents the results of an experiment designed to determine the unsteady lift and drag response of a hydrofoil running in regular waves at low chord Froude numbers. It is believed that these experiments are unique in that they were run at low Froude numbers, at the corresponding frequency range of interest, using a relatively large (0.406 meter chord and 2.43 meter span) hydrofoil model and in that tare data was removed to isolate the foil only response. A literature search revealed no other low Froude number test data.

The measured lift response is compared to the prediction obtained from several theories. Extensive theoretical work concerning the prediction of unsteady loads on air foils is available. References 1, 2, and 3 summarize and list the outstanding works applicable to the prediction of airfoil response. In this report the theoretical predictions of Theodorsen[4] (2-dimensional), Reisner[5], Reisner and Stevens[6] (3-D)and Lawrence and Gerber[7] (3-D) as transformed by Henri and Ali[8] from the case of forced oscillations in an infinite medium to the response in regular waves, are compared to the measured data. In addition, a lifting surface theory prediction as computer programmed by Widnall and computed by Besch and Rood[9] for a foil very similar to the one tested here is compared to the experimental lift response.

---

[1]References are listed on page 24.

The U.S. Navy's interest in the test data presented here arises from possible design applications for control foils (pitch and roll) on SWATH (Small Waterplane Area Twin Hull Ship) and on conventional surface ships operating at slow speed. In addition, these tests may be of use in the design of pure hydrofoil ships with very large chord foils. For example the test covers the full scale speed range from 18.3 knots to 55.3 knots for a hydrofoil having a 20 ft (6.1 m) mean foil chord.

OBJECTIVES

The object of these experiments was to determine the lift and drag response of a hydrofoil operating in regular waves at low chord Froude numbers, and to compare the experimental response with the theoretical response using existing gust response theories available from aeronautical or marine literature. The development of any new response theory was not intended even though it was recognized that the available prediction methods were not likely to take into account the low Froude number effects.

DESCRIPTION OF EXPERIMENT

The experiments were conducted in the Deep Water Basin of the David W. Taylor Naval Ship Research and Development Center. The Deep Water Basin is 2775 ft. (845.8m) long 51 feet (15.5 m) wide and 22 ft. (6.70 m) deep. The model was attached to the vertical rails of Towing Carriage 2 and the Pneumatic Wavemaker was used to generate regular waves. For the wave portion of the tests, the water level was lowered to a depth of 19.5 ft. (5.94 m). Additional information on the towing facilities is contained in Ref. 10.

The foil model used in these experiments has been extensively tested in calm water to determine the effect of low chord Froude number on the wave making drag. These calm water test results are expected to be published subsequent to this report. Figure 1 shows a photograph of the foil and Table 1 lists the principal dimensions and other important information concerning the foil.

The general layout of the test set-up, Figure 1 shows the tilt yaw table which can move on the vertical rails for height adjustment, a forward strut, aft strut and the top pipe which provide a structural base for block gauge stacks, forward and aft fairings around the block gauge stacks, and lower pipe and nose piece combination which supports the foil. The fairings were removed in Figure 2 to show details of the forward block gauge stack and the aft block gauge flexure combination. In Figure 2, the foil has been removed and the nose piece slot filled with a faired

wooden block for the purpose of making tare measurements. In addition, a faired tail-cone fitted when making test runs has been removed from the aft end of the sting. This tail cone is approximately 1 ft. (0.304 m) long and matches the 6 inch (15.24 cm) outside diameter of the sting.

TABLE 1

Foil Principal Dimensions and Characteristics

Foil span	8 ft. (2.438 m)
Foil chord	1.33 ft. (0.406 m)
Planform shape	Rectangular
Planform area, A_p	10.66 ft.^{2} (0.99 m^2)
Aspect ratio AR	6
Foil material	Solid aluminum
Foil incidence angle at zero speed	4^o
Flap angle	0^o
Section shape	NACA 64 A010
Trip wire	0.016 inch. (0.04 cm)

The primary measurements taken and the instruments used for taking these measurements are shown in Table 2.

TABLE 2

Primary Test Measurements

Forward lift	5000 lb (22.24 kN) capacity, DTNSRDC 4 inch (10.2 cm) block gauge
Aft lift	2000 lb (8.89 kN) capacity, DTNSRDC 4 inch (10.2 cm) block gauge
Drag	200 lb (889 N) capacity, DTNSRDC 4 inch (10.2 cm) block gauge
Wave height	Wesmar sonic probe
Carriage speed	DTNSRDC magnetic pickup

The forward lift and drag block gauge stack was located 3 feet (0.914 m) behind the foil ¼ chord position and the aft lift gauge was 9 ft. (2.74 m) aft of the ¼ chord position. A plan-view of the foil sting set up is shown in Figure 3. A total of four basic foil/sting test configurations were tested as shown in Table 3.

TABLE 3

Test Configurations

Configuration	Type of run	Water depth
1) sting only	Calm water tare	22 ft. (6.71 m)
2) sting only	Regular wave-tare runs, head seas	19.5 ft. (5.94 m)
3) sting + foil	Calm water	22 ft. (6.71 m)
4) sting + foil	Regular waves - head seas	19.5 ft. (5.94 m)

By subtracting the tare runs from the sting + foil runs, the lift and drag of the foil only were isolated. In order to run in waves, the water depth had to be lowered from the calm water level. The difference in water depth is not expected to introduce any measurable error into the tare subtraction process.

The matrix of test runs involved a variation of foil depth, foil forward speed, wave period and wave height. Foil depth was fixed for each run at foil depth to foil chord ratios of 0.5, 1.0 and 2.0. Foil speed varied from 8.0 to 24.0 fps (2.43 to 7.32 m/s) corresponding to a chord Froude numbers of 1.22 to 3.66. Wave period varied from 1.75 to 4.25 sec. The nominal wave amplitude for the test was 3.5 inches (8.89 cm) with linearity checks at nominal wave amplitudes of 2.0 inches (5.08 cm) and 5.0 inches (12.7 cm).

The primary test speeds corresponded to the chord Froude numbers F_{nc} of 1.22, 1.83, 2.60 and 3.66. Additional speeds were run as required in order to obtain test data where the reduced frequency of encounter, k_e, was held constant. Dynamic lift and drag data for k_e = 1.83, 2.50, and 3.14 were obtained for a range of chord Froude numbers.

EXPERIMENTAL RESULTS

The force response in waves was harmonically analyzed to determine the amplitude and phase at the fundamental and twice the fundamental frequency. The

measured lift and drag response was expressed in the following form:

$$C_L = C_{L1} \cos (\omega_e t + \Phi_{L1}) + C_{L2} \cos (2\omega_e t + \Phi_{L2}) + \bar{C}_L \quad (1)$$

$$C_D = C_{D1} \cos (\omega_e t + \Phi_{D1}) + C_{D2} \cos (2\omega_e t + \Phi_{D2}) + \bar{C}_D \quad (2)$$

where

C_L is the total measured lift coefficient

$\bar{C}_L$ is the mean value of the lift response coefficient

C_{L1}, C_{L2} is the amplitude of the oscillatory part of the response at the fundamental and twice the fundamental frequency

Φ_{L1}, Φ_{L2} is the phase angle of the oscillatory part of the lift response at the fundamental and twice the fundamental frequency

C_D is the total measured drag coefficient

$\bar{C}_D$ is the mean value of the drag response coefficient

C_{D1}, C_{D2} is the amplitude of the oscillatory part of the response at the fundamental and twice the fundamental frequency

Φ_{D1}, Φ_{D2} is the phase angle of the oscillatory part of the fundamental and twice the fundamental frequency drag response

The subscript 1 and 2 associated with the force coefficients and phase angles indicate the value at the fundamental frequency or twice the fundamental frequency. Assuming that C_{L2} is zero, the measured lift with respect to the incoming wave then can be shown as in Figure 4. In order to isolate the foil only response from the combination foil and sting dynamometer response, tare values (sting only) were subtracted from the magnitude and phase of the response for the sting and foil combination at both the fundamental frequency and twice the fundamental frequency. For example, for determining the fundamental frequency lift response of the foil only configuration the following equations are used.

$$C_{L1_f} = \left[(C_{L1_{fs}} \cos \Phi_{L1_{fs}} - C_{L1_s} \cos \Phi_{L1_s})^2 + (C_{L1_{fs}} \sin \Phi_{L1_{fs}} - C_{L1_s} \sin \Phi_{L1_s})^2 \right]^{1/2} \quad (3)$$

and

$$\Phi_{Ll_f} = \tan^{-1} \frac{(C_{Ll_{fs}} \cos \Phi_{Ll_{fs}} - C_{Ll_s} \cos \Phi_{Ll_s})}{(C_{Ll_{fs}} \sin \Phi_{Ll_{fs}} - C_{Ll_s} \sin \Phi_{Ll_s})} \tag{4}$$

and

$$\overline{C}_{L_f} = \overline{C}_{L_{fs}} - \overline{C}_{L_s} \tag{5}$$

The subscripts f, s, and fs are defined below

- s - measured response of sting only (tare) configuration
- fs - measured response of configuration with sting and foil
- f - response for the foil only condition as calculated in Equations (3) and (4)

The drag response for the foil only condition at the fundamental frequency and twice the fundamental frequency was calculated using Equations 3-5 by substituting drag coefficients and phases for the lift coefficients and phases. The subscript "f" indicating a foil only condition will be dropped from here on in this report and it will be understood that the tare values have been removed from all the response data presented. A tabulation of the unsteady experimental data corrected for tare values is presented in Appendix A.

LIFT AND DRAG RESPONSE AT NOMINAL WAVE HEIGHT

The amplitude and phase of the lift response at the fundamental frequency for three different depth chord ratios are shown in Figures 5A through 5F. Almost all of the data was collected at a nominal wave amplitude to semi-chord ratio r equal 0.44. In order to maintain clarity, Figure 5D shows phase data for only selected chord Froude numbers. The data for other chord Froude numbers is tabulated in Appendix A. The few dashed symbols indicate that the data was collected at some other wave height at which good linearity was observed. Figure 6A through 6F and 7A through 7F show the drag response and phase at the fundamental and twice the fundamental frequency.

The data for the lift response at twice the fundamental frequency is not shown because the amplitude of the response C_{L2} was very small. Typically C_{L2} was 0.01 to 0.02 times the primary frequency response C_{L1}. Almost all of the energy dissipated in lift response went into the fundamental frequency response. Values of ROOTQO for virtually all of the test runs ranged from 0.96 to 1.00. As mentioned in Appendix B of this report describing the sample output, ROOTQO is equal to the standard deviation of the oscillating part of the response multiplied by $\sqrt{2}$. In our case a ROOTQO value equal to 1.00 indicates that the response is a perfect sine wave of the fundamental frequency. The ROOTQO value can be considered as a measure of the energy in the response concentrated at or near the fundamental frequency, and ROOTQO values near unity indicate that the energy of the response is concentrated at the fundamental frequency.

In contrast to the nature of the lift response, the drag response showed a strong component at the second harmonic. C_{D2} values as high as 70 percent of the C_{D1} values were recorded. Compare Figure 6A and 7A at $k_e = 0.5$ and $F_{nc} = 1.22$. This strong second harmonic drag component should not be surprising since reference 11 states that under certain conditions the amplitude of the second harmonic drag response may be 50 percent of the fundamental. A tabulation of the lift and drag response data appears in Appendix A grouped according to depth chord ratio. Tare values have been substracted from all the response data and the run numbers correspond to the foil and sting dynamometer runs.

In general the phase response, especially for the first and second harmonic of the drag, has more scatter than the amplitude of the response. One should keep in mind however, that where the amplitude of the response is small or near zero the associated phase is a meaningless quantity that may be random.

LINEARITY OF THE RESPONSE

The bulk of the test data was taken at a nominal wave amplitude to semi-chord ratio, r, equal to 0.44. Linearity checks at nominal values of $r = 0.22$ and $r = 0.6$ were run at three chord Froude numbers and corresponding constant reduced frequency of encounter k_e. At all three depth chord ratios the linearity of the fundamental lift response is very good as shown by the almost horizontal lines in Figures 8A to 8C. The linearity of the amplitude is better than that of the phase.

The drag response, in contrast to the lift response, shows poor linearity (see Figures 9A to 10C). One should keep in mind that, as stated in the accuracy section of this report, the drag response measurement is much less accurate than the lift response measurement. In addition, the drag response is much smaller than the lift response and therefore the linearity is more susceptible to the influence of scatter.

RESPONSE TRENDS WITH CHORD FROUDE NUMBER, DEPTH FROUDE NUMBER AND DEPTH-CHORD RATIO

a) Chord Froude number (F_{nc}) variation at constant reduced frequency of encounter and depth.

The lift and drag response obtained from the faired lines through the data shown in Figures 5A, 5C, and 5D were plotted holding k_e and depth as a constant parameter. See Figures 11A, 11B, and 11C. The constant k_e values 0.183, 0.25 and 0.315 were selected prior to the experiment and the proliferation of data at these encounter frequencies was planned. One can see from Figures 11A, 11B, and 11C that the amplitude of fundamental frequency lift response strongly increases as chord Froude number F_{nc} decreases from 3.66 to 1.22. This trend agrees with other experimental lift response trends taken at high chord Froude numbers. (The AG (EH) data shows a C_{L1}/r change from 0.065 to 0.092 for a chord Froude number change from 7.18 to 4.98, see Figures 26 and 27 of this report). The data for the fundamental drag response, Figures 12A, 12B, and 12C show a different trend with chord Froude number variation. The fundamental frequency drag response curves show a general hollow at $F_{nc} = 2.5$ instead of the steadily decreasing nature of the lift response curves. The second harmonic drag response, Figures 13A, 13B, 13C, shows the same trend as the fundamental lift response, that is, decreasing response amplitude with increasing chord Froude number. While it would be of academic interest to find an explanation for this trend, in any practical application the variation in the drag response would probably be ignored, since its value is very small.

The solid point on Figure 11B represents a theoretical prediction for a similar foil. This prediction is discussed in the theory section of this report. The two data points on Figure 11C were taken from Reference 8 and represent results on an aspect ratio 4 rectangular hydrofoil. They are shown for comparison with our aspect ratio 6 hydrofoil lift response trend.

b) Chord Froude number, F_{nc}, variation at constant depth Froude number, F_{nh}, and reduced frequency of encounter k_e.

Figures 14A, 14B, and 14C shows the variation of the fundamental lift response with chord Froude number holding depth Froude number and k_e constant. These curves are all in a narrow band indicating that the response is sensitive to chord Froude number and not so sensitive to depth Froude number. For example, at $k_e = 0.25$ and $F_{nc} = 2.4$, Figure 14B,the change in C_{L1}/r corresponding to the F_{nc} change from 1.72 to 2.58 is only 0.22 to 0.26. Furthermore, where the curves cross there is no dependence on F_{nh}.

c) Variation of the fundamental lift response with F_{nh} at constant k_e, F_{nc}, and h/c.

A carpet plot of the fundamental lift response vs F_{nh} with F_{nc} and h/c held constant is shown in Figures 15A, 15B and 15C for three different reduced frequencies of encounter. The symbols shown are data points. These plots show a strong dependence of the lift response on chord Froude number and depth. Note that as k_e decreases the sensitivity of the response to depth Froude number diminishes.

MEAN LIFT AND DRAG IN WAVES AND IN CALM WATER

The mean lift and drag coefficients $\overline{C}_L$ and $\overline{C}_D$ in head seas is presented in Figures 16A to 16G along with the lift and drag coefficient C_L and C_D in smooth water. All these coefficients include turbulence stimulator drag. For almost all of the depth chord ratios and chord Froude numbers the mean drag in waves is less than the smooth water drag while the added lift in waves is dependent on the depth-chord ratio, reduced frequency of encounter and the chord Froude number.

In order to assess the significance of the lift and drag response in terms of the mean lift and drag in waves the ratio $C_{L1}/\overline{C}_L$ and $C_{D1}/\overline{C}_D$ are plotted in Figures 17Ato 17F. These figures show that the amplitude of the fundamental lift response as compared to the mean lift is always much larger than the amplitude of the drag response compared to the mean drag. The highest C_{L1}/C_L ratio is 2.25 and occurs at depth chord ratio, 0.5, reduced frequency of encounter, 0.43, and chord Froude number, 1.22. At these same conditions the $C_{D1}/\overline{C}_D$ ratio is only 1.1. In fact the amplitude of the fundamental frequency drag response is very small, probably negligible for most control surface applications at depth chord ratio 1.0 and 2.0,

but in contrast the amplitude of the lift response is still significant, 1.0 to 0.8 times the mean lift for $F_{nc} = 1.22$.

THEORETICAL PREDICTION OF LIFT RESPONSE

The aerodynamic response of wings has been under investigation for many years. Several texts, (References 1, 2, and 3) deal with the more encompassing aeroelastic problems encountered on wings and they should be consulted for background information and extensive bibliographies. There appear to be two general approaches to predicting the slightly different problem of hydrofoil response in waves. One approach relies on the existing aerodynamic theories (and supporting experimental data) as discussed in the above texts for predicting the aerodynamic response of a wing due to forced sinusoidal oscillations in infinite uniform flow and transforms this response to that of a hydrofoil operating under regular waves. Examples of this approach include response predictions by Theodorsen[4], or Reisner[5] or Lawrence and Gerber[7] transformed to the hydrofoil response in waves by the approximate method of Henry and Ali[8]. The other general approach is a direct attack on the problem of a hydrofoil moving under regular waves. These methods such as Crimmi's[12] and Widnalls[13] 2-D theory, are potential flow problems which satisfy the Laplace equation, associated kinematic and dynamic free surface boundary conditions, and the Kutta condition for finite pressure at the trailing edge of the foil. A lifting surface program developed by Ashley et al[14] and Widnall[15] and computer programmed by Widnall is described, summarized and evaluated by Besch and Rood[9]. Further details and a comparison of predictions with the experimental results reported herein follow.

a. THEODORSEN'S THEORY (References 4, and 16)

This is a 2-dimensional inviscid, incompressible linearized potential flow solution satisfying the Kutta condition. The foil of semi chord b is assumed to be in uniform flow traveling at a constant speed U and oscillating with a circular frequency ω. The prime motivation for the theory was to predict flutter speed and the lift and moment response on airplane wings.

Results are expressed as a tabulation of the reduced frequency $k = \omega b/V$ versus a function $C(k) = F + iG$. Since the publication of the original paper, the function C(k) has become known as Theodorsen's function.

It is convenient to express the uniform flow response to forced oscillations in terms of the non-dimensional aerodynamic coefficients L_h and L_α. They are

related to Theodorsen's function by the following expressions

$$L_h = 1 - \frac{2i}{k}(F+iG) \tag{6}$$

$$L_\alpha = \frac{i}{2} - \frac{i}{k}[1 + 2(F+iG)] - \frac{2}{k^2}(F+iG) \tag{7}$$

L_h and L_α are then separated into their real and imaginary parts:

$$L_h = L_{hr} + iL_{hi} \text{ and} \tag{8}$$

$$L_\alpha = L_{\alpha r} + iL_{\alpha i} \tag{9}$$

The Theodorsen 2-dimensional prediction of these aerodynamic coefficients as a function of k is presented in Figures 18A to 18D. It should be noted here that the Theodorsen function C(k) is equal to an algebraic combination of the Bessel function J_o, J_1 and Y_o, Y_1 and could be calculated rapidly by computer. However, since Reference 6 provides a very extensive tabulation of Theodorsen's function it was not necessary to write a computer program for performing this calculation.

For the case of the hydrofoil oscillating in simple harmonic motion defined by

$$h = h_o e^{i\omega t} \text{ and} \tag{10}$$

$$\alpha = \alpha_o e^{i(\omega t+\Phi_1)} \tag{11}$$

the expression for lift forces per unit span is given by

$$L' = \pi\rho b^3 \omega^2 \left[L_h \frac{h}{b} + \alpha(L_\alpha - (\tfrac{1}{2} + a))L_h\right] \tag{12}$$

where h, a and α are defined in Figure 19 and Φ_1 represents the phase lag of the pitch motion relative to the heave motion.

Equation 12 predicts the response for an oscillating foil in calm water. It was not used to compare our experimental results with the theoretical predictions,

because all of the dynamic experiments were run in waves with the foil fixed (within the limits of the dynamometer stiffness). The equation is presented in order to illustrate that the total lift response has contributions from both the L_h and L_α aerodynamic derivatives. The comparison of these functions, as predicted by this and other theories, is shown in Figures 18A to 18D.

In order to predict the lift response for the fixed hydrofoil operating in regular waves the theory of Henry & Ali[8] is used instead of Equation 12. This theory obtains the approximate gust response operator $R(k_e)$ from the non-dimensional aerodynamic coefficients L_h and L_α. It assumes a fluid vertical velocity distribution given by the following equation:

$$v(x,y,t) = (\frac{\bar{c}}{2})r\omega \exp(-\frac{\omega\pi y}{\lambda} \sin \frac{2\pi}{\lambda})[x - (V + c)\ t] \tag{13}$$

It shows that by the application of certain simple transformations the vertical velocity distribution on a fixed airfoil in a sinusoidal gust can be made nearly the same as that on an oscillating airfoil in uniform flow. Figure 20 shows the definition of the terms used in Equation 13.
The wave elevation is given by:

$$\zeta(x,t) = (\bar{c}/2)r \cos \frac{2\pi}{\lambda} [x - (V+c)\ t] \tag{14}$$

The wave celerity c, dimensionless wave number K and wave length λ are given by

$$c = g/\omega \tag{15}$$

$$K = \pi\bar{c}/\lambda \tag{16}$$

$$\lambda = \frac{2\pi g}{\omega^2} \text{ (in deep water)} \tag{17}$$

Henry and Ali's theory constrains the gust response operator $R(k_e)$ to be of the form given by

$$R(k_e) \cos \omega_e t = \frac{C_{L1}}{r} \cos (\omega_e t + \Phi_{L1}) \tag{18}$$

The response to a sinusoidal gust is sinusoidal at the same fundamental frequency with a phase shift Φ_{L1}. No harmonics are permitted. C_{L1}, the amplitude of the oscillating part of the lift response is defined previously in Figure 6, and r is the wave amplitude (1/2 the crest to trough distance) to semi chord ratio

$$r = \frac{2\zeta_a}{c} \quad . \tag{19}$$

The predicted response in terms of the aerodynamic coefficients is

$$\frac{C_{L1}}{r} = \pi k \, k_e \, e^{-kd} \, (X^2 + Y^2)^{\frac{1}{2}} \tag{20}$$

$$d = 2h/\bar{c} \tag{21}$$

where

$$X = L_{hr} \, (1 + \frac{K}{k_e}) + K \, L_{\alpha i} \tag{22}$$

$$Y = K \, L_{\alpha r} - (1 + \frac{K}{k_e}) \, L_{hi} \tag{23}$$

and the phase of the response is

$$\Phi_{L1} = \tan^{-1} \, (Y/X) \, . \tag{24}$$

The reduced frequency of encounter k_e for head waves is defined as

$$k_e = \frac{\pi f_e}{\bar{c}V} = \frac{\omega \bar{c}}{2V} \, (1 + \frac{\omega V}{g}) \tag{25}$$

with

$$f_e = \frac{\omega_e}{2\pi} \tag{26}$$

The phase angle Φ_{L1} is the phase lead of the lift time history (at midchord) with respect to the wave time history.

It is important to note that when the foil is oscillating in uniform flow the forcing frequency is characterized by the reduced frequency k whereas when it is operating in waves the forcing frequency is characterized by the reduced frequency of encounter, k_e, in order to take into account the effect of wave celerity.

b. REISNER'S THEORY (References 5 and 6)

Reisner developed a theory to take into account the effect of finite span on the airload distribution of an oscillating wing of aspect ratio ≥ 3.0. The final results of this theory are formulas for the spanwise distribution of air forces and moments on a wing of finite span. In these formulas the effect of the three-dimensionality is a correction term σ to the basic function C(k) of the two-dimensional Theodorsen theory. Tabulated results of the correction factor σ are presented for wings of elliptical planform and wings of rectangular planform. In both cases the aspect ratios are 3 and 6 and a range of values of the reduced frequency k are covered.

The aspect ratio 6, rectangular planform correction factor, σ was used to calculate the aerodynamic coefficients L_h and L_α. The tabulated correction factors, σ, as presented by Reisner are for the semi-span locations 0.0, 0.4, 0.8 and 1.0 and they were graphically integrated as defined by Equations 29 through 32.

At each semispan location

$$L_h' = 1 - \frac{2i}{k} \left(C(k) + \sigma\right) \tag{29}$$

$$L_\alpha' = \tfrac{1}{2} - \frac{2}{k^2} \left(C(k) + \sigma\right) - \frac{2i}{k} \left[\tfrac{1}{2} + C(k) + \sigma\right] \tag{30}$$

and the aerodynamic coefficients are

$$L_h = \frac{1}{b} \int_{-b/2}^{b/2} L_h' \, dy \tag{31}$$

$$L_\alpha = \frac{1}{b} \int_{-b/2}^{b/2} L_\alpha' \, dy \tag{32}$$

Symmetry about the central zero semispan station is assumed. The calculated coefficients are shown in Figures 18A to 18D. Once the aerodynamic coefficients L_{hi}, L_{hr}, $L_{\alpha i}$, and $L_{\alpha r}$ are determined, the Henri and Ali[8] theory was used to predict the response in waves just as in the case of the Theodorsen theory.

The Reisner theory is compared to experimental results for depth-to-chord ratio 2.0 in Figures 21 and 22. Note the general overprediction of the amplitude of the lift response by 11 to 16 percent. This agreement is remarkable. The trends in the lift amplitude data are accurately predicted. The phase response is overpredicted by as much as 40 percent; however, the predicted trend with chord Froude Number is similar to that obtained in the experiments (Figure 22).

c. LAWRENCE & GERBER THEORY (Reference 7)

Lawrence and Gerber developed a low aspect ratio (AR $\leq$ 4) potential flow theory for calculating the forces on a harmonically oscillating wing in inviscid incompressible flow. The theory is limited to wings with straight trailing edges. The starting point for the theory is an exact two variable integral equation for an oscillating lifting surface in incompressible flow, from which an approximate integral equation in one variable for unsteady flow is derived. The aerodynamic lift and moment coefficients for the limiting case of aspect ratio approaching zero are shown to agree with the Jones[17] theory extended to unsteady forces. As aspect ratio approaches infinity, the two dimensional result is obtained for rectangular wings; and as the reduced frequency approaches zero the

steady state case of Reference 18 is reproduced. In Reference 7 the aerodynamic coefficients are tabulated for wings with rectangular and triangular planforms of aspect ratio 0.25, 0.50, 1.0, 2.0, and 4.0 for a range of reduced frequencies k from 0.0 to 1.0.

In order to obtain results for aspect ratio equal to 6.0, the aerodynamic coefficients were interpolated from the rectangular planform aspect ratio 1.0, 2.0 and 4.0 values as predicted by Lawrence and Gerber and from the infinite aspect ratio two-dimensional Theodorsen results. The interpolated coefficients for aspect ratio 6 are shown in Figures 18A to 18D along with the Reisner results.

Again, in order to obtain the response in regular waves, the theory of Henry & Ali[8] is applied. Comparison with the experimental data are shown in Figures 23 and 24.

The theories mentioned so far, Theodorsen's, Reisner's and the Lawrence and Gerber theory use the response from infinite fluid forced oscillation and therefore would not be expected to predict the effect of the free surface on the response. Any effect due to the presence of the free surface could be the result of a hydraulic jump over a very shallowly submerged foil or to a modification of the wave pattern by the response. According to Reference 19 there is no uniform agreement as to whether these free surface effects should be characterized by chord Froude number or depth Froude number. The Henri and Ali transformation of the aerodynamic coefficients to response in regular waves take into account only the effects due to wave celerity. In order to take Froude number effects into account in the Theordorsen, Reisner or Lawrence and Gerber theories one would have to modify the aerodynamic coefficients.

It can be seen from Figures 21 and 23 that the amplitude of lift response prediction by the Lawrence and Gerber theory is in closer agreement with the experimental data than the Reisner theory predictions, although the difference is probably not significant. The Lawrence & Gerber theory prediction is generally 6.0 to 10.0 percent too high at the depth chord ratio 2.0.

One would expect the best agreement with experimentally determined lift response at the deepest submergence for the Reisner and the Lawrence and Gerber theories, since they do not take free surface effects into account. The Lawrence & Gerber prediction at shallower depths are shown in Figures 25A to 25F. Only the Lawrence & Gerber prediction is shown, since the Reisner lift amplitude predictions were just slightly higher for the depth chord ratio 2.0 case and one would expect

this trend between the two theories to hold independent of depth. The predicted trend of the response is similar to that obtained from the experiments,showing decreasing lift amplitude with increasing submergence for h/c greater than 1.0. However, the decrease in response as submergence appraoches zero is not predicted. Note also that the predicted phase of the lift response, Figures 25D to 25F, is constant with depth chord ratio whereas the experimental data is not.

d. WIDNALL & LANDAHL THEORY

Widnall and Landahl[13] derived an acceleration potential theory for the lift and moment response of an oscillating three-dimensional hydrofoil at infinite chord Froude number and a two dimensional theory at finite chord Froude number. The two-dimensional theory contains the effects of the unsteady wake, surface waves generated by the motion and the depth of the foil below the surface. At infinite depth, this theory is claimed to reproduce the Theodorsen results.

e. WIDNALL LIFTING SURFACE PROGRAM

A lifting surface theory for calculating the fluid dynamic loading on airfoils and hydrofoils was developed by Ashley[14] et al and Widnall and was subsequently programmed into computer code by Widnall. Besch and Rood[9] performed extensive calculations and comparison to existing data using this program and have shown that with empirical corrections, lift predictions can be made with an accuracy of about 15 to 20 percent. The computer program is capable of calculating both steady and unsteady loading on hydrofoils (camber taken into account, thickness effects ignored) and includes finite depth effects and cavitation effects. A summary of the lifting surface theory, a program listing and user's guide is presented by Besch and Rood[9].

Besch and Rood[9] used the Widnall program to predict the lift response for an aspect ratio 6 foil, on which lift response tests were performed by Wetzel and Maxwell[11]. This foil was similar to the one tested here except that it has NACA 16-509 section and had a much smaller chord = 0.25 ft (7.62 cm). It has the same rectangular planform and the lift response prediction was made for k_e equal to 0.237 and depth chord ratio 1.0 as shown in Figure 12B. The prediction for the Wetzell and Maxwell foil which is very similar to the present configuration compares well with the present data.

In order to compare the various prediction methods, the Lawrence and Gerber and the Theodoresen 2-dimensional theories were used to predict the lift response

amplitude of the AG(EH) main foil. Widnall 2-dimensional and 3-dimensional predictions as well as experimental data are available for this foil as shown in Figures 26 and 27. The AG(EH) main foil is a trapezoidal aspect ratio 3 foil. Trapezoidal planforms can be predicted by the Lawrence and Gerber theory; however, the aerodynamic coefficients were available in tabulated form only for the triangular and rectangular planforms. It is assumed that the prediction for the trapezoidal planform would fall between the triangular and rectangular planforms aspect ratio 3 prediction. It can be seen from Figure 26 and 27 that the Widnall 3-dimensional prediction as calculated by Besch and Rood[9] is the best. As expected, the two-dimensional Theodorsen theory greatly overpredicts the response. The Lawrence and Gerber theory also overpredict the response but not by much. Based on previous trends, the Lawrence and Gerber theory would probably be more accurate at a deeper submergence. The Reisner theory, not shown, would be expected to be very close to the Lawrence and Gerber theory. An anomaly in the prediction is the underprediction by the two-dimensional Widnall theory obtained from Reference 20. One would expect the two-dimensional theory to overpredict the experimental response as well as the three-dimensional theory.

DYNAMOMETER CALIBRATION AND ACCURACY

The set-up and calibration for the experiment consisted of calibrating the individual block gauges, and re-calibrating and checking out the assembled gauges using the Carriage V heavy bridge as a calibration stand. Then, without disassembly, the dynamometer was moved to the Carriage II dry dock and a final calibration was performed.

Based on past experience, an interaction between the lift and drag measurement was expected. This interaction is basically caused by small deflections in the sting and sting supports when they are under a lift load and by possible misalignment of the flexure. The interaction was minimized by using shims to adjust the vertical angle of the flexure within the limits allowed by the clearance in the flexure bolt holes. The angular deflection of the nose piece at the 1/4 chord position was determined by applying varying lift loads. The final deflection calibration performed on the assembled dynamometer in the Carriage II drydock showed 3.74×10^{-4} degrees of deflection per pound (4.48 N) of lift applied at the 1/4 chord position of the foil.

The excess interaction drag produced by various lift loads was found to be consistently repetitive and was calibrated. The calibration curve was fitted with the following polynomial expression

$$\Delta D = -0.035 + 0.00146\ L + 1.9375 \times 10^{-6}\ L^2 \qquad (30)$$

where ΔD is the excess interaction drag in pounds (4.448N) due to the applied lift, L in pounds (4.418 N). ΔD is equal to the channel 1 mean DRAG minus the channel 12 DRAG COR mean drag as shown on the sample outputs, Appendix B. From the equation for ΔD it can be seen that the maximum interaction drag is 10.7 lb. (47.59 N) for 2000 lb (8896 N) applied lift. The accuracies of the primary measurements used in this experiment are shown in Table 4.

TABLE 4

Primary Measurement Accuracies

Measurement	Accuracy
Lift	$\pm$ 5% of reading for lift $<$200 lb.
	$\pm$ 1.5% of reading for lift $\geq$200 lb.
Drag	$\pm$ 1.5% of reading for drag $<$50 lb.
	$\pm$ 0.5% of reading for drag $\geq$50 lb.
Speed	$\pm$ 0.01 knot
Wave height	$\pm$ 2% of reading
Wave period	$\pm$ 0.05 sec.

The lift and drag accuracies were determined by the calibration of the assembled dynamometer. The drag accuracy includes the correction for interaction drag caused by lift. The wave height and speed accuracies are based on previous calibration and experience with the instruments and the wave period accuracy is based on the scan rate of the data collection system.

The above instrument accuracies were used to calculate the error range of the measured lift and drag coefficients, lift and drag response and reduced frequency of encounter for two typical data sets which were chosen to represent the best and the worst expected errors. These errors are shown in Table 5 both as an absolute value and as a percentage error.

TABLE 5

Accuracy of the Reduced Data

	Low Speed F_{nc} = 1.22			High Speed F_{nc} = 3.66		
	Nominal Value	Error (absolute)	% Error	Nominal Value	Error (absolute)	% Error
Lift coefficient C_L	0.202	$\pm$0.011	$\pm$5.4	0.266	$\pm$0.004	$\pm$1.5
Drag coefficient C_D	0.0234	$\pm$0.004	$\pm$1.7	0.0247	$\pm$0.00014	$\pm$5.7
Lift response C_{L1}/r (fundamental freq)	0.4204	$\pm$0.027	$\pm$6.4	0.165	$\pm$0.010	$\pm$6.1
Drag response C_{D1}/r (fundamental freq)	0.0066	$\pm$0.0013	$\pm$19.7	0.0034	$\pm$0.00079	$\pm$23.2
Reduced frequency of encounter k_e						
Low wave period at τ_o = 2.0	0.466	$\pm$0.017	$\pm$3.6	0.291	$\pm$0.012	$\pm$4.1
High wave period at τ_o = 4.0	0.182	$\pm$0.003	$\pm$1.6	0.0947	$\pm$0.0018	$\pm$1.9

It can be seen that the lift coefficient C_L, drag coefficient C_D, lift response C_{L1}/r, and reduced frequency of encounter, k_e, have low error values. The drag response, C_{D1}/r, on the other hand has a very large error $\pm$19.7% and 23.2% for the two cases considered. This is primarily the result of trying to measure a very small alternating drag with a block gauge which must have the capacity to measure at least an order of magnitude larger steady state force. It should be emphasized that the error limits in Table 6 are strictly instrument errors and as such they do not account for scatter in the test data which is due to a variation in test conditions or the non repeatability of any possible flow that is in the transition stage between the laminar and turbulent regime.

In addition to static calibrations, the dynamic response of the dynamometer (with the foil mounted) was explored. A small mechanical shaker shown in Figure 28 was used to impart dynamic lift and drag forces to the dynamometer at various frequencies. In order to measure the lift dynamic response a small A-frame was constructed which held the shaker above and out of the water at the 1/4 chord foil positions while the foil was submerged to a depth chord ratio 1/2. The drag dynamic response was taken with the foil raised out of the water, the tail cone removed and the shaker bolted in its place so as to produce sinusoidal horizontal forces in line with the center of the sting.

The drag amplification factor was taken in air; however, it is felt that the results would be nearly the same in water because the added mass associated with the drag direction is expected to be small. The resonant frequency of the drag response in water was double checked by striking the dynamometer with a rubber mallet and analyzing the strip chart record of the drag gauge output as it decayed over approximately 10 cycles. The above method yielded a 4.8 hertz natural frequency in water versus the 4.5 measured in the air shake test. Although one would expect a slightly lower natural frequency in water it is felt that for the purposes of this experiment the drag amplification factor could be considered the same in water and in air. The results shown in Figures 29 and 30 indicate that the amplification factor is unity for both lift and drag, in the low frequency range, where the experiments were conducted. Note that in Figure 29 the shaker lift force is double that of the force in block gauge #2 for the low, less than 2.0 hertz, frequencies because by static analysis, the #2 block gauge records only 1/2 the lift force. The maximum encounter frequency run during the tests was 1.65 hertz while the bulk of the test data, over 80% of the runs, were at encounter frequencies

between 033 and 1.1 hertz. Thus, both lift and drag amplifications, in the frequency range of interest are considered to be 1.0.

The lift amplification curve, Figure 29, has a double peak which is typical of a "vibration absorber" (see Reference 21) that is made of a pair of idealized spring-mass dampers in series. The analogy could be made to the test set up, where the struts and the frame supports consist of one spring mass system and the foil-sting-block gauge-combination is the other spring mass system.

CONCLUSIONS AND RECOMMENDATIONS

Based upon experimental results and theoretical predictions the following conclusions and recommendations can be made:

CONCLUSIONS

1. Chord Froude number has a strong influence on the amplitude and phase of the first harmonic lift, first harmonic drag and second harmonic drag response. Chord Froude number effects become more important as depth chord ratio decreases. At constant reduced frequency of encounter, the fundamental frequency lift response increases with decreasing chord Froude number for all depth to chord ratios and chord Froude numbers from 1.22 to 3.66 that were tested.
2. The second harmonic lift response is zero.
3. The amplitude and phase of the lift and drag response vary with the reduced frequency of encounter.
4. Of the three depth chord ratios tested, 0.5, 1.0 and 2.0, the amplitudes of the lift and drag response were least for depth chord ratio 2.0.
5. The first harmonic lift response amplitude and phase are linear with wave amplitude.
6. The drag-response amplitude (both first and second harmonic), in general, does not appear to be linear with wave amplitude. The magnitude of the measured oscillating drag component was very small, posing difficulties in data-resolution. Guidance from theoretical predictions is needed for establishing data trends.
7. Prediction of the fundamental lift response amplitude at depth chord ratio 2.0 by the theory of Reisner is generally within 11 to 16 percent of the

experimental data. The predictions of Lawrence and Gerber for fundamental frequency lift amplitude are within 6 to 10 percent. These predictions do not take into account the presence of the free surface. As depth-chord ratio decreases, they deviate more and more from the experimental data.

RECOMMENDATIONS

1. Exercise the Widnall lifting surface program and compare the lift response predictions to the present experimental data. Concentrate on the low chord Froude number F_{nc} = 1.22, low depth chord ratio, h/c = 0.5 case.
2. Repeat some of the present tests with a geosim model of smaller size (representative of typical SWATH model appendages) in order to determine any scale effects, and verify Froude number effects by varying the chord.
3. Develop a drag response prediction method for the three dimensional case that meets the need for accurate prediction at low chord Froude numbers near 1.0 and at low depth chord ratios near 0.5.

REFERENCES

1. Scanlan, R.H. and Rosenbaum, R., "Aircraft Vibration and Flutter", Dover Publications Inc., New York, 1968.

2. Fung, Y.C., "The Theory of Aeroelasticity", John Wiley & Sons Inc., New York, 1955.

3. Bispinghoff, R. L., Ashley, H., and Halfman, R.L., "Aeroelasticity", Addison-Wesley Publishing Co., Inc., Reading, Massachusetts, 1957.

4. Theodorsen, T., "General Theory of Aerodynamic Instability and the Mechanism of Flutter", NACA TR #496, 1934.

5. Reisner, E., "Effect of Finite Span on the Airload Distribution for Oscillating Wings Part I - Aerodynamic Theory of Oscillating Wings of Finite Span", NACA TN #1194, 1947.

6. Reisner, E., and Stevens, J.E., "Effect of Finite Span on the Airload Distributions for Oscillating Wings Part II - Methods of Calculation and Examples of Application", NACA TN #1195, 1947.

7. Lawrence, H.R., and Gerber, E.H., "Aerodynamic Forces on Low Aspect Ratio Wings Oscillating in an Incompressible Flow", Journal of the Aeronautical Sciences, November 1952.

8. Henry, C.J., and Ali, R.M., "Hydrofoil Lift in Head Seas", Stevens Institute of Technology, Report 982, October 1963.

9. Besch, P.K. & Rood, E.P., "Accuracy of Hydrofoil Loading Predictions Obtained from a Lifting Surface Computer Program", DTNSRDC, Report 79/039, September 1979.

10. "Research Facilities at the David Taylor Model Basin", DTMB Report 1913, October 1964.

11. Wetzel, J.M., and Maxwell, W.H. C., "Tandem Interference Effects of Flat Noncavitating Hydrofoils", St. Anthony Falls Hydraulic Laboratory, Report #61, University of Minnesota, May 1962.

12. Crimi, P., "Forces and Moments on a Hydrofoil Running Under Regular Waves" Cornell Aeronautical Laboratory Inc., Report BB-2143-6-1, March 1966.

13. Widnall, S. and Landahl, M., "Digital Calculation of Steady and Oscillatory Hydrofoil Loads Including Free Surface Effects," Mass. Inst. Technol. Tech. Note, Navy Contract Nonr 1841 (81), July 1965.

14. Ashley, et al, "New Directions in Lifting Surface Theory", Journal of the American Institute of Aeronautics and Astronautics, Vol. 3, No. 1 P. 3-16, January 1965.

15. Widnall, S.E., "Unsteady Loads on Supercavitating Hydrofoils of Finite Span", Journal of Ship Research, Vol. 10, No. 2, June 1966.

16. Theodorsen, T., and Garrick, I. E., "Mechanism of Flutter, a Theoretical and Experimental Investigation of the Flutter Problem", NACA TR #685, 1940.

17. Jones, R.T., "Properties of Low-Aspect-Ratio Pointed Wings at Speeds Below and Above the Speed of Sound, NACA TN #1032, 1946.

18. Lawrence, H.R., "The Lift Distribution of Low-Aspect-Ratio Wings at Subsonic Speeds", Journal of the Aeronautical Sciences, Vol. 18, October 1951.

19. Pattison, J.H., "Unsteady Hydrodynamic Loads on a Two Dimensional Hydrofoil", DTNSRDC Report 3245, November 1970.

20. O'Neill, W.C., "Unsteady Lift and Hinge Moment Characteristics of the AG(EH) Main Foil and Strut Assembly", NSRDC Report 2805, July 1966.

21. Thomson, W.T., "Mechanical Vibrations 2nd Edition," Prentice Hall Inc., Englewood Cliffs, N.J., 1962.

Figure 1 - Photograph of Hydrofoil & Dynomometer Arrangement

forward lift block gauge

wood block

drag block gauge pivot nose piece

aft lift block gauge

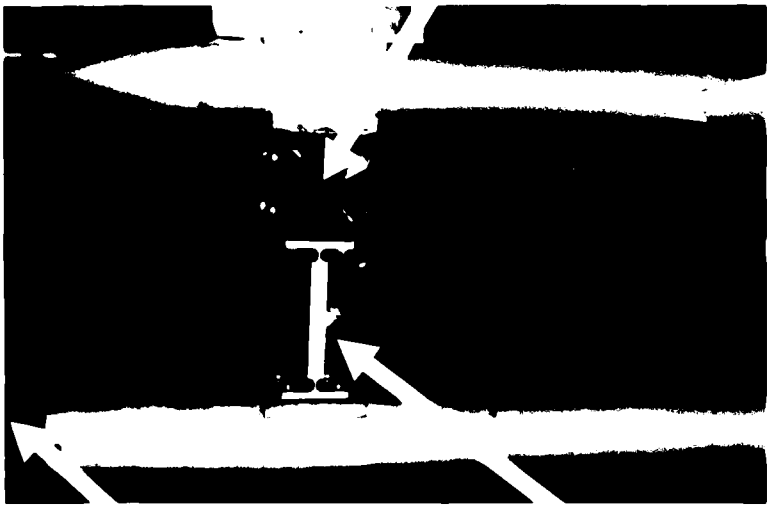

ton pipe support

tail cone position flexure

(tailcone not shown)

Figure 2 - Details of Forward & Aft Block Gauge Stacks

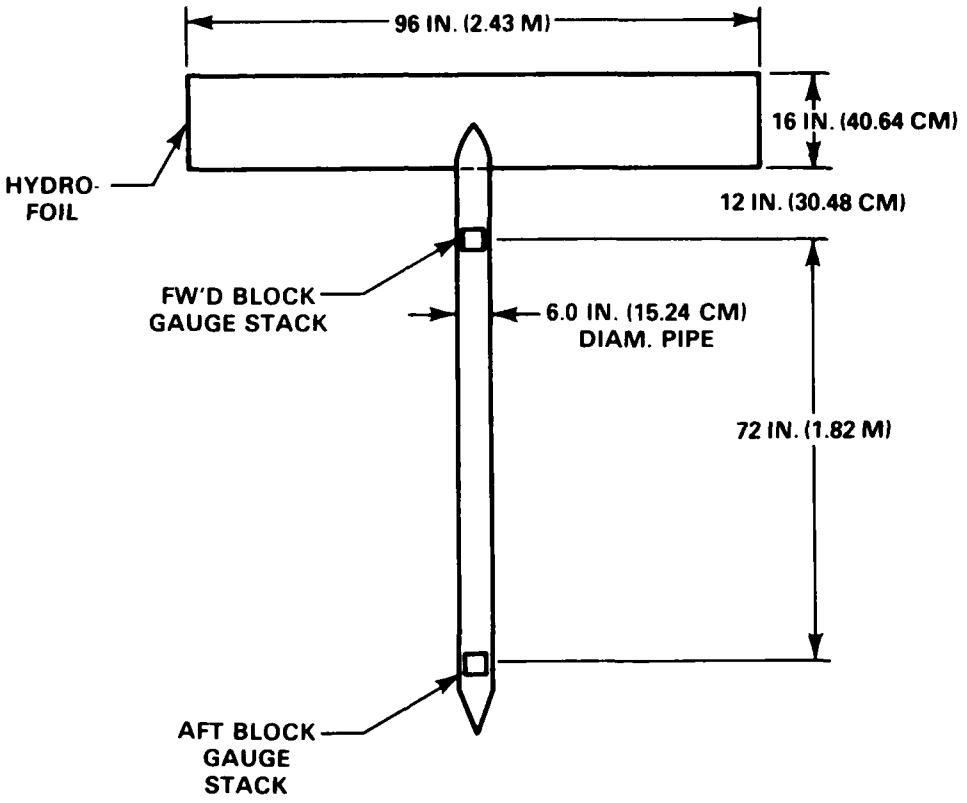

Figure 3 - Plan View of Hydrofoil & Sting

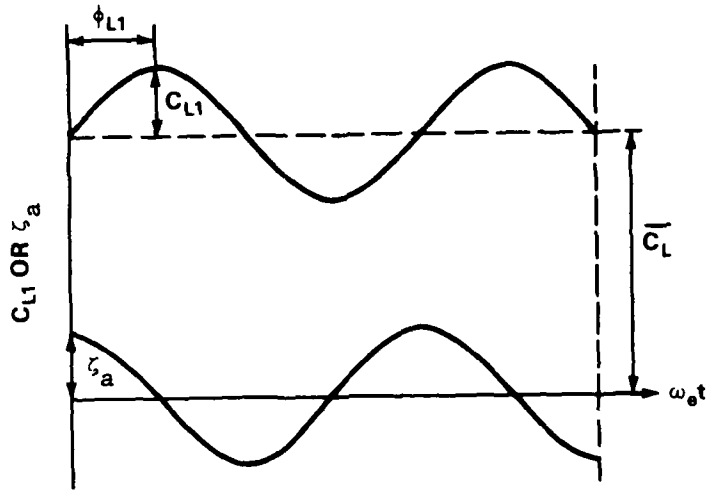

Figure 4 - Definition of Lift Response Amplitude & Phase

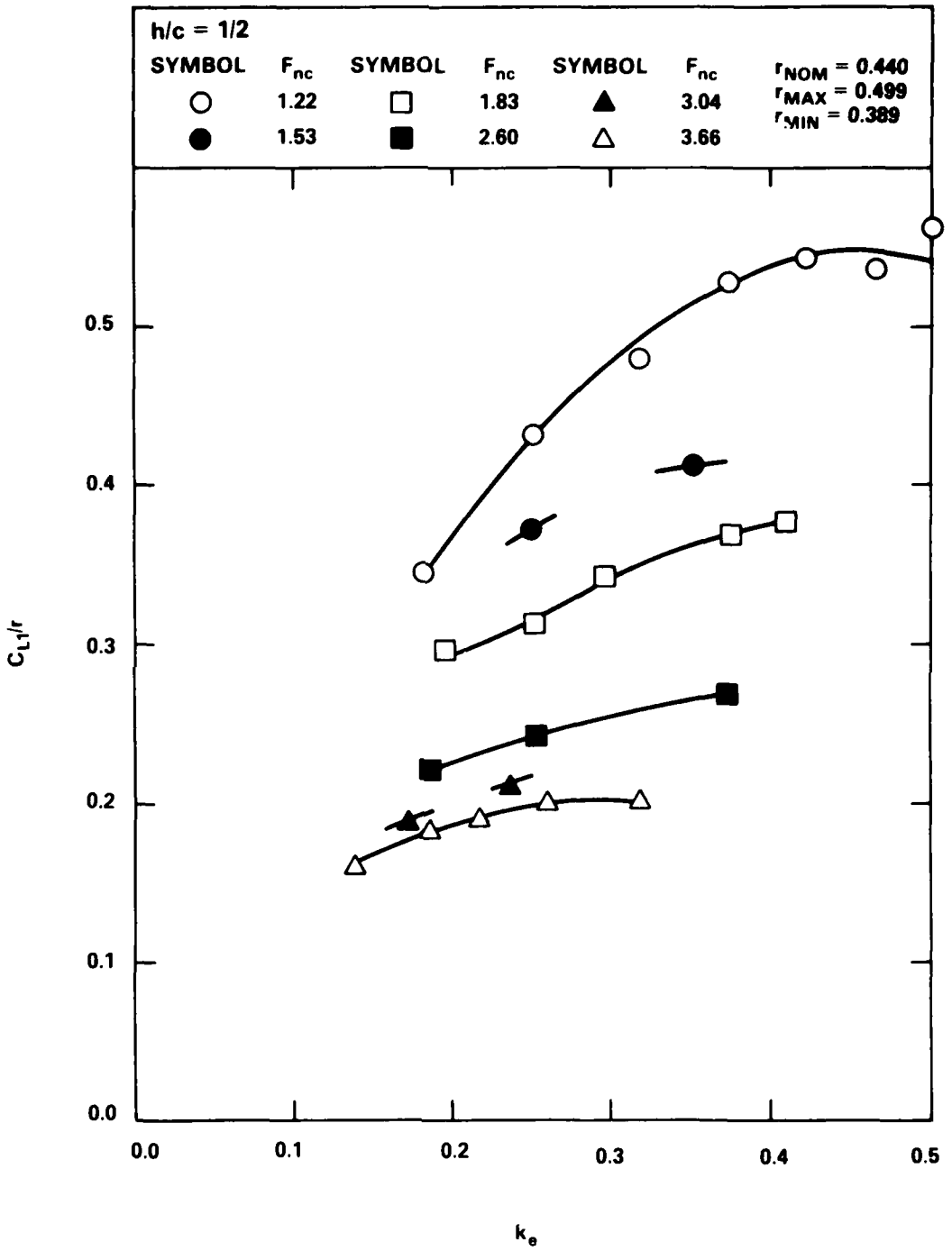

Figure 5A - Lift Amplitude Response at the Fundamental Frequency; h/c = 0.5

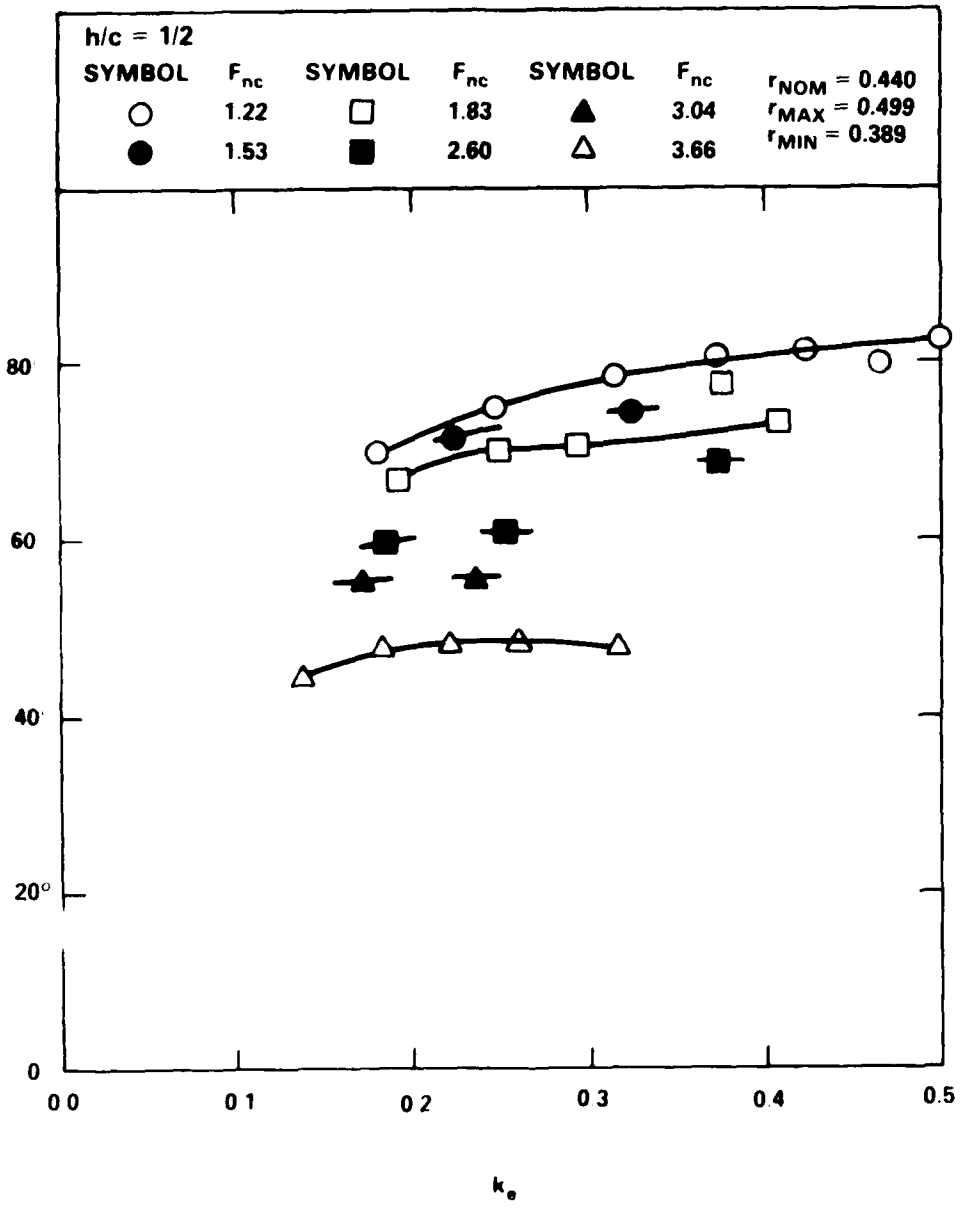

Figure 5B - Lift Phase Response at the Fundamental Frequency; h/c = 0.5

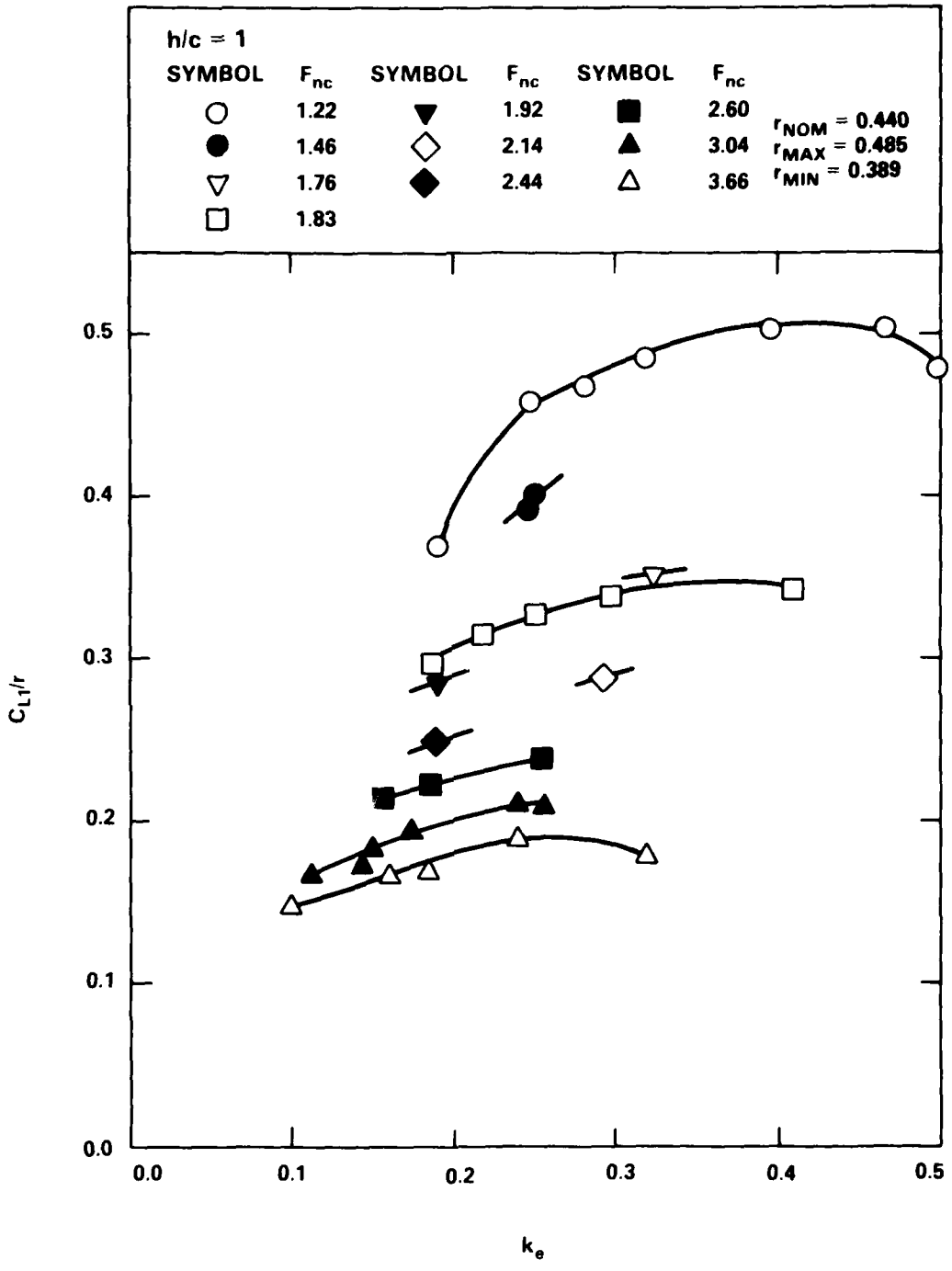

Figure 5C - Lift Amplitude Response at the Fundamental Frequency; h/c = 1.0

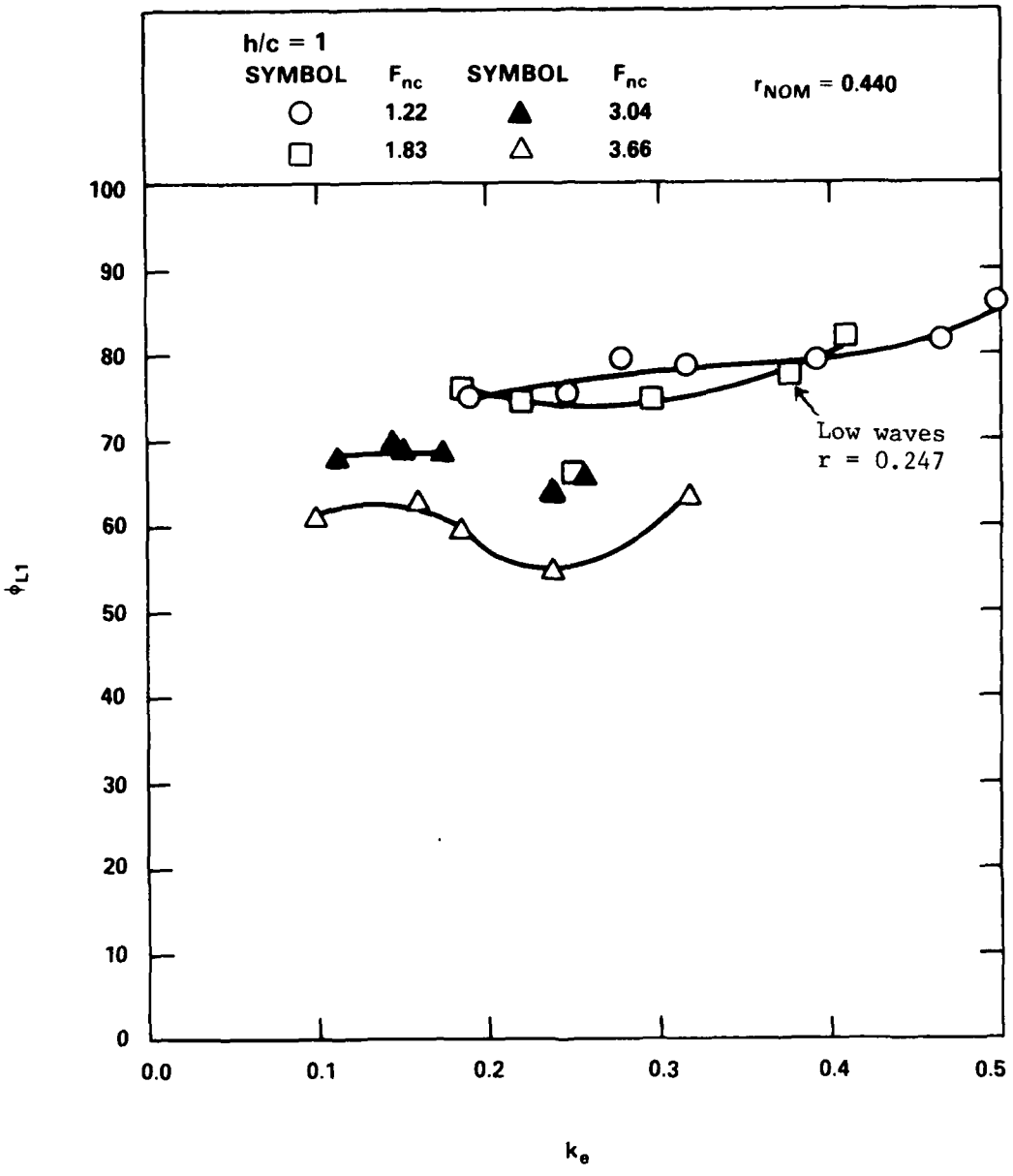

Figure 5D - Lift Phase Response at the Fundamental Frequency; h/c = 1.0

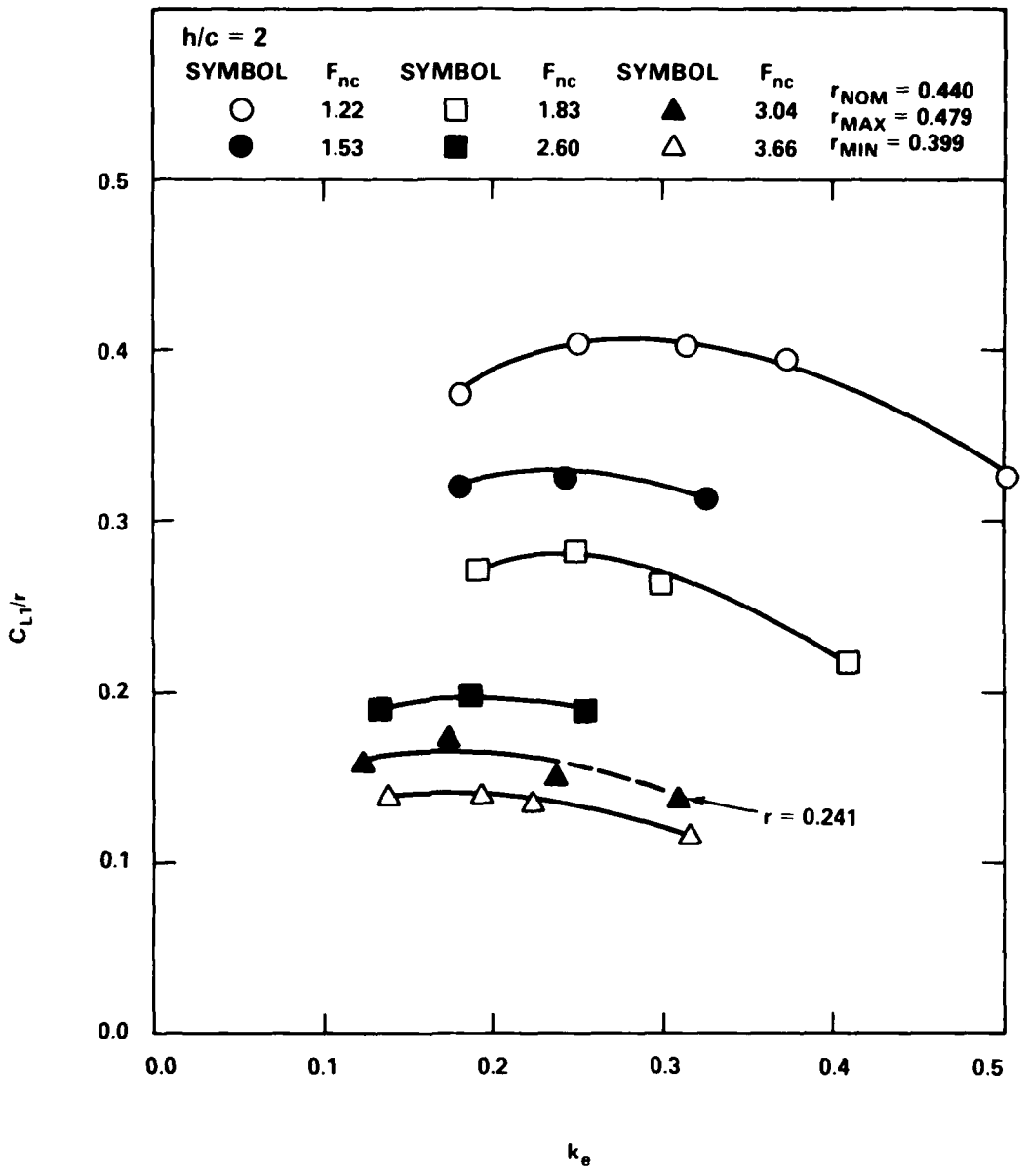

Figure 5E - Lift Amplitude Response at the Fundamental Frequency; h/c = 2.0

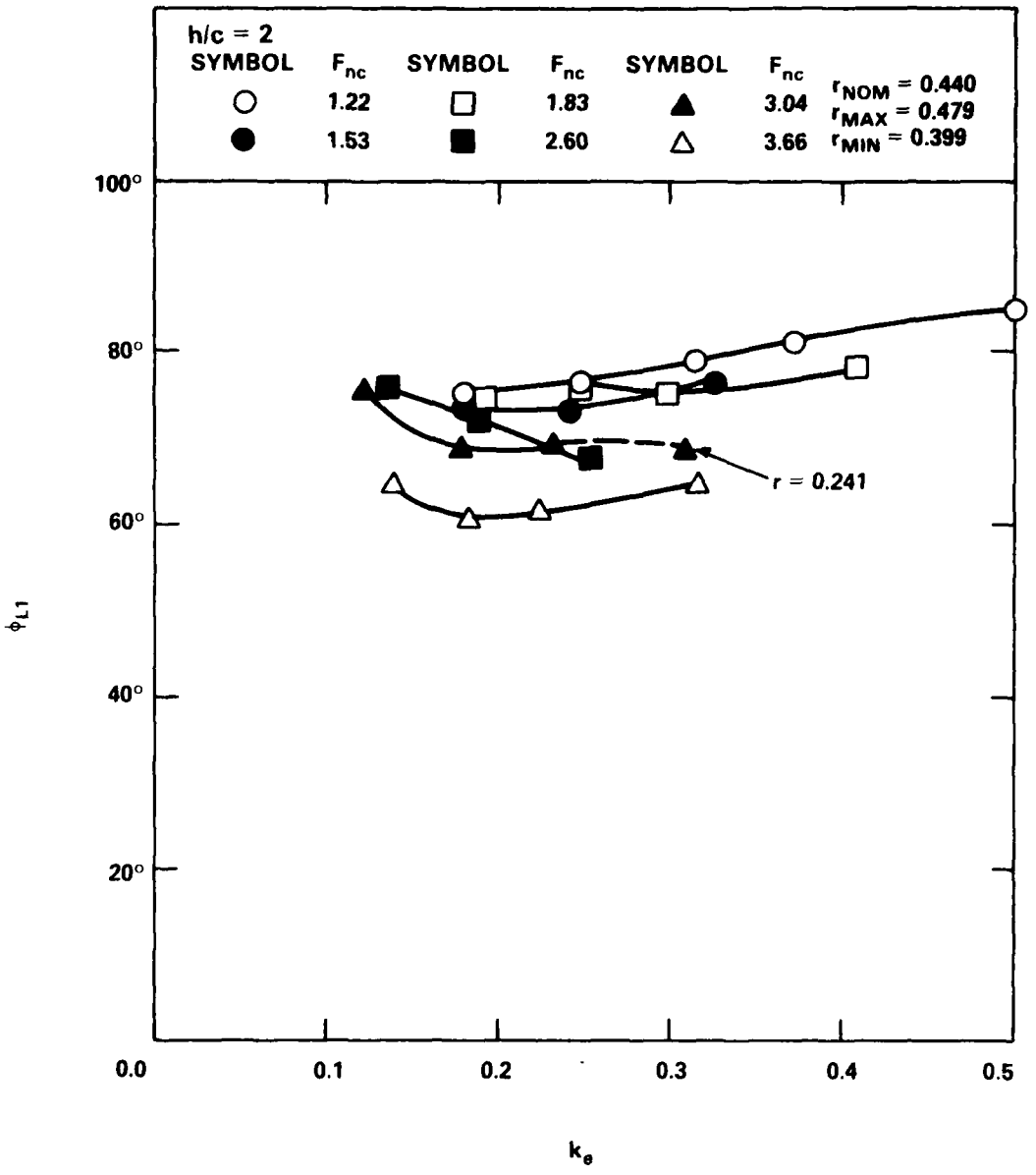

Figure 5F - Lift Phase Response at the Fundamental Frequency; h/c = 2.0

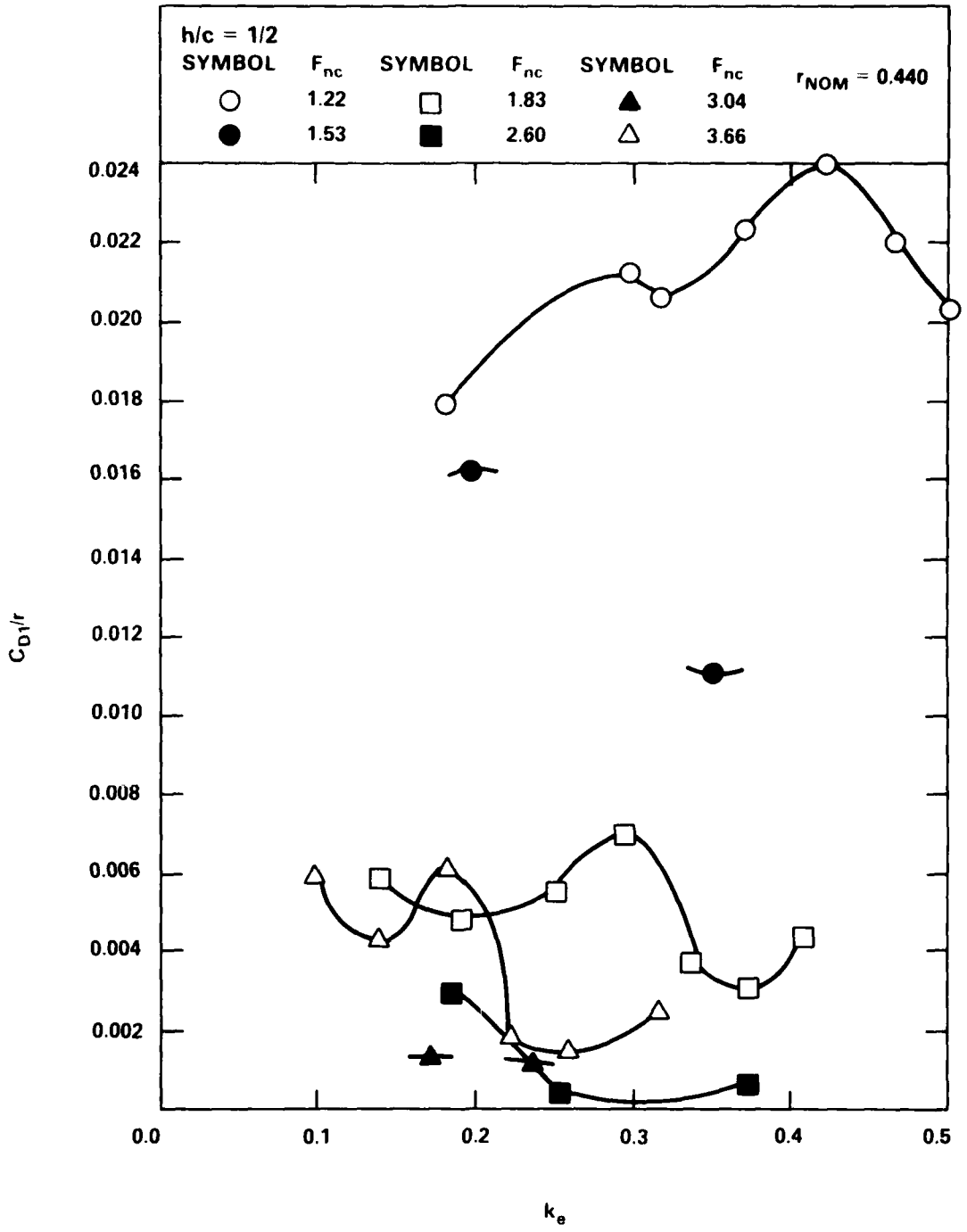

Figure 6A - Drag Amplitude Response at the Fundamental Frequency; h/c = 0.5

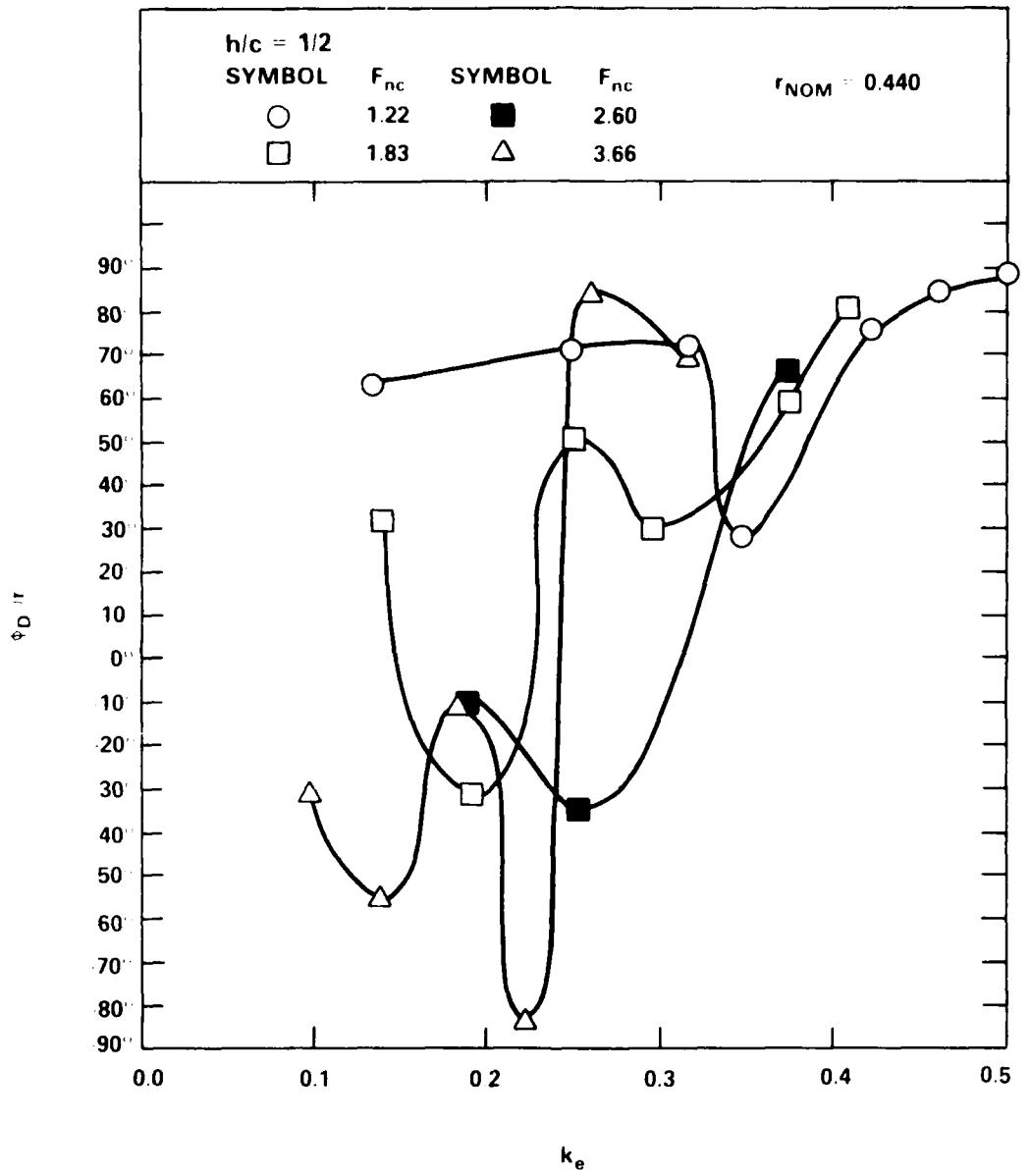

Figure 6B - Drag Phase Response at the Fundamental Frequency; h/c = 0.5

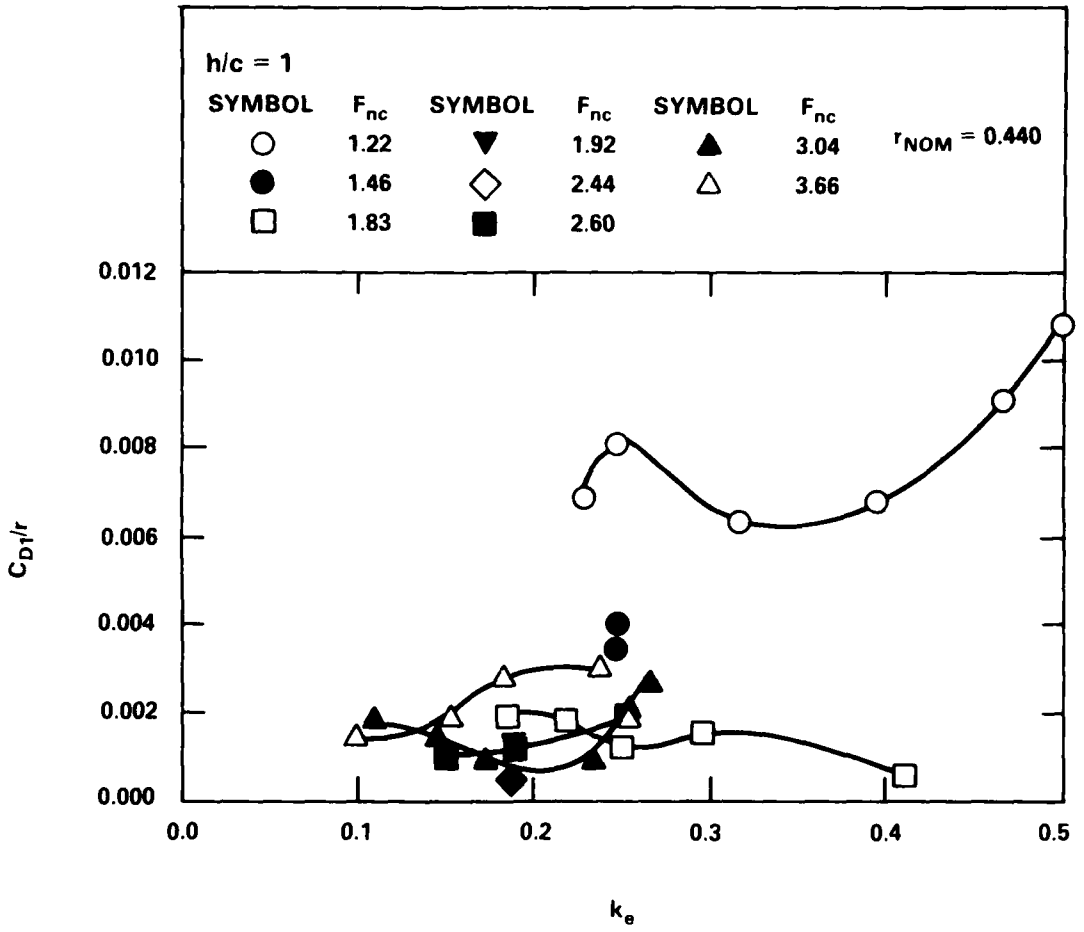

Figure 6C - Drag Amplitude Response at the Fundamental Frequency; h/c = 1.0

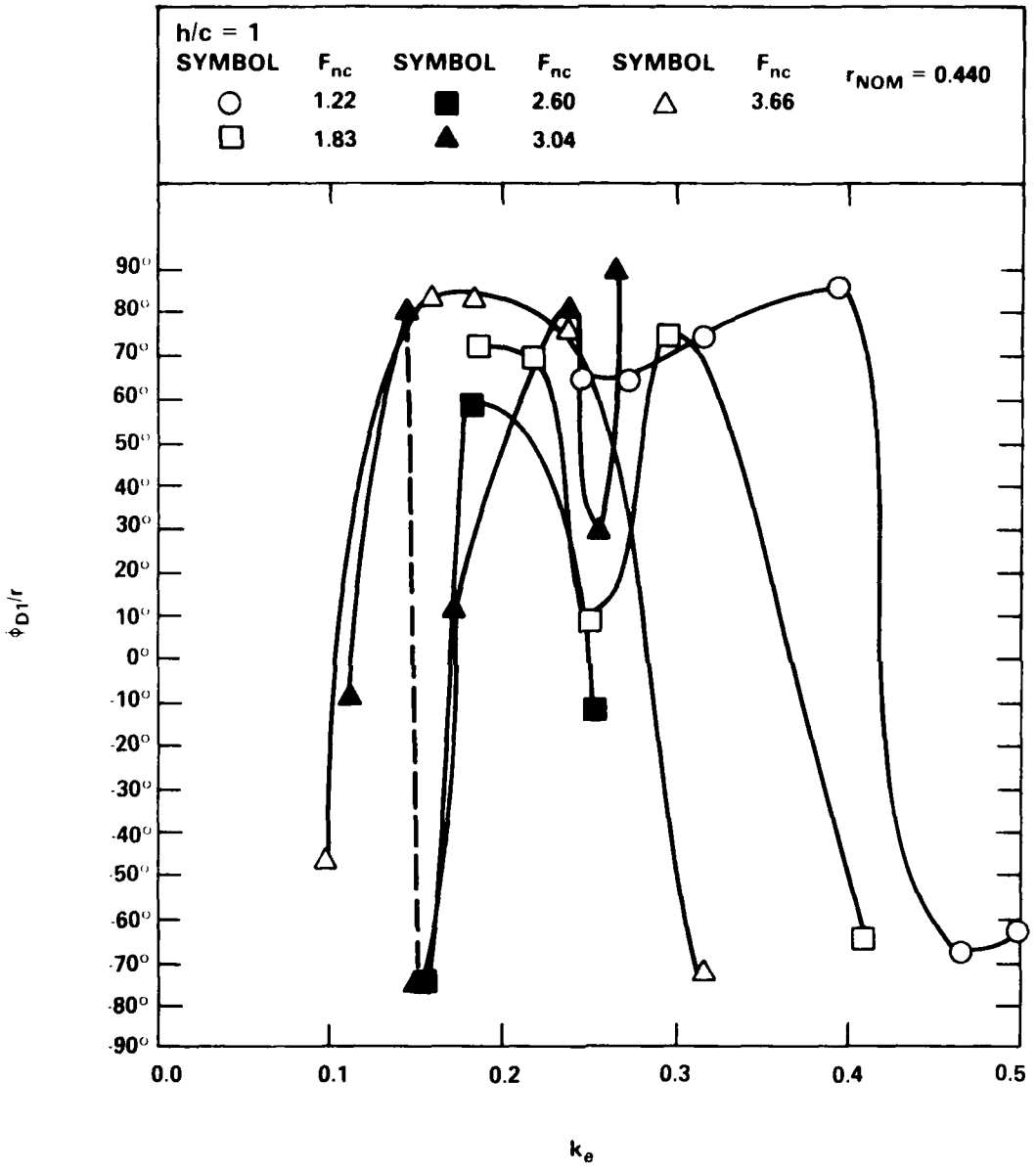

Figure 6D - Drag Phase Response at the Fundamental Frequency; h/c = 1.0

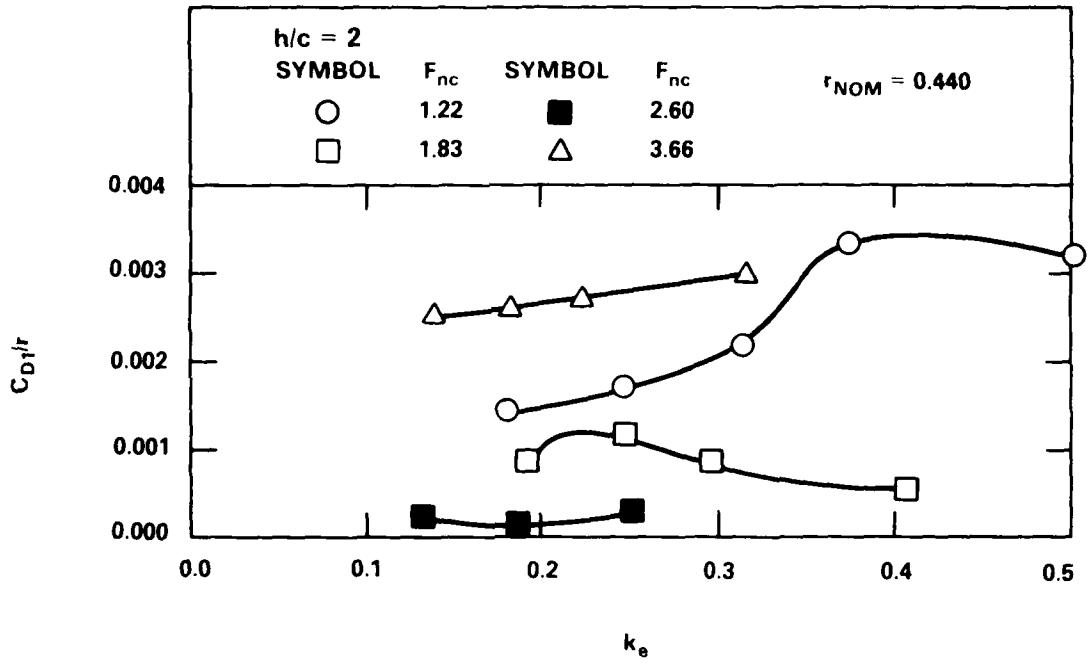

Figure 6E - Drag Amplitude Response at the Fundamental Frequency; h/c = 2.0

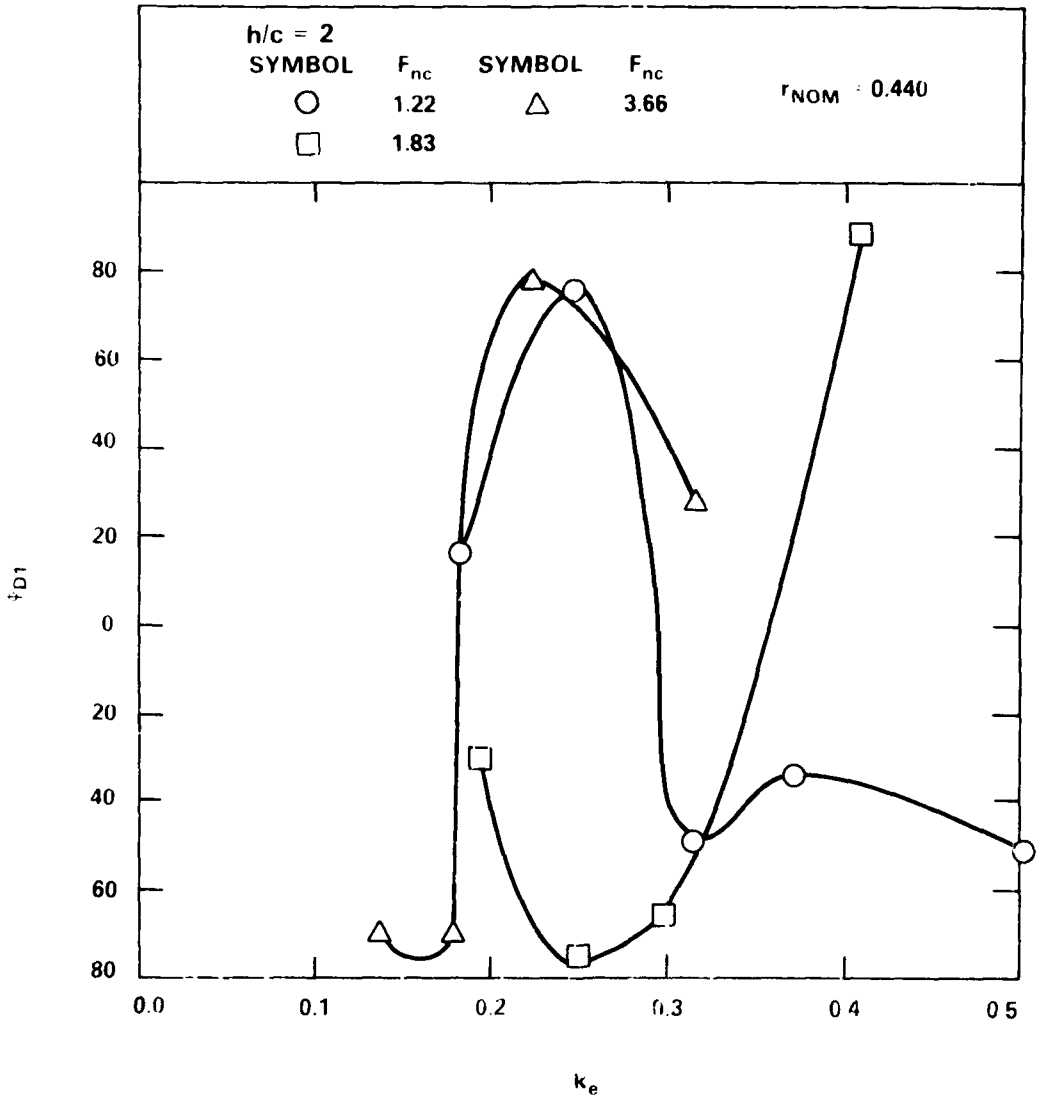

Figure 6F - Drag Phase Response at the Fundamental Frequency; h/c = 2.0

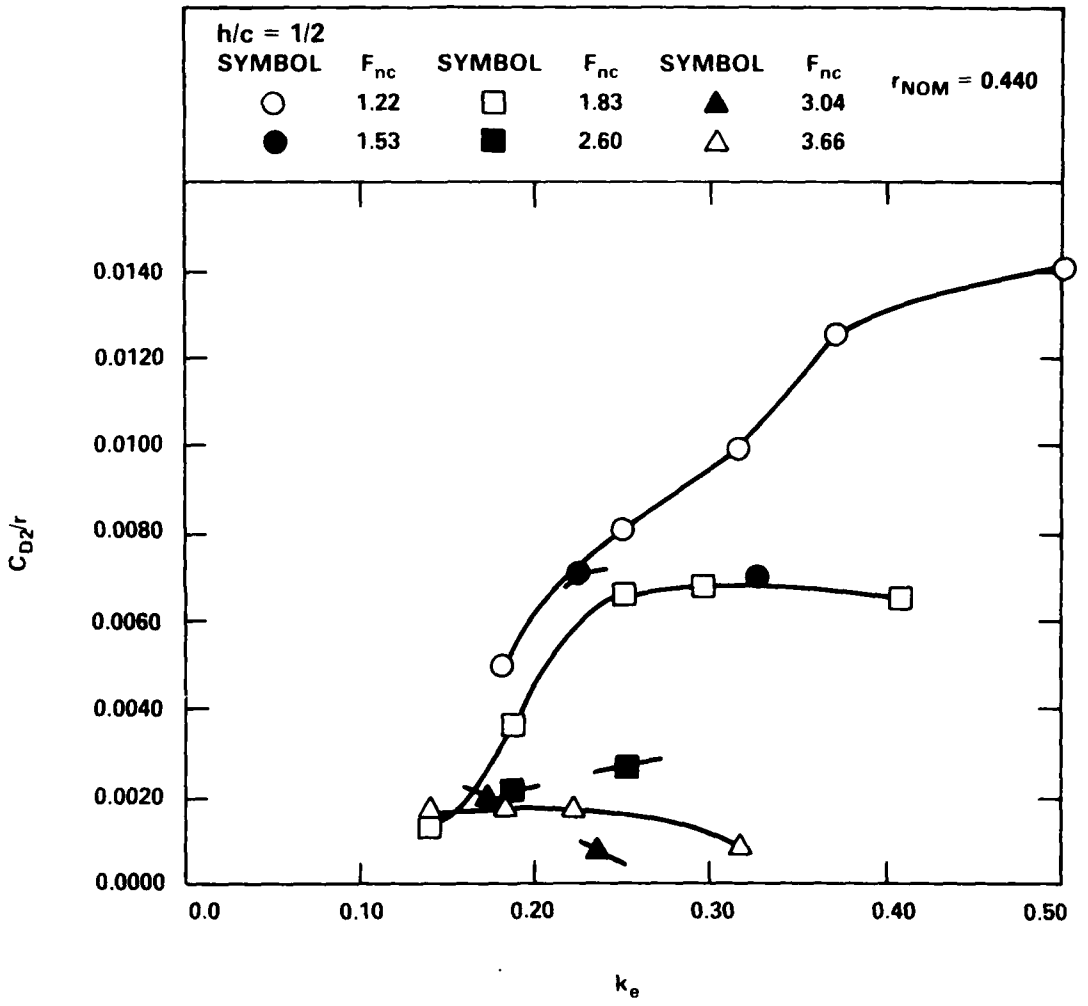

Figure 7A - Second Harmonic Drag Amplitude Response; h/c = 0.5

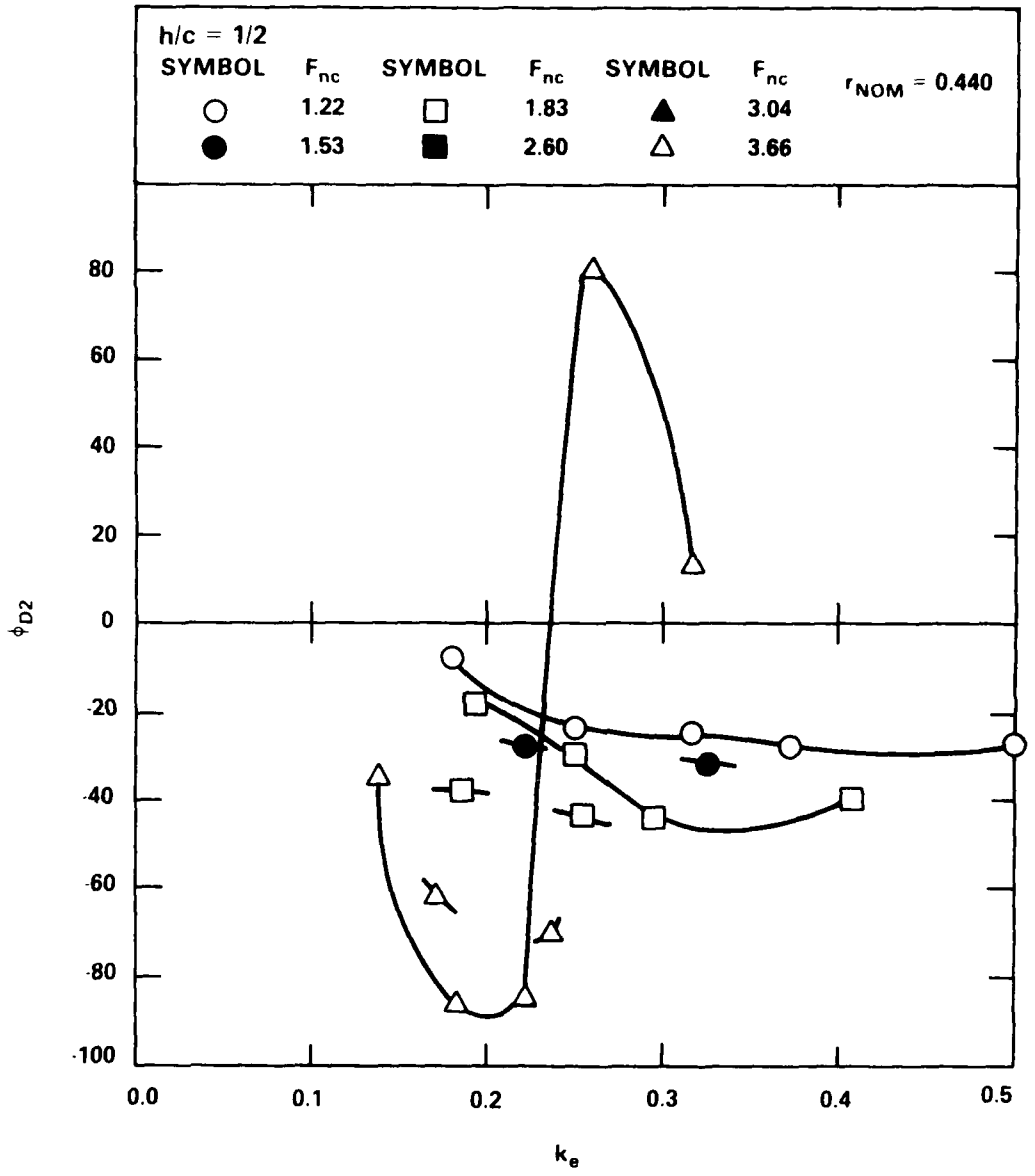

Figure 7B - Second Harmonic Drag Phase Response; h/c = 0.5

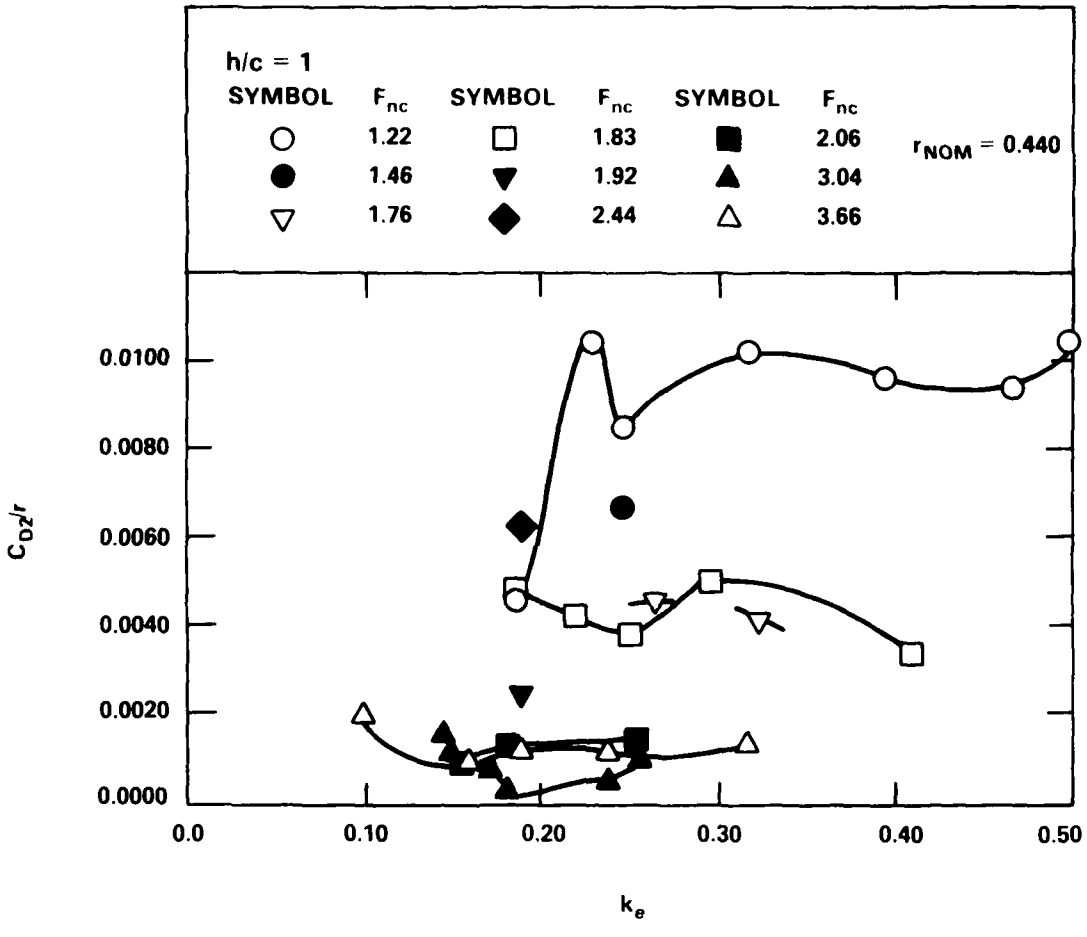

Figure 7C - Second Harmonic Drag Amplitude Response; h/c = 1.0

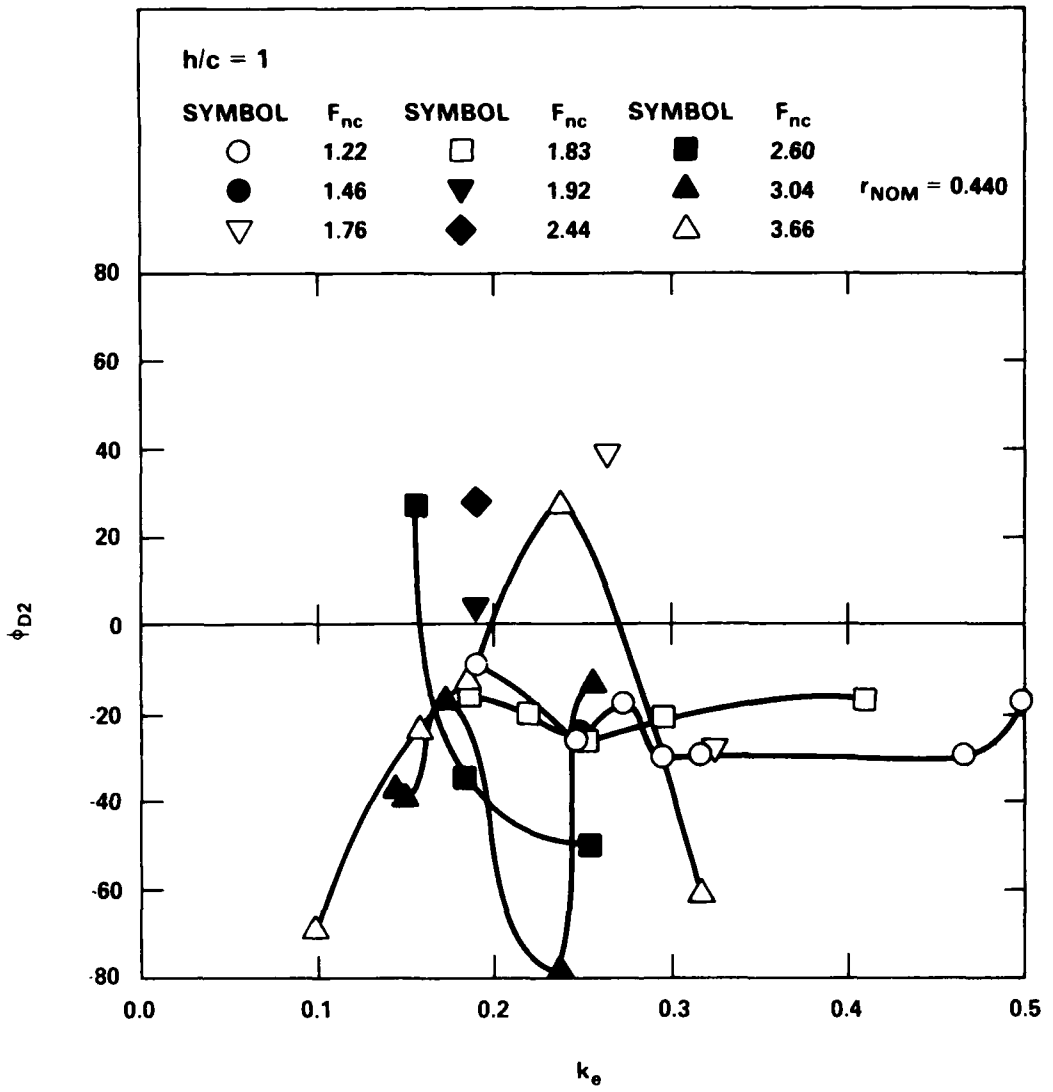

Figure 7D - Second Harmonic Drag Phase Response; h/c = 1.0

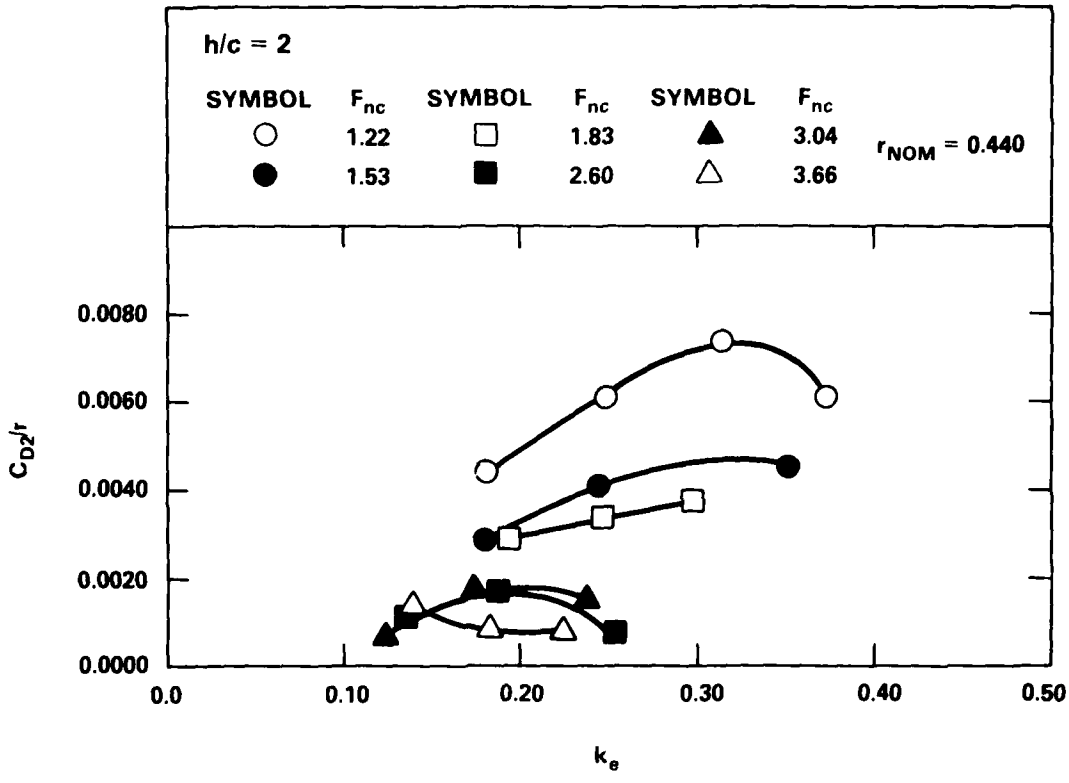

Figure 7E - Second Harmonic Drag Amplitude Response; h/c = 2.0

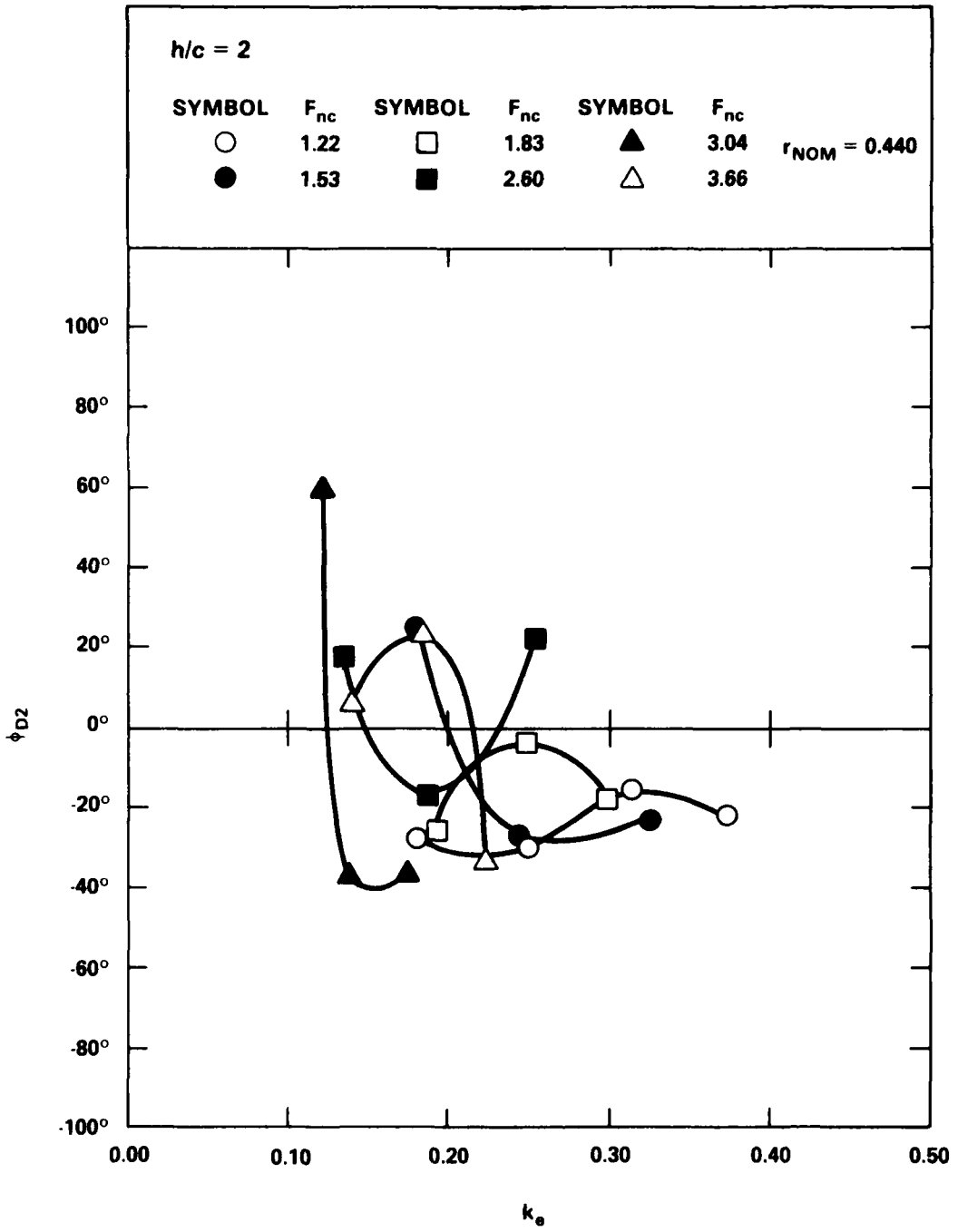

Figure 7F - Second Harmonic Drag Phase Response; h/c = 2.0

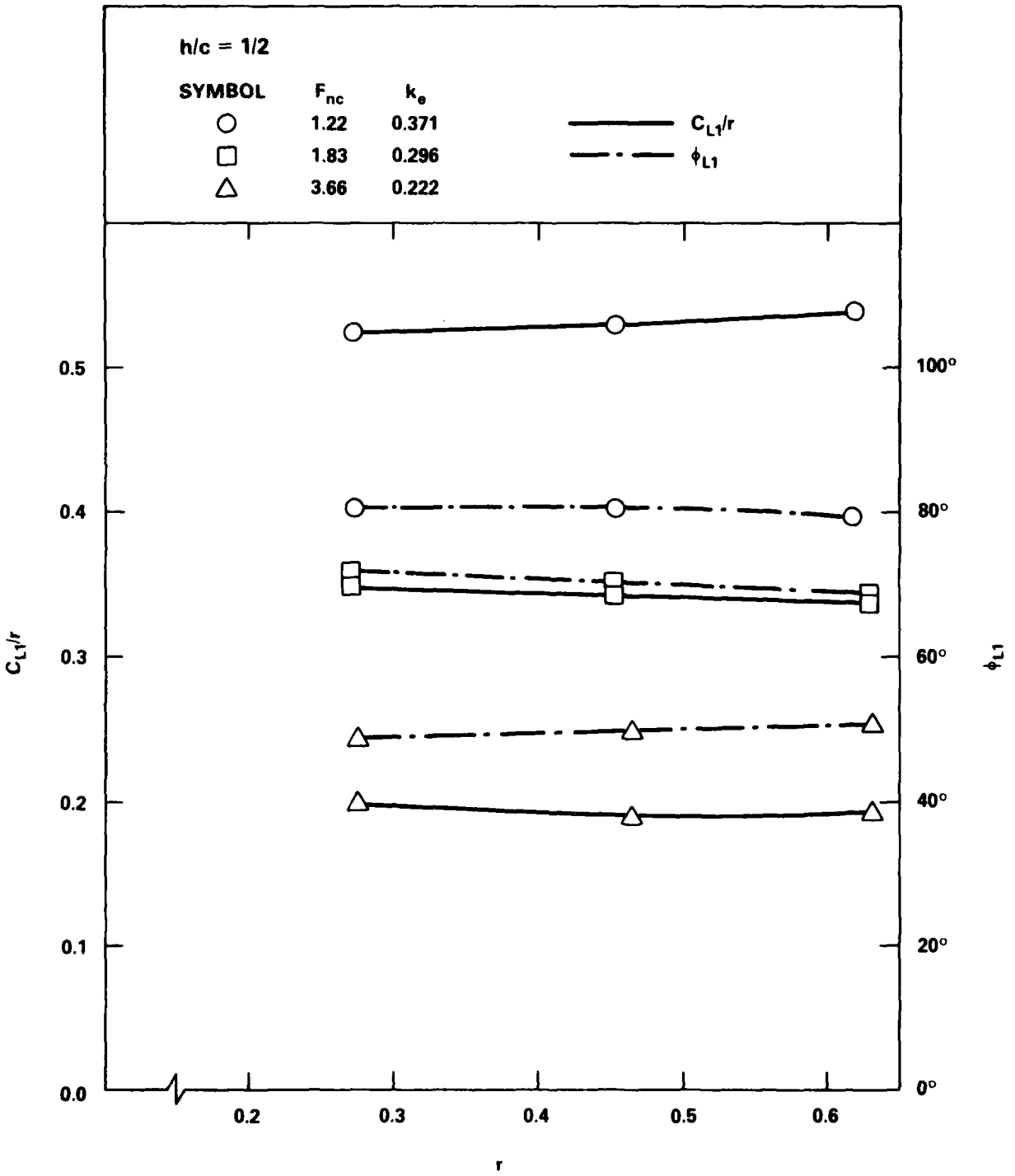

Figure 8A - Fundamental Frequency Lift Response Linearity; h/c = 0.5

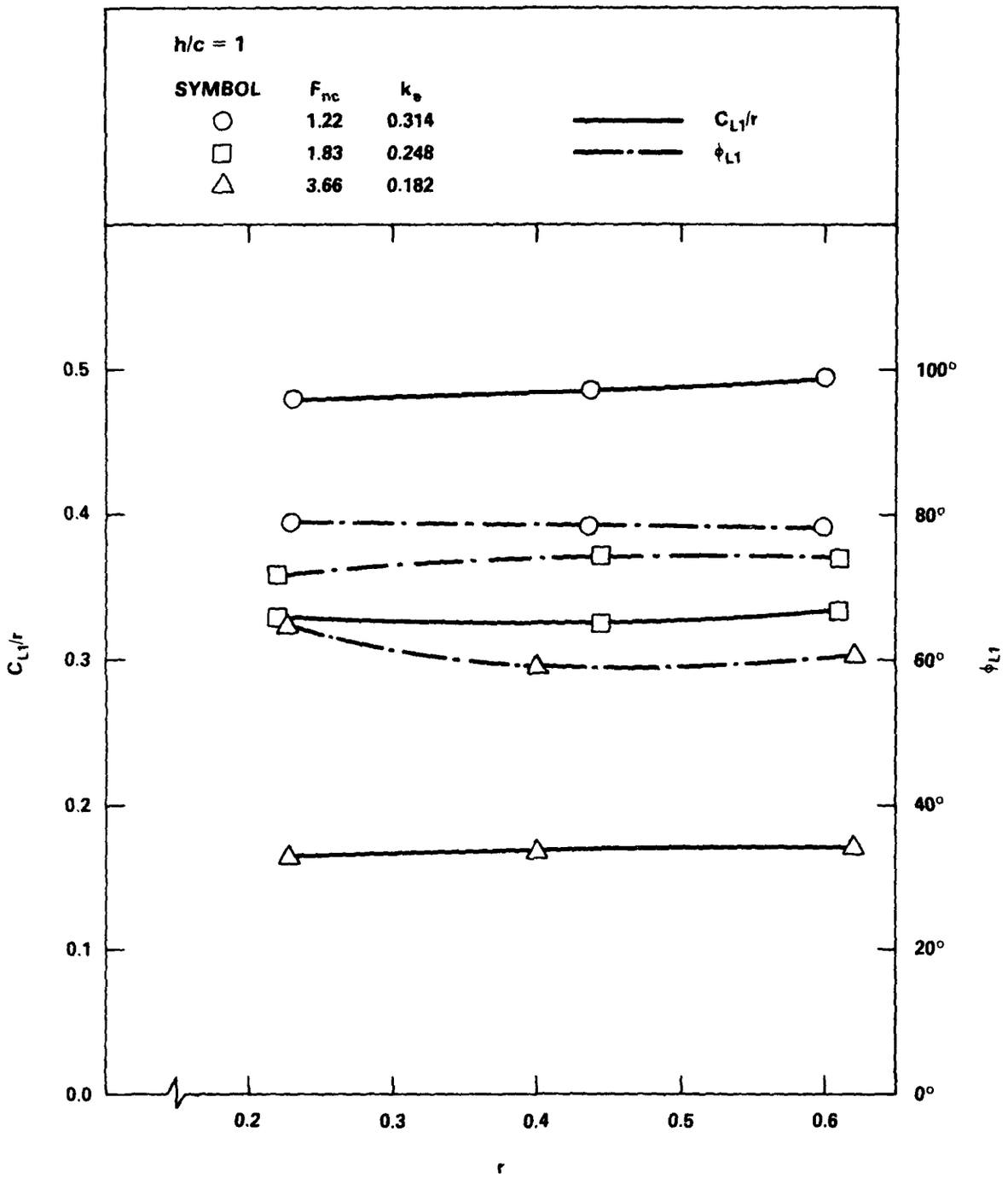

Figure 8B - Fundamental Frequency Lift Response Linearity; h/c = 1.0

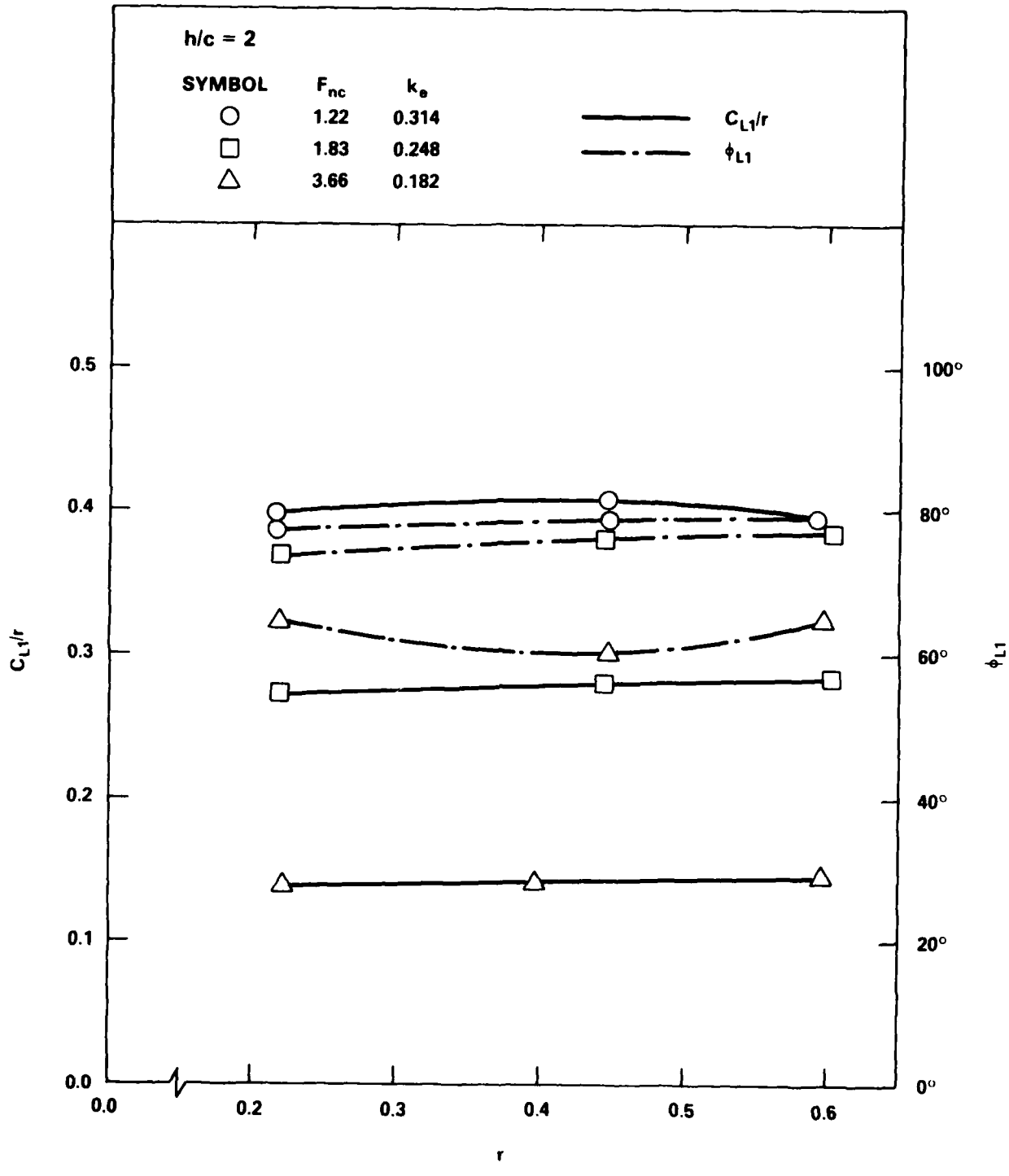

Figure 8C - Fundamental Frequency Lift Response Linearity; h/c = 2.0

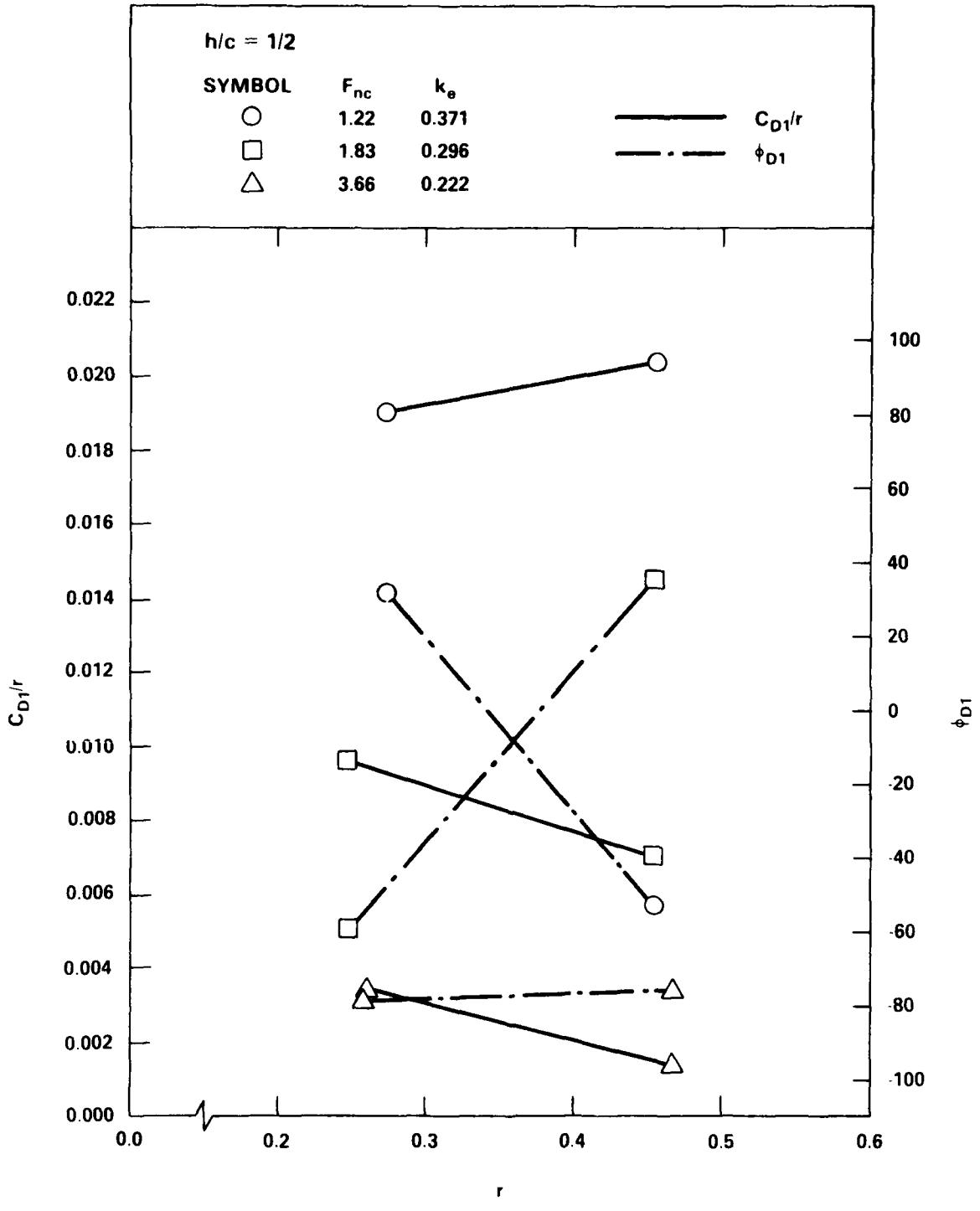

Figure 9A - Fundamental Frequency Drag Response Linearity; h/c = 0.5

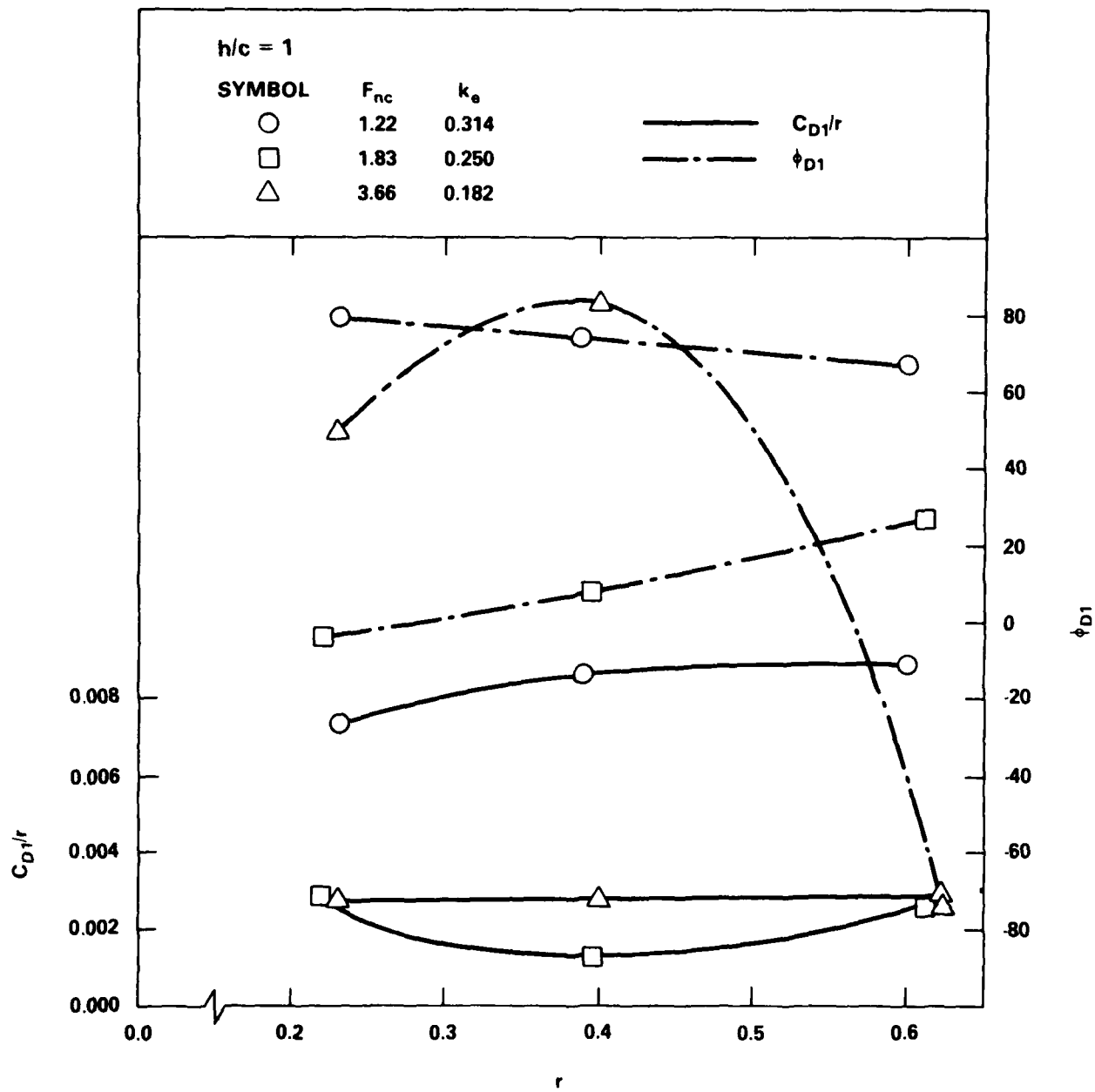

Figure 9B - Fundamental Frequency Drag Response Linearity; h/c = 1.0

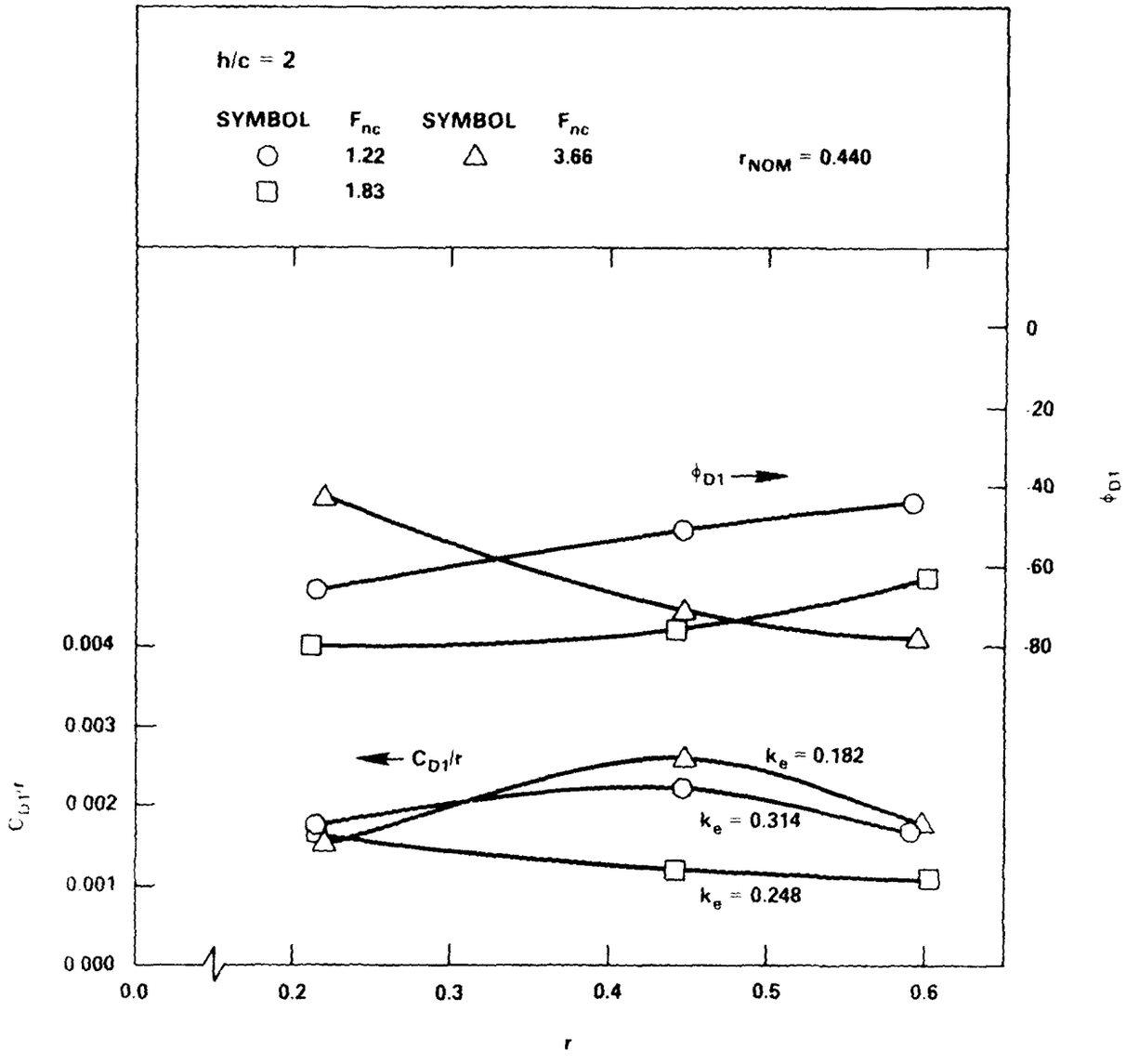

Figure 9C - Fundamental Frequency Drag Response Linearity; h/c = 2.0

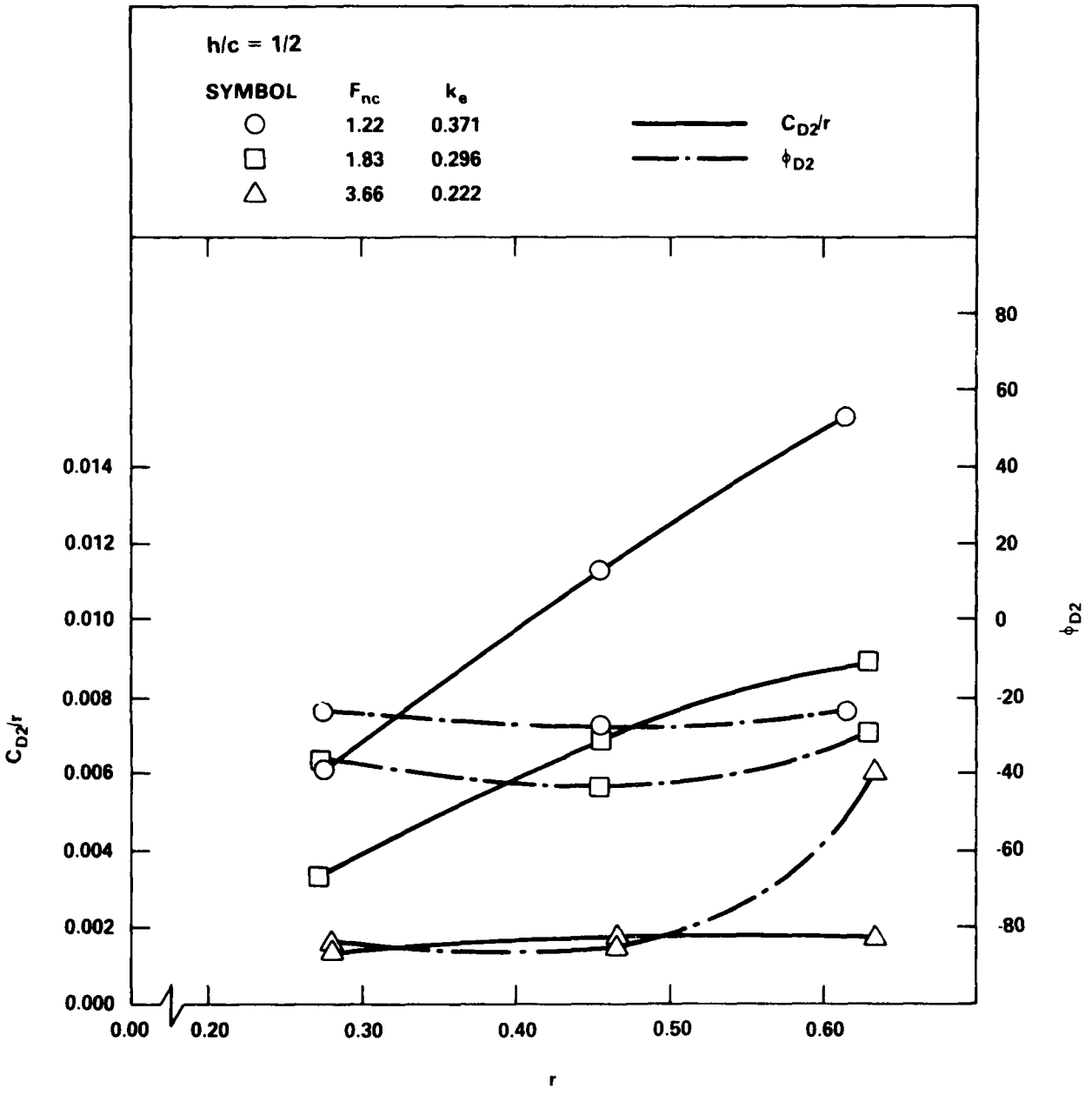

Figure 10A - Second Harmonic Drag Response Linearity; h/c = 0.5

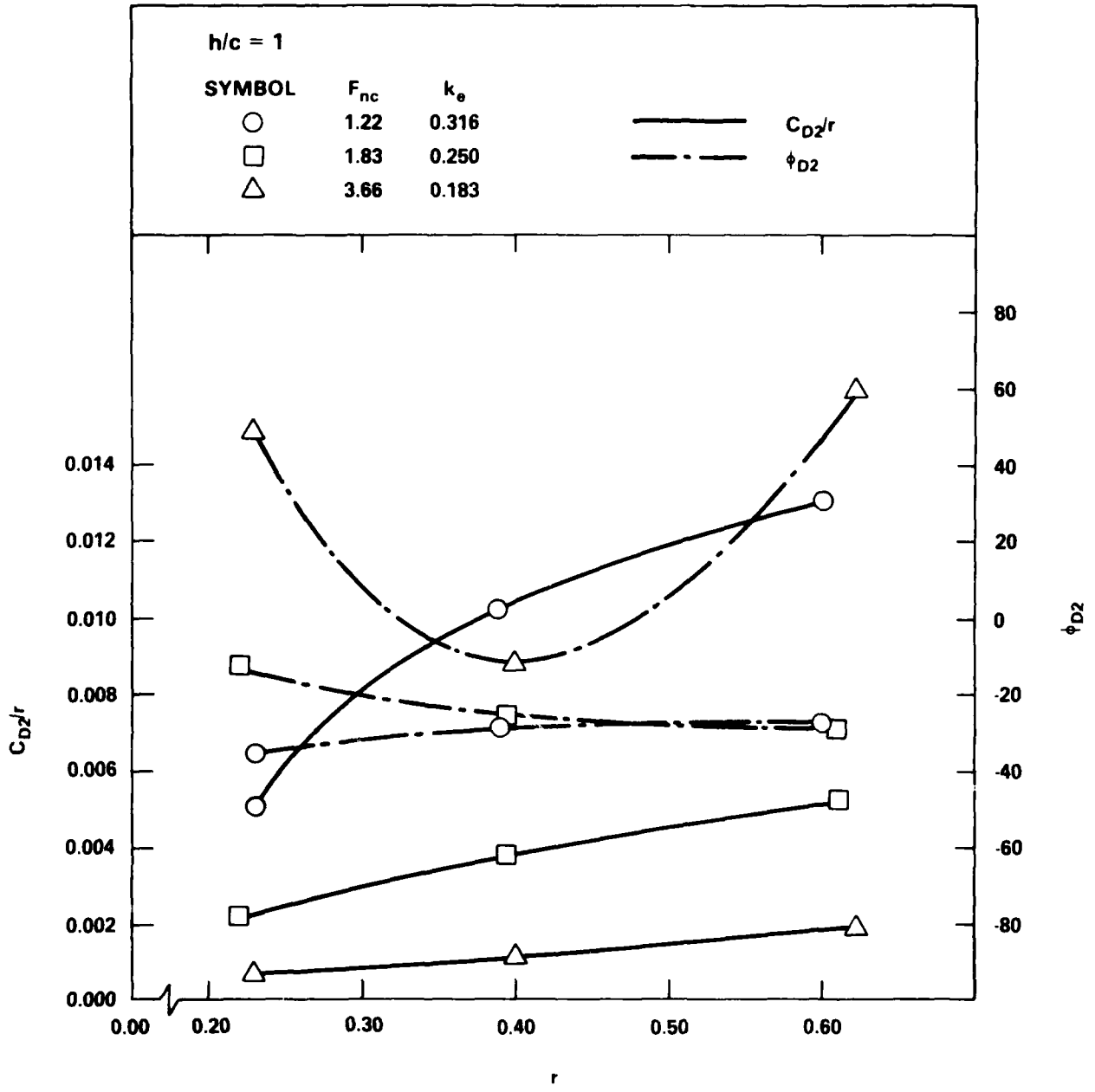

Figure 10B - Second Harmonic Drag Response Linearity; h/c = 1.0

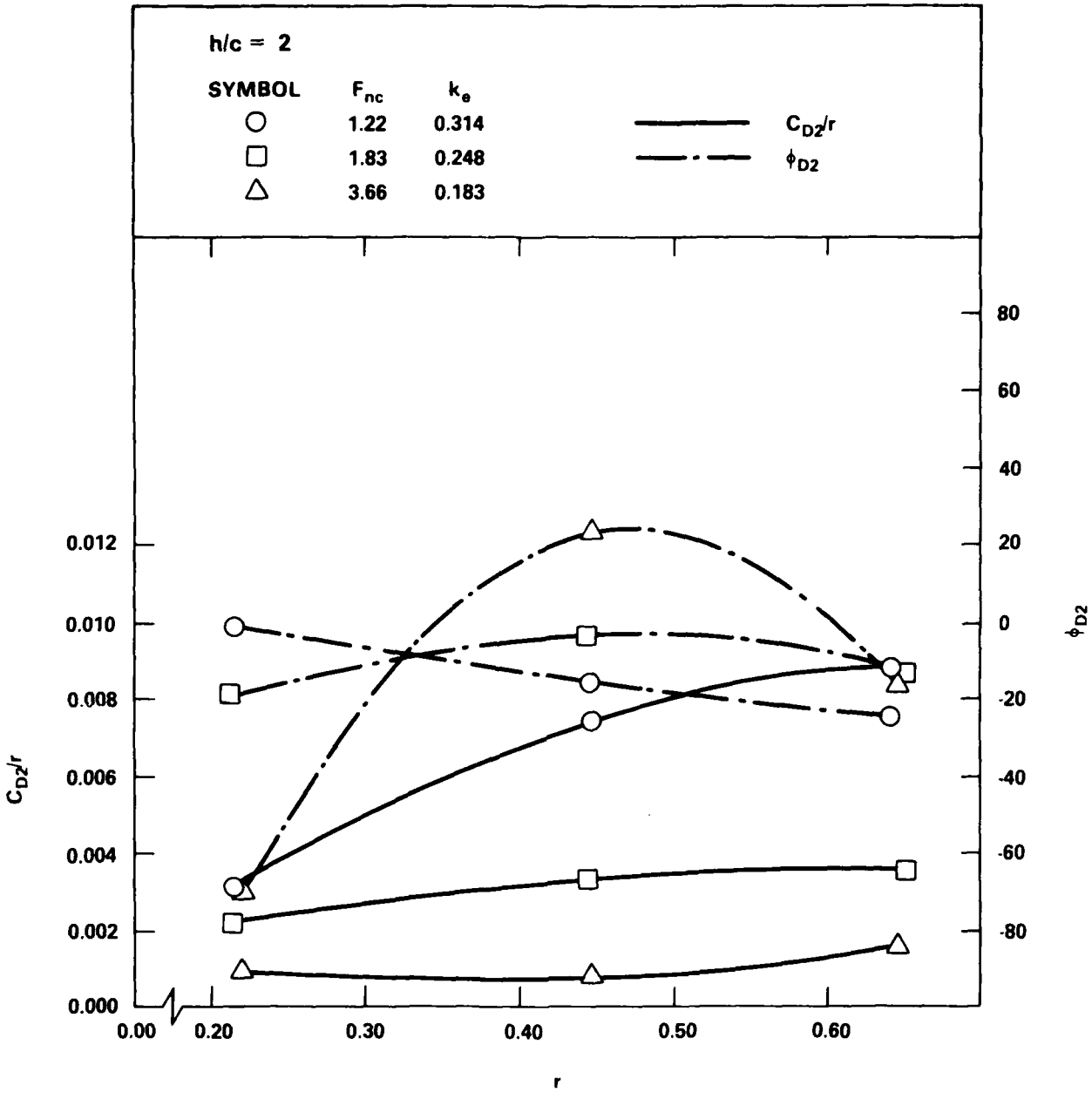

Figure 10C - Second Harmonic Drag Response Linearity; h/c = 2.0

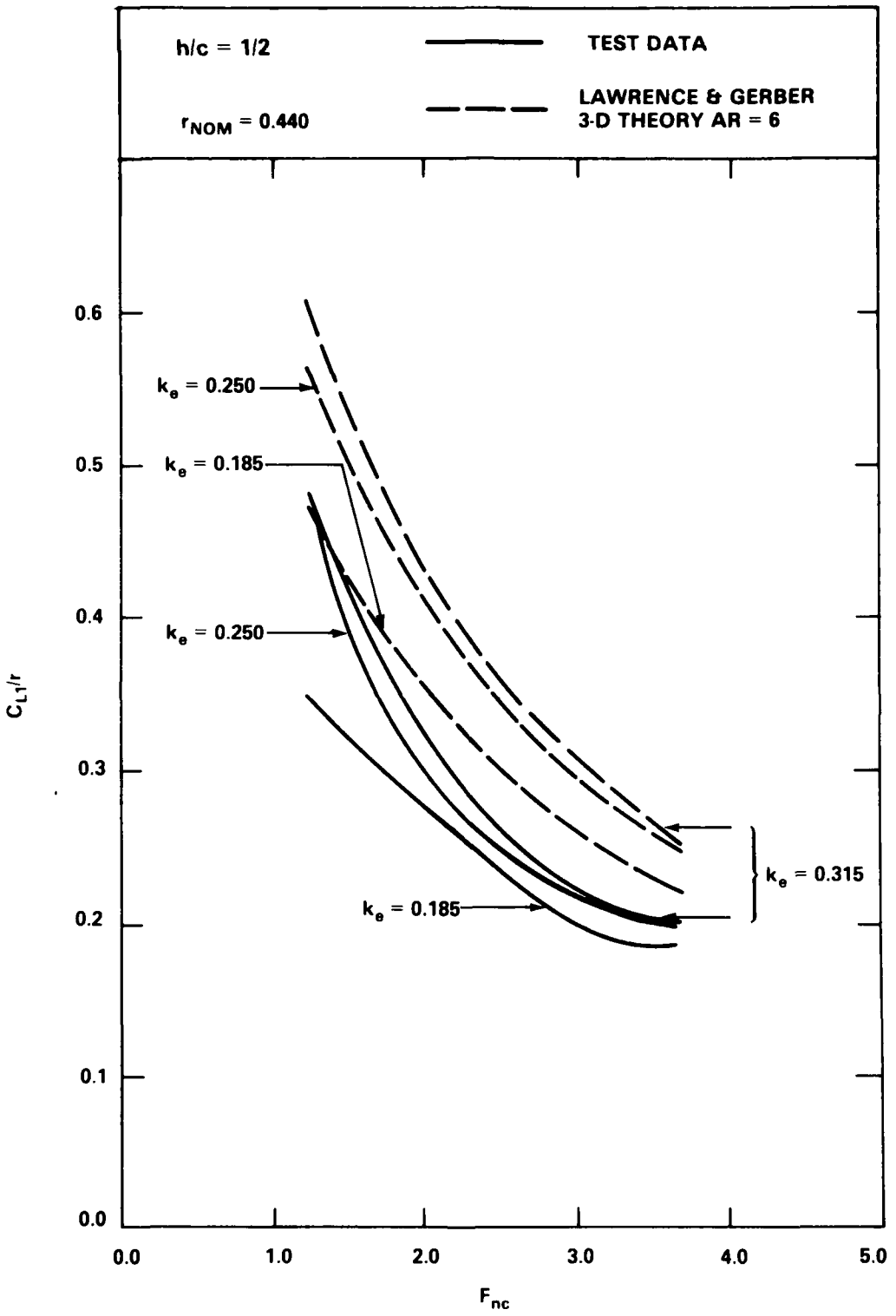

Figure 11A - C_{L1}/r vs F_{nc}; k_e = Constant; h/c = 0.5

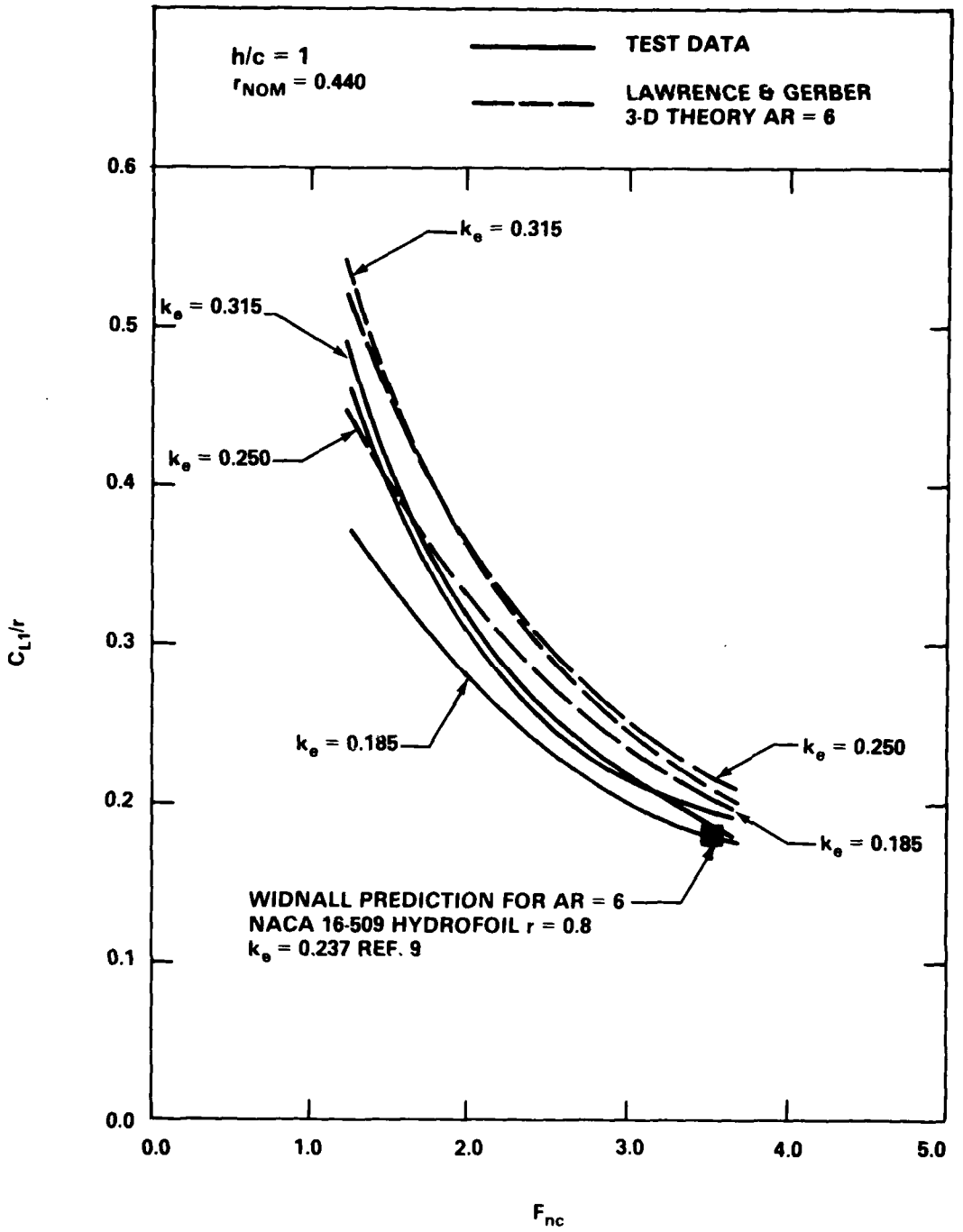

Figure 11B - C_{L1}/r vs F_{nc}; k_e = Constant; h/c = 1.0

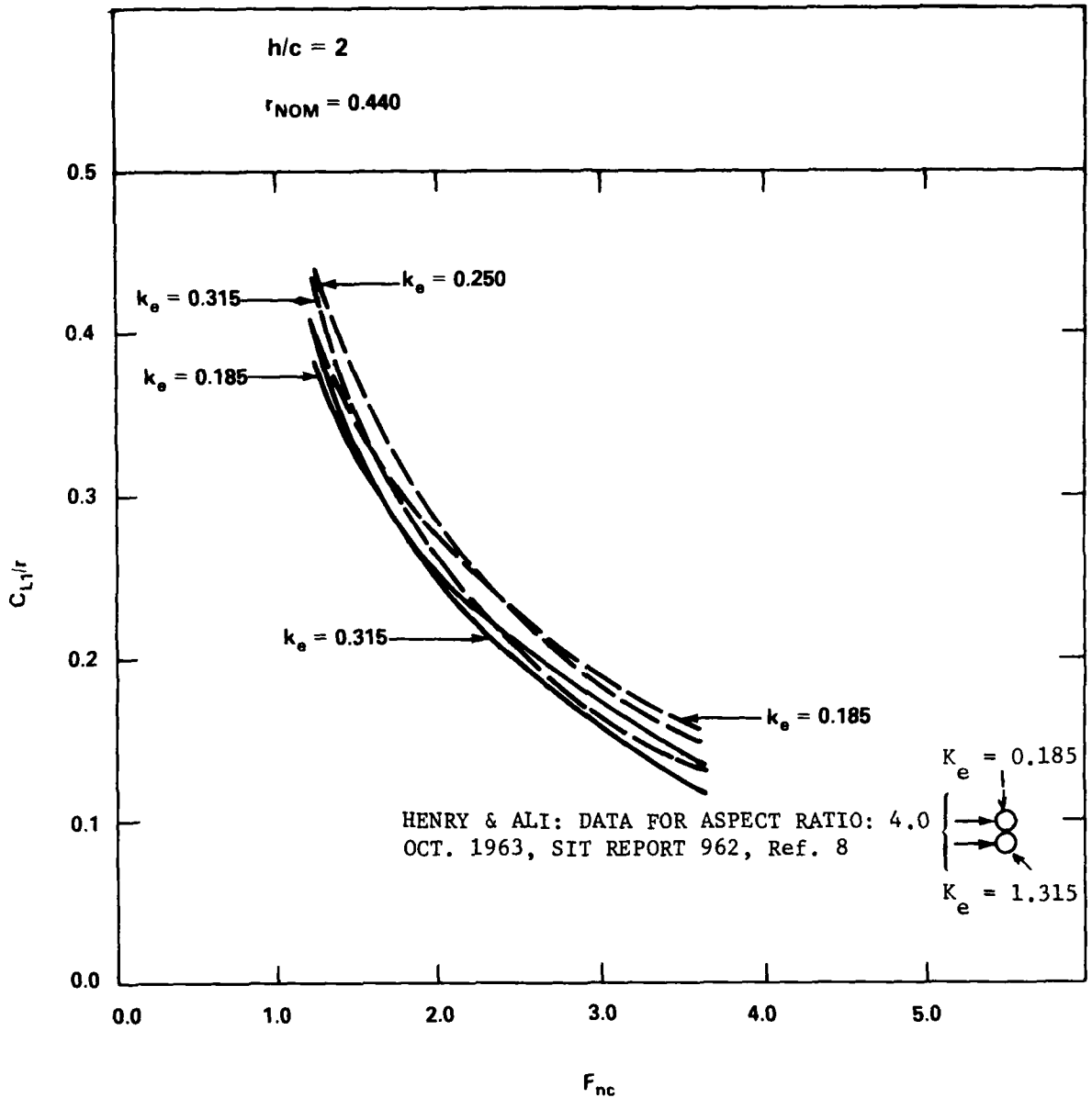

Figure 11C - C_{L1}/r vs F_{nc}; k_e = Constant; h/c = 2.0

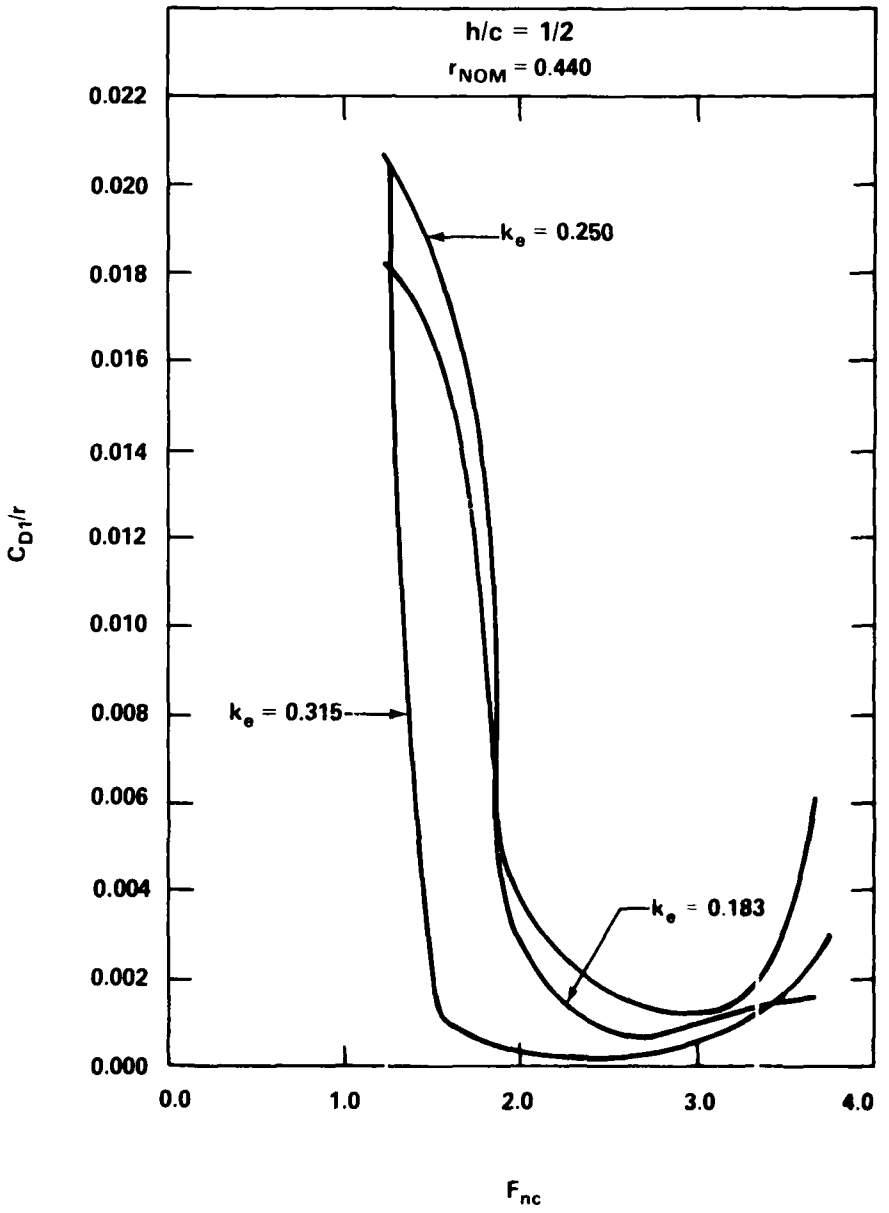

Figure 12A - C_{D1}/r vs F_{nc}; k_e = Constant; h/c = 0.5

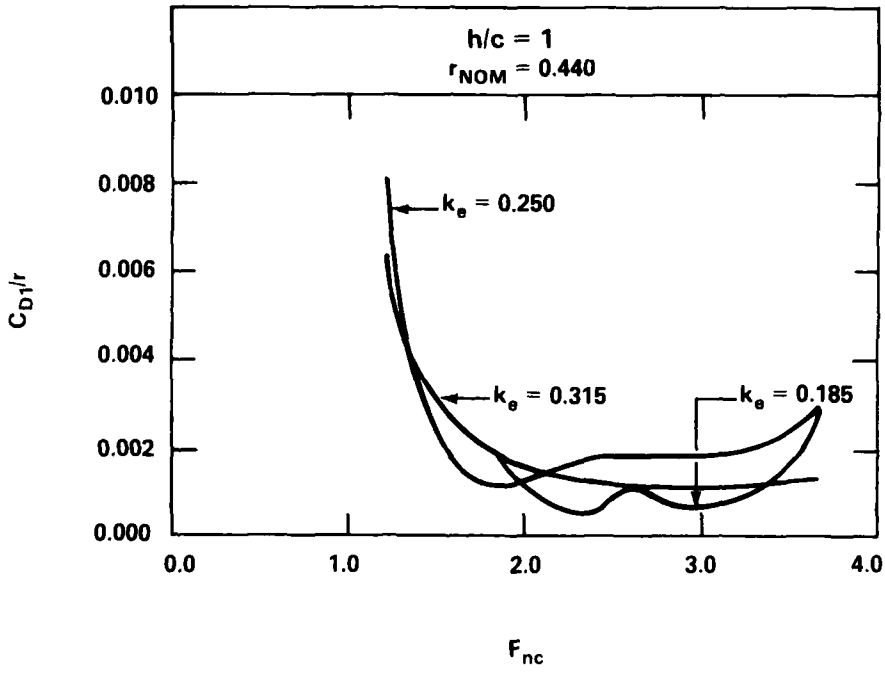

Figure 12B - C_{D1}/r vs F_{nc}; k_e = Constant; h/c = 1.0

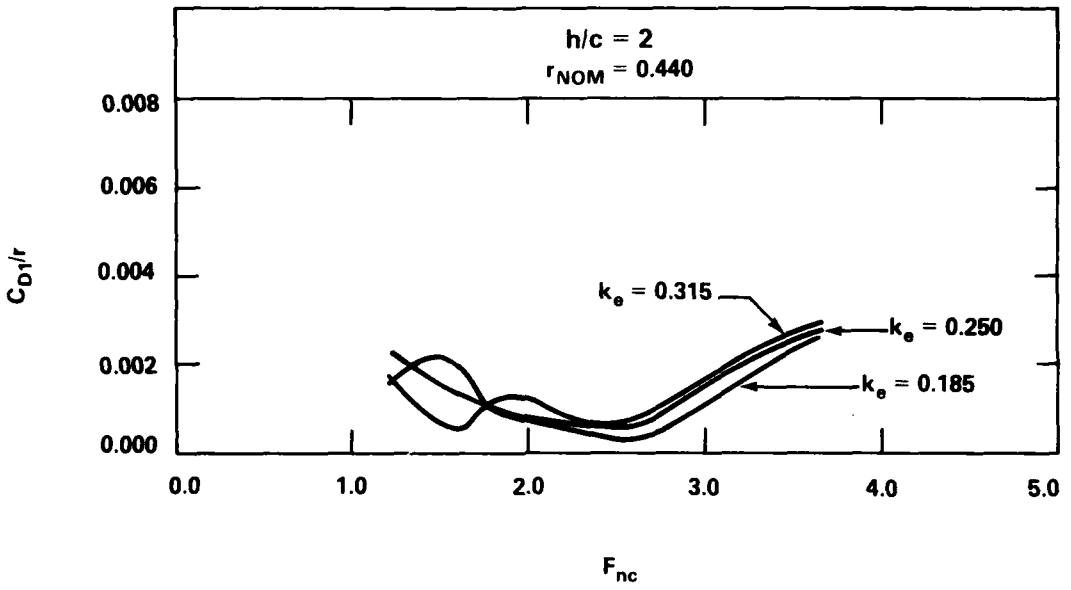

Figure 12C - C_{D1}/r vs F_{nc}; k_e = Constant; h/c = 2.0

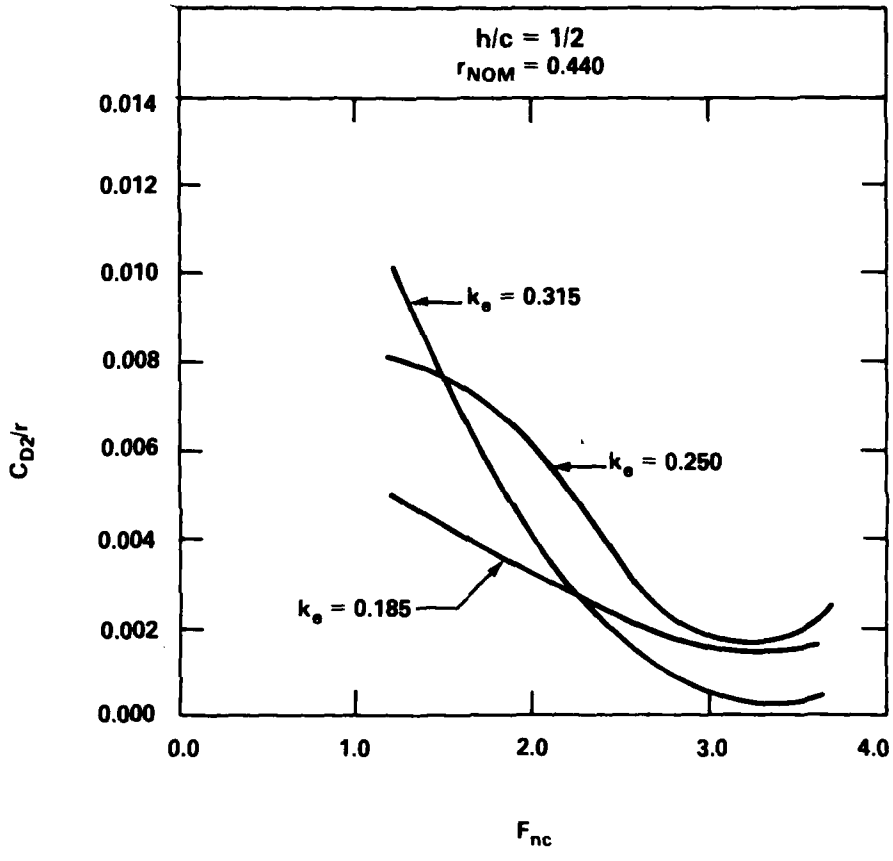

Figure 13A - C_{D2}/r vs F_{nc}; k_e = Constant; h/c = 0.5

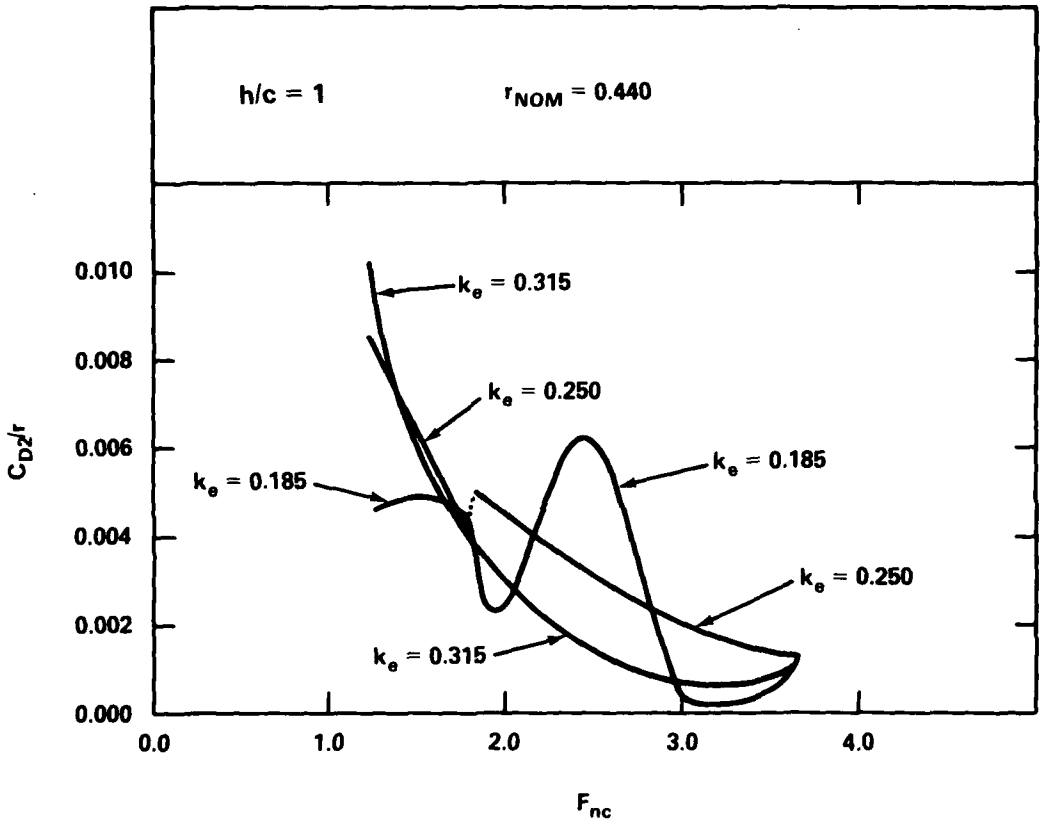

Figure 13B - C_{D2}/r vs F_{nc}; k_e = Constant; h/c = 1.0

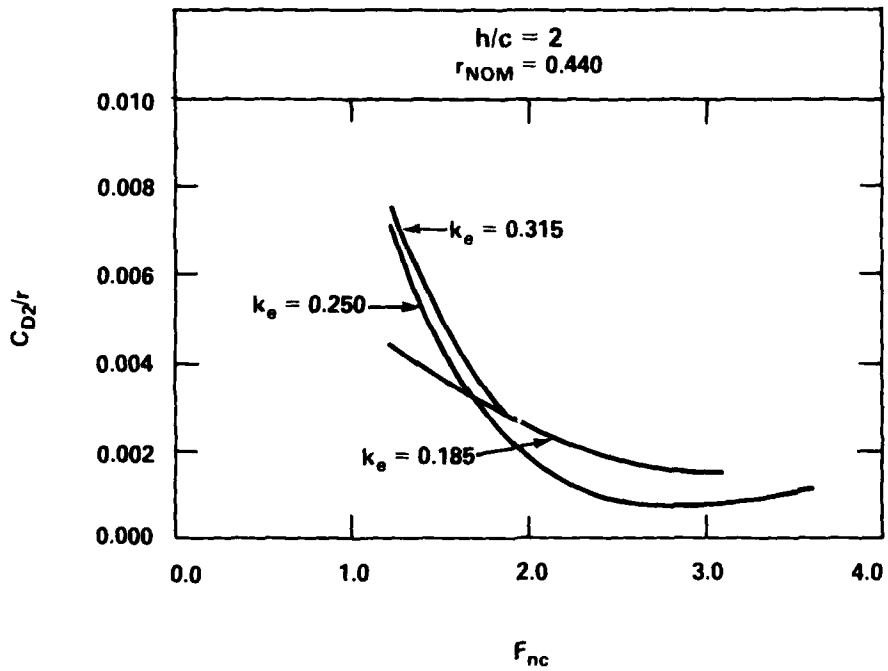

Figure 13C - C_{D2}/r vs F_{nc}; k_e = Constant; h/c = 2.0

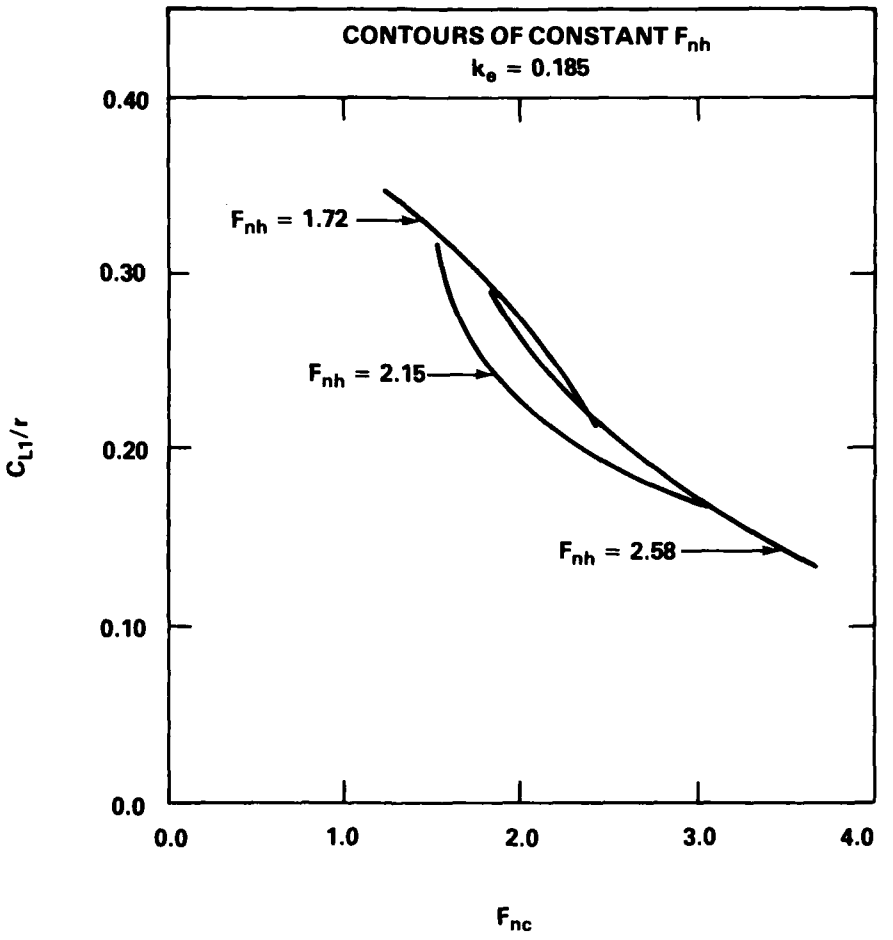

Figure 14A - C_{L1}/r vs F_{nc}; F_{nh} = Constant; k_e = 0.185

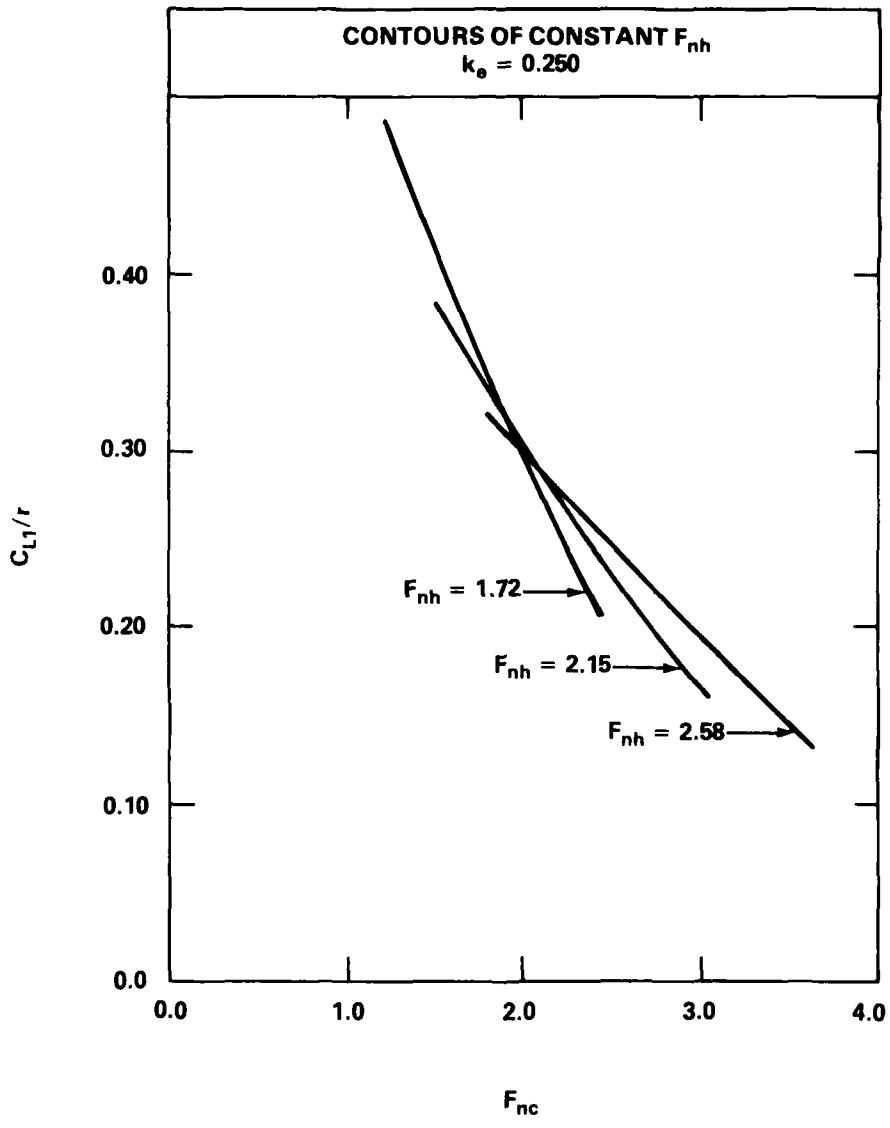

Figure 14B - C_{L1}/r vs F_{nc}; F_{nh} = Constant; k_e = 0.250

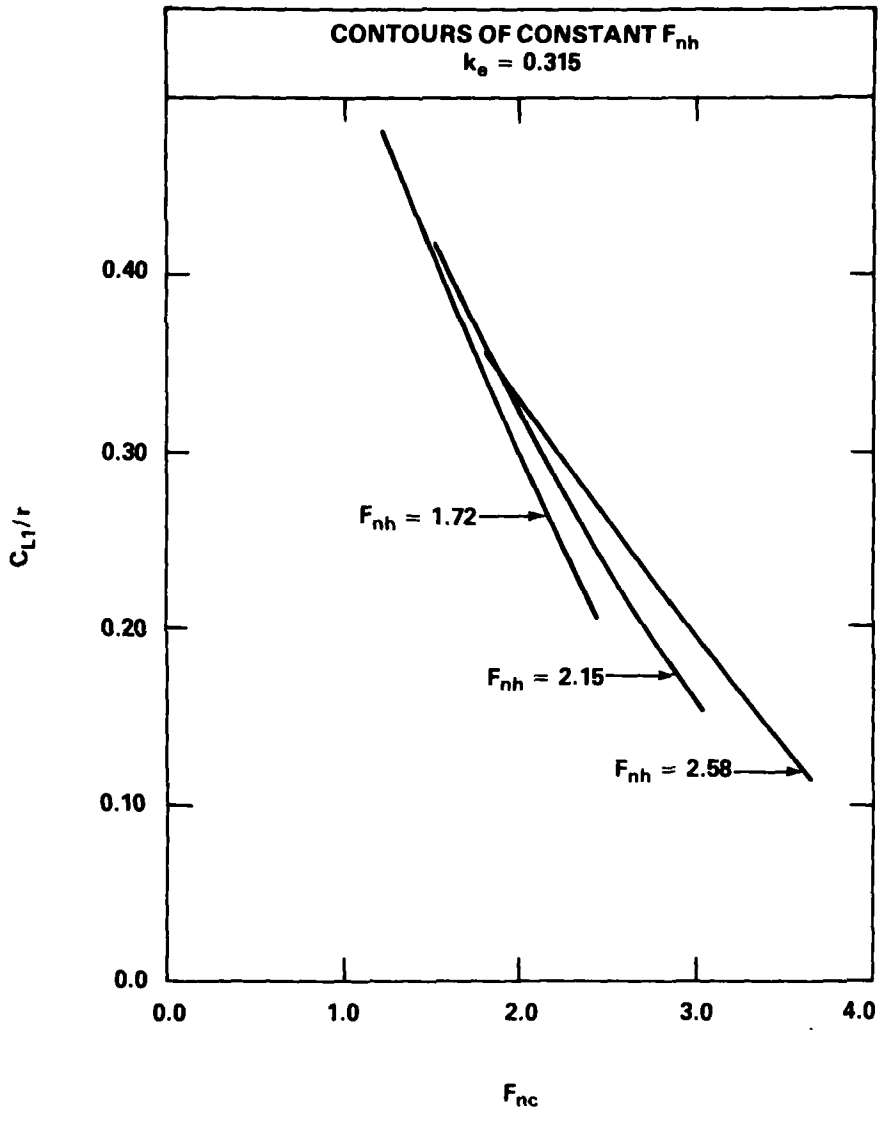

Figure 14C - C_{L1}/r vs F_{nc}; F_{nh} = Constant; k_e = 0.315

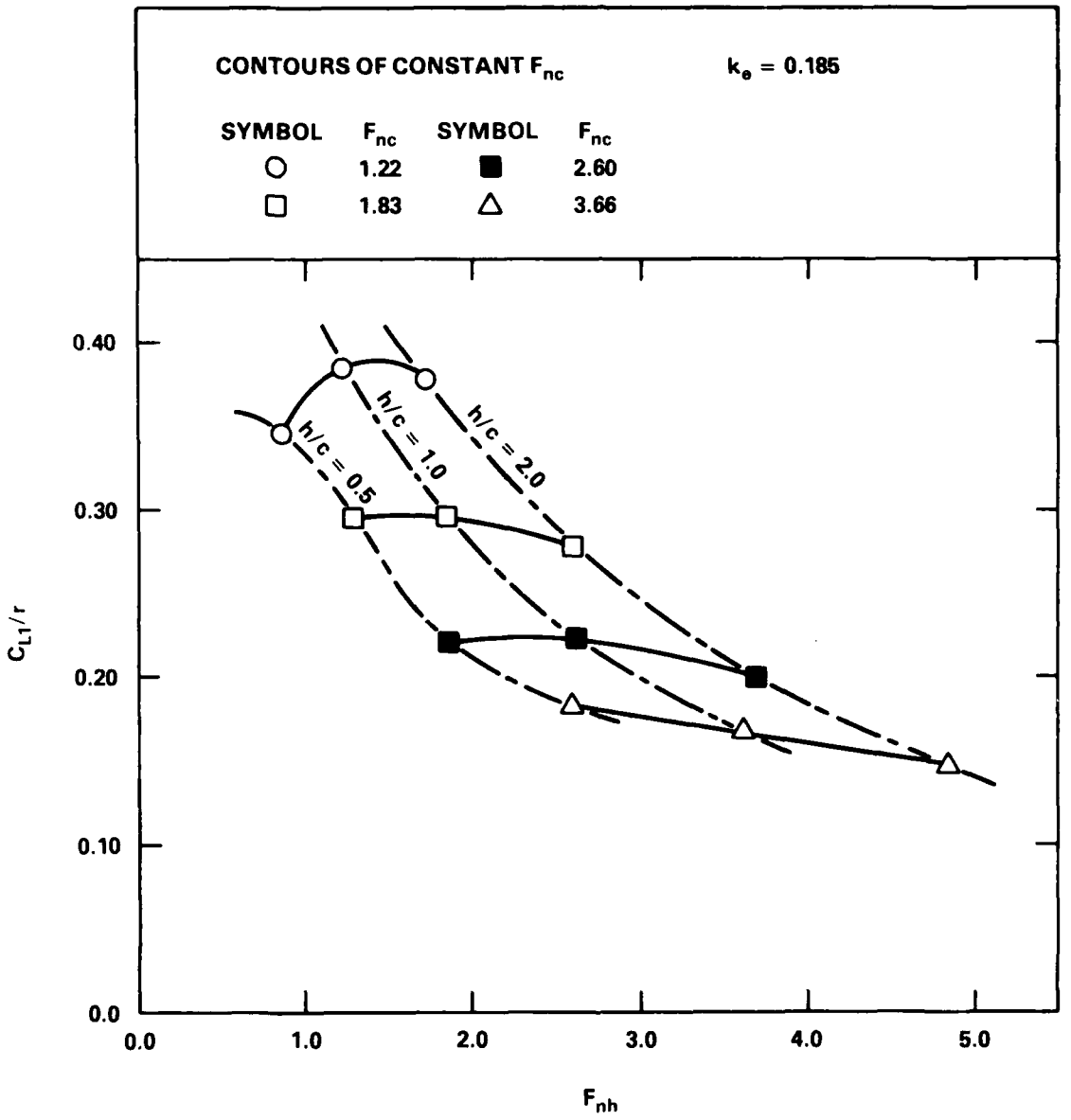

Figure 15A - C_{L1}/r vs F_{nh}; F_{nc} = Constant; k_e = 0.185

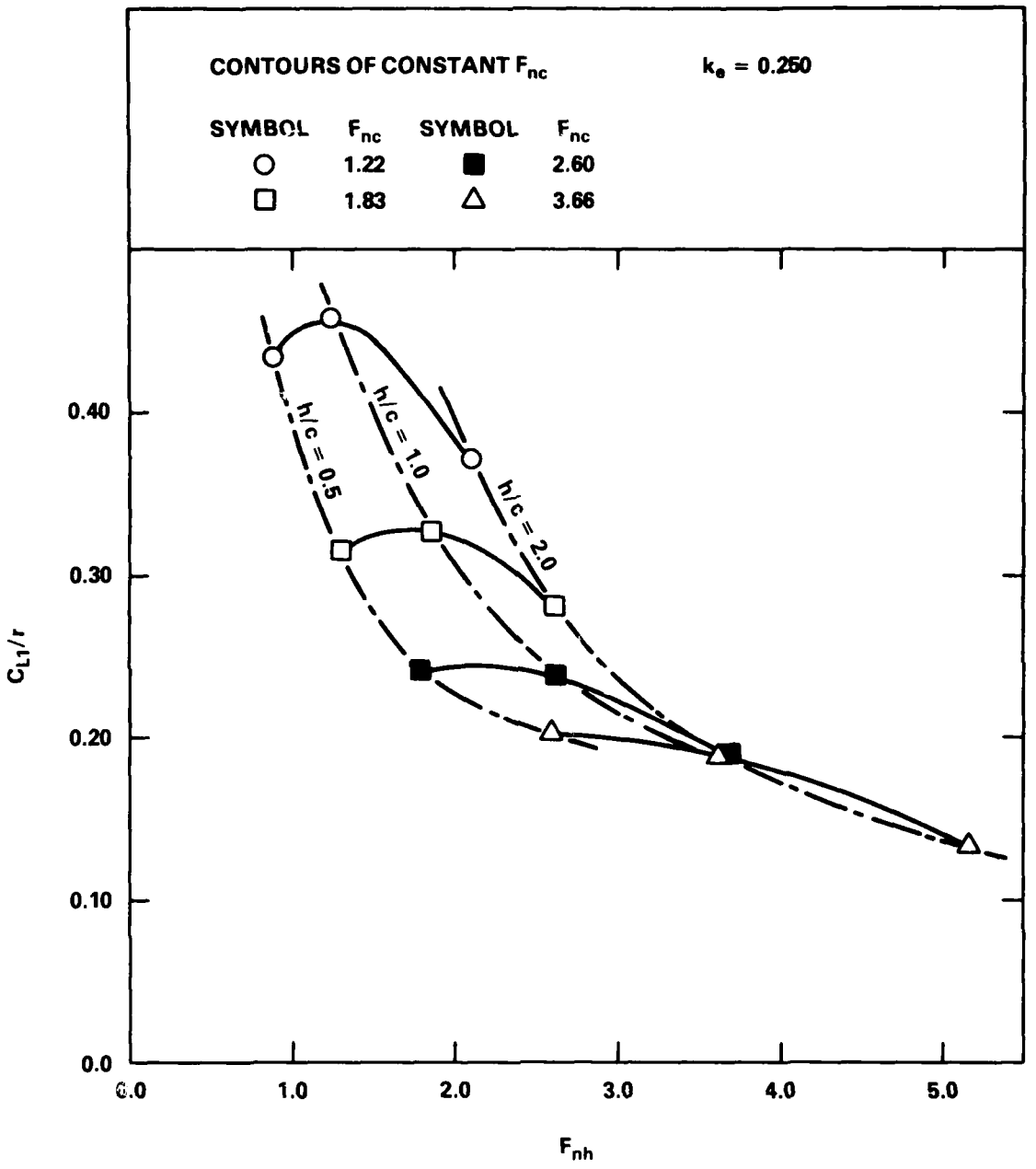

Figure 15B - C_{L1}/r vs F_{nh}; F_{nc} = Constant; k_e = 0.250

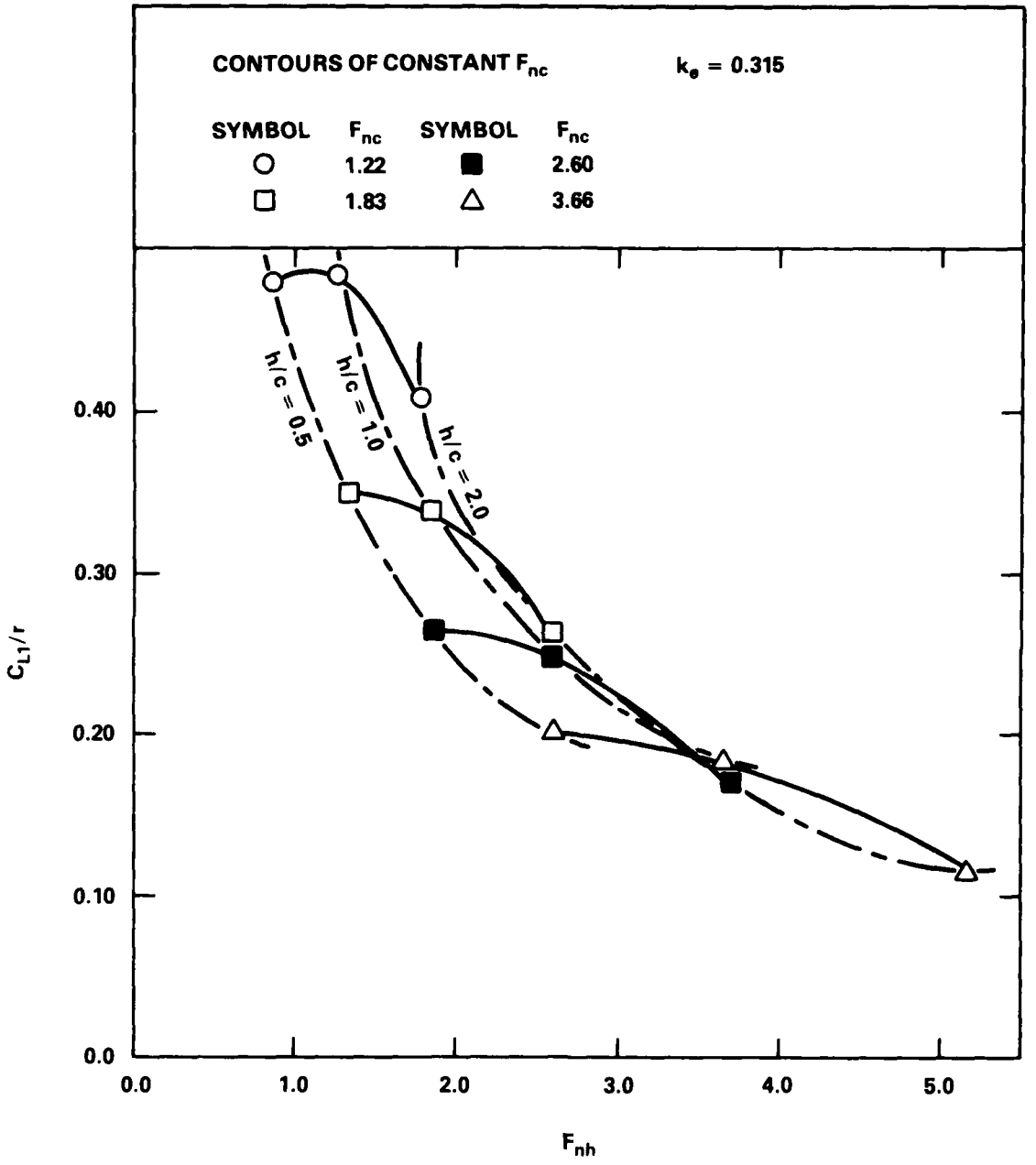

Figure 15C - C_{L1}/r vs F_{nh}; F_{nc} = Constant; k_e = 0.315

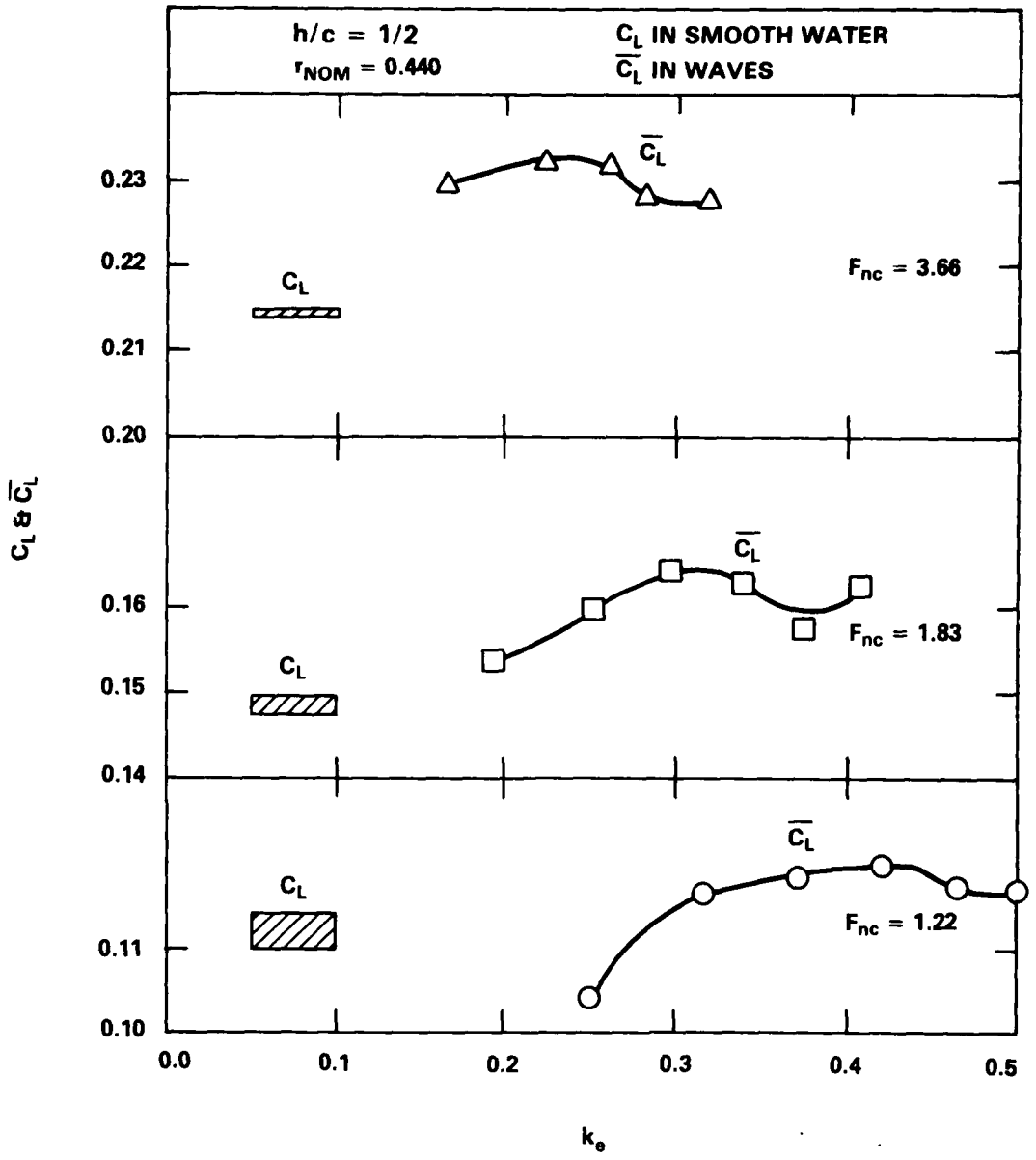

Figure 16A - Mean Lift in Waves Compared to Calm Water Lift; h/c = 0.5; F_{nc} = 1.22, 1.83 and 3.66

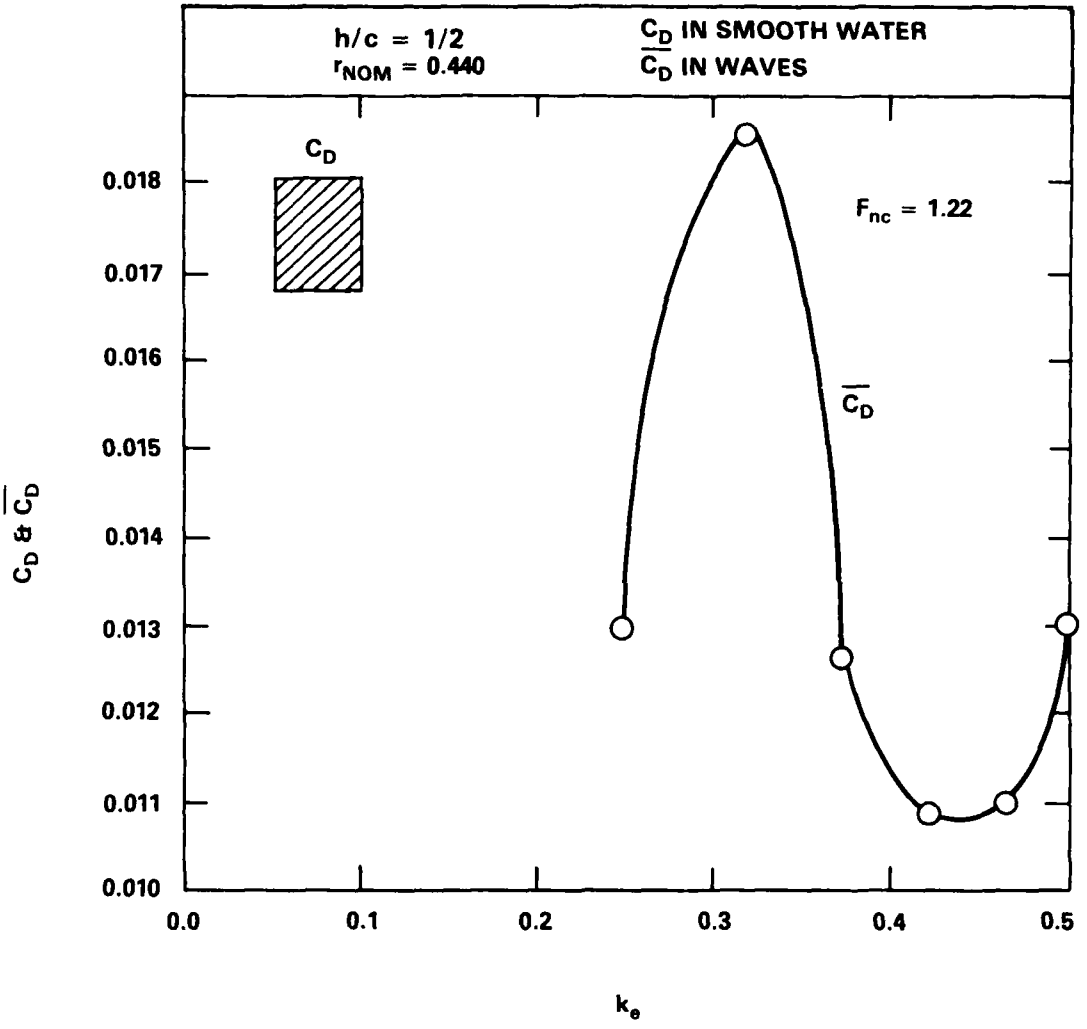

Figure 16B - Mean Drag in Waves Compared to Calm Water Drag; h/c = 0.5; F_{nc} = 1.22

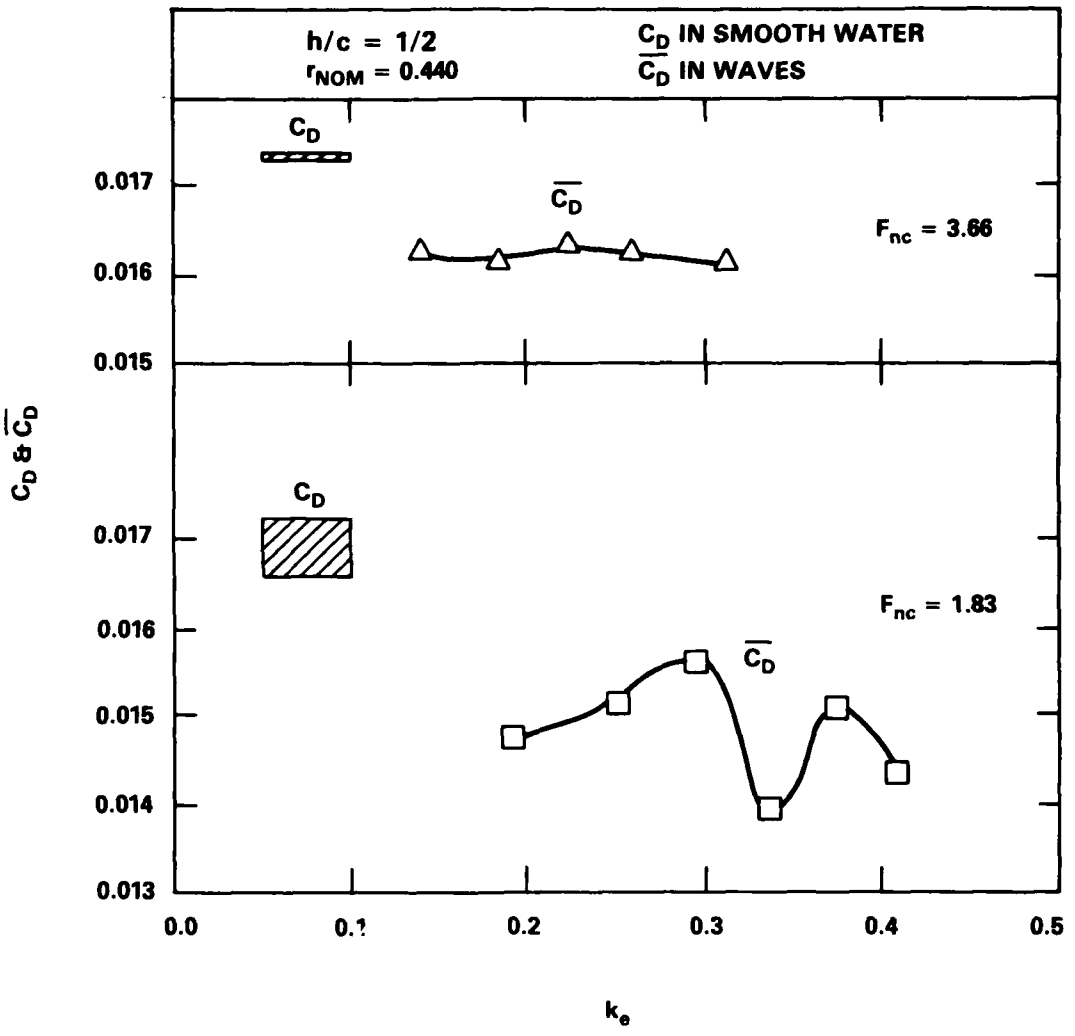

Figure 16C - Mean Drag in Waves Compared to Calm Water Drag; h/c = 0.5; F_{nc} = 1.83 and 3.66

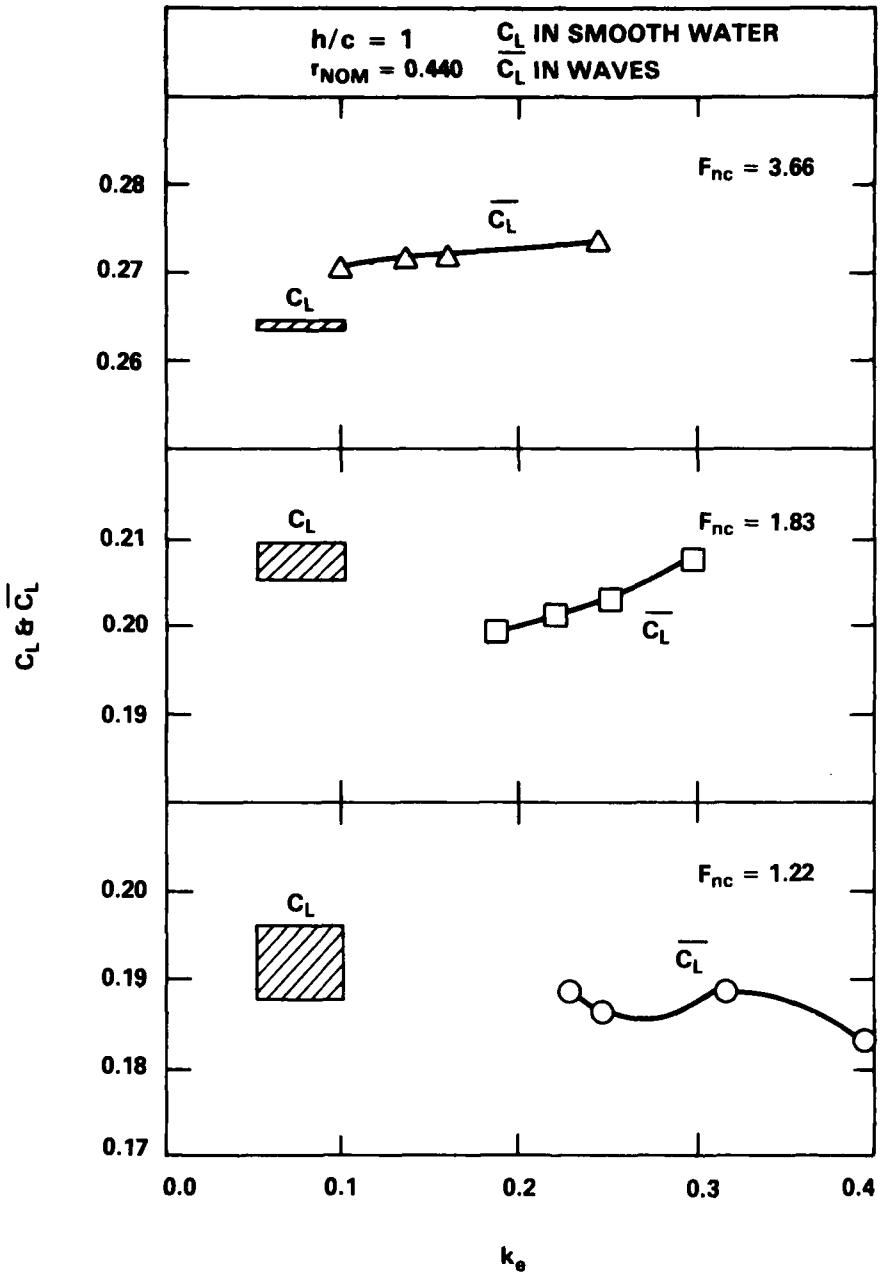

Figure 16D - Mean Lift in Waves Compared to Calm Water Lift; h/c = 1.0

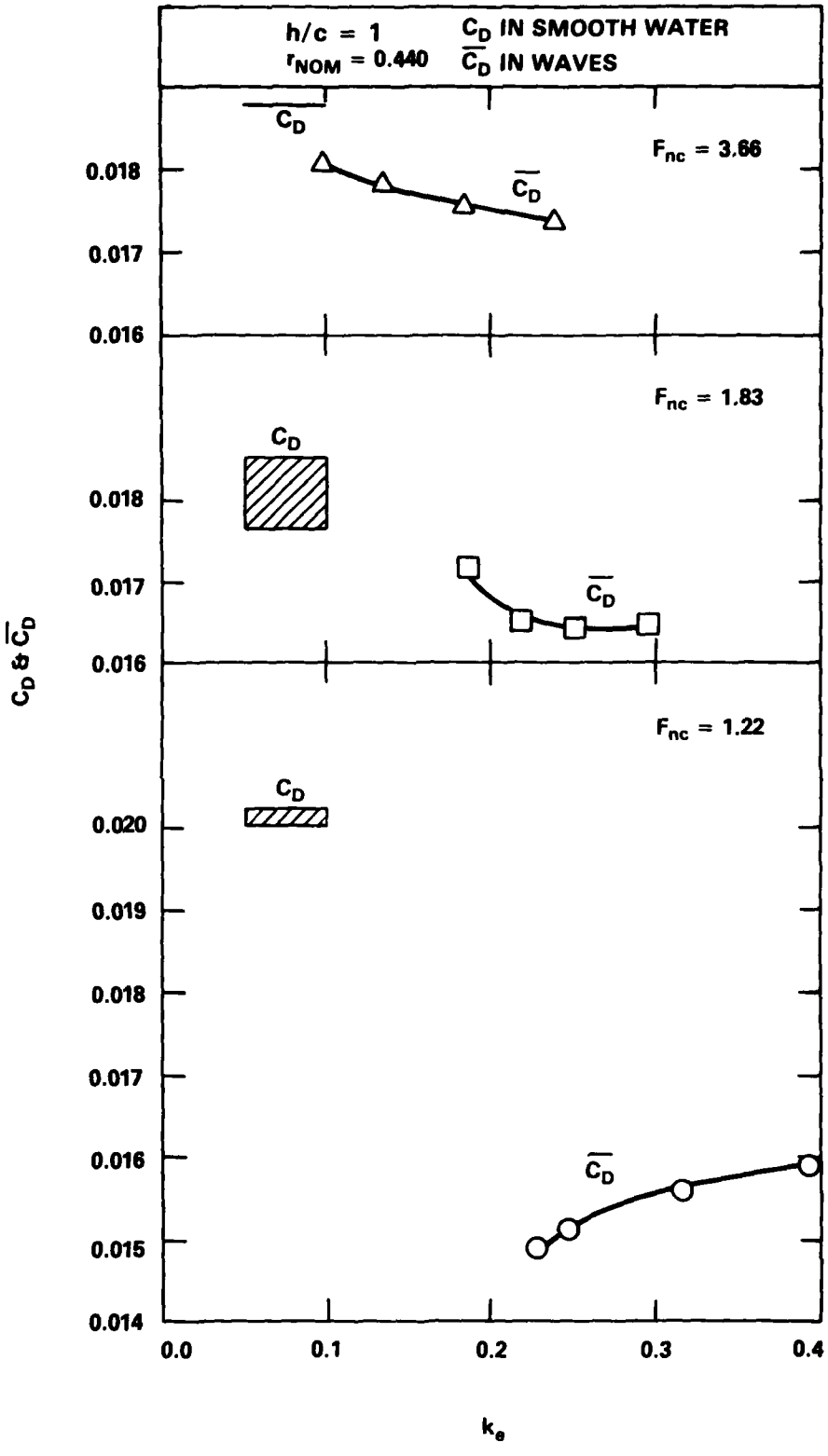

Figure 16E - Mean Drag in Waves Compared to Calm Water Drag; h/c = 1.0

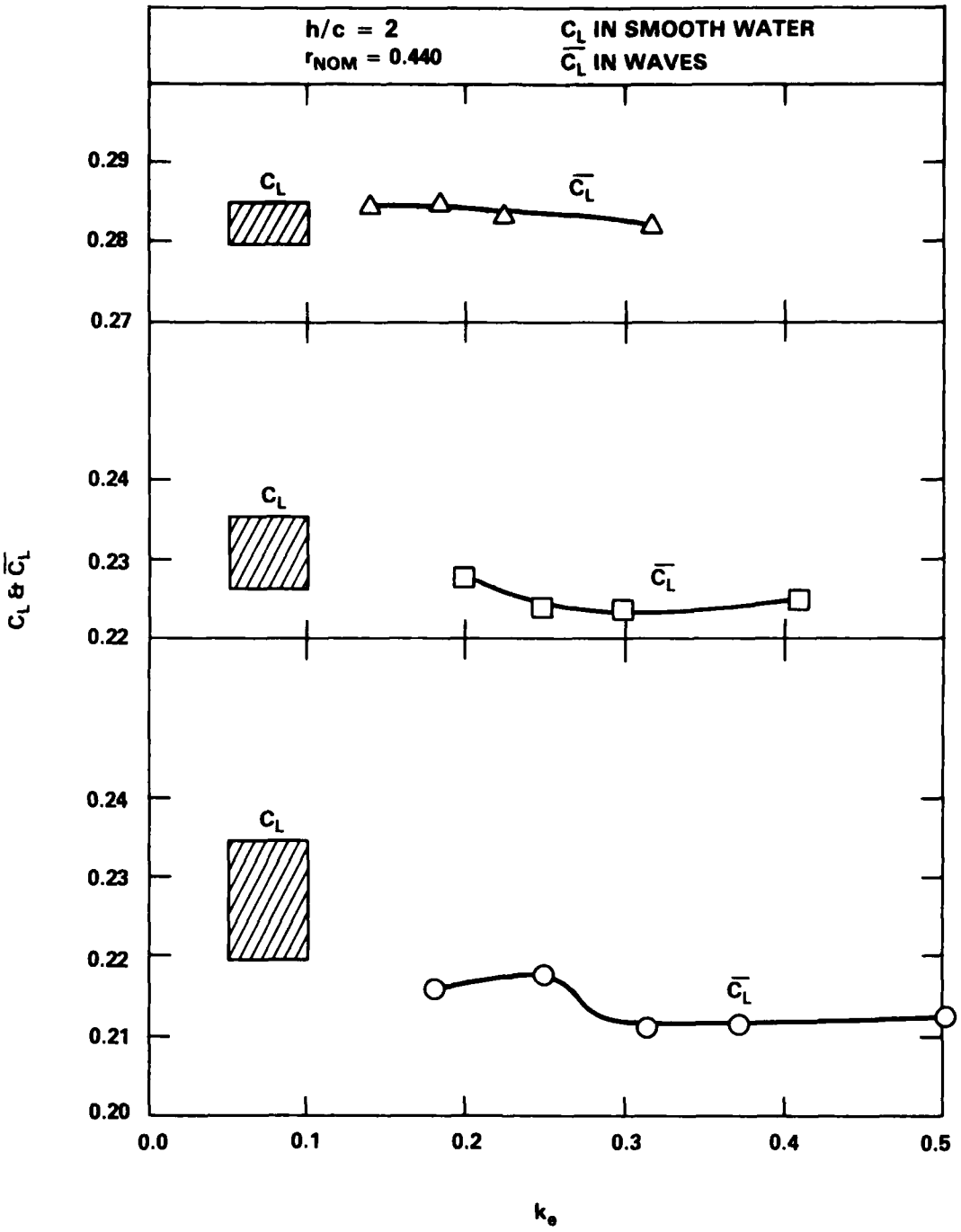

Figure 16F - Mean Lift in Waves Compared to Calm Water Lift; h/c = 22.0

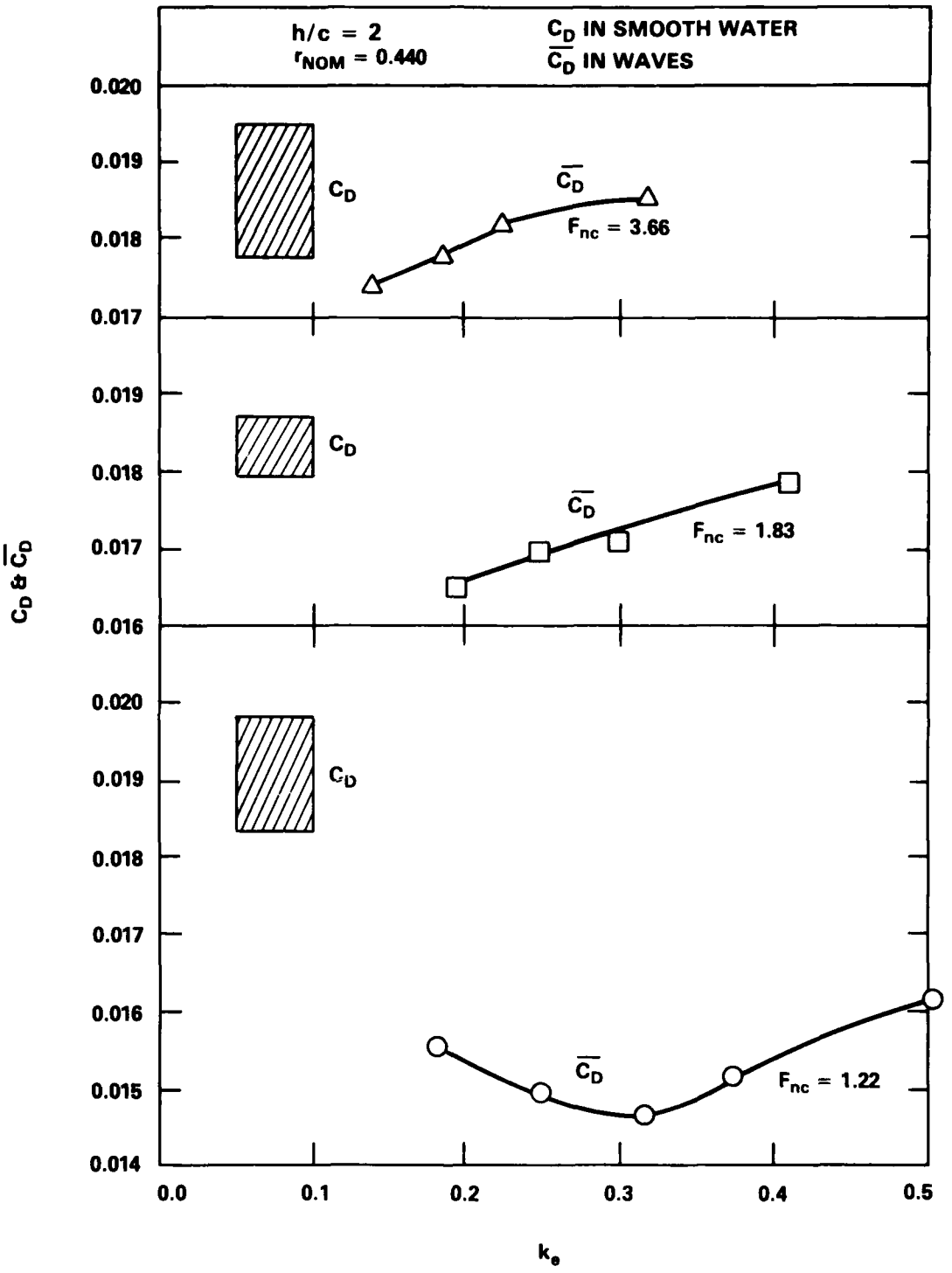

Figure 16G - Mean Drag in Waves Compared to Calm Water Drag; h/c = 2.0

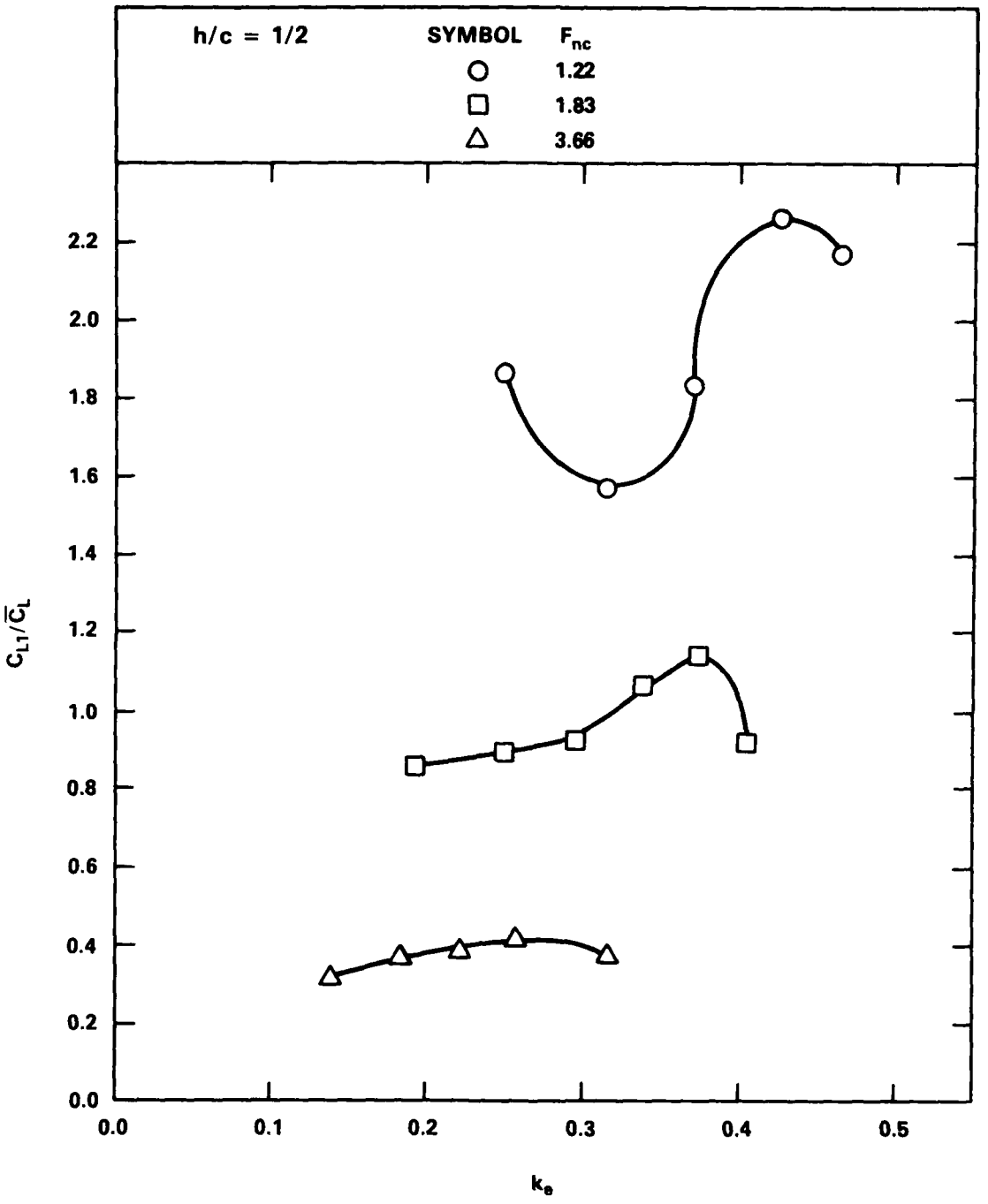

Figure 17A - Fundamental Frequency Lift Amplitude Response to Mean Lift Ratio; h/c = 0.5

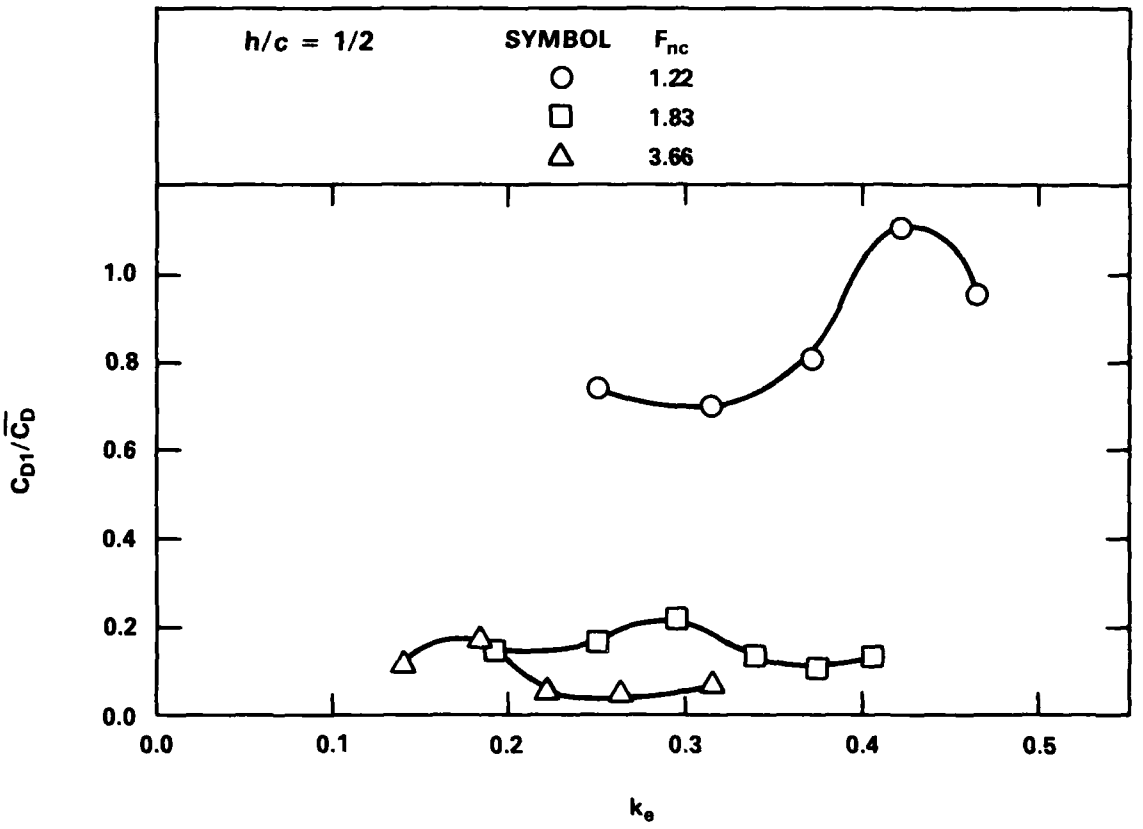

Figure 17B - Fundamental Frequency Drag Amplitude Response to Mean Drag Ratio; h/c = 0.5

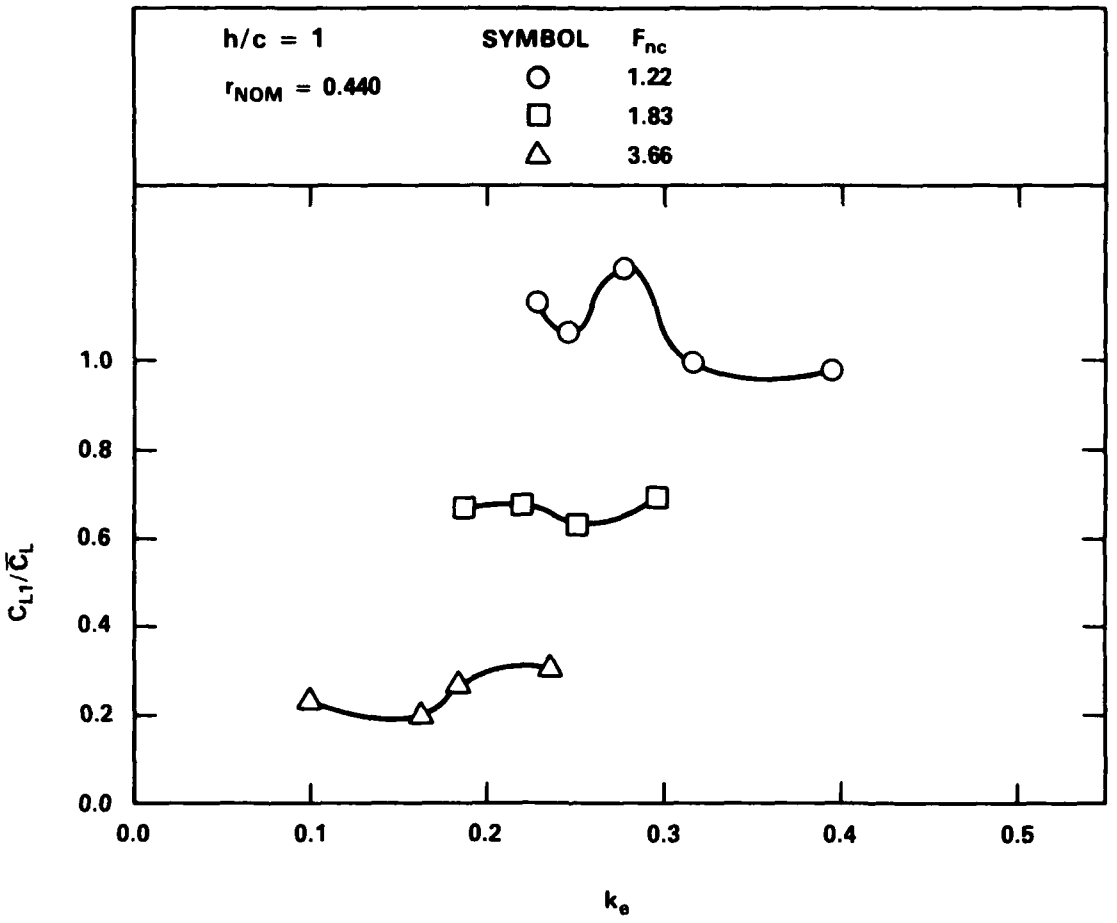

Figure 17C - Fundamental Frequency Lift Amplitude Response to Mean Lift Ratio; h/c = 1.0

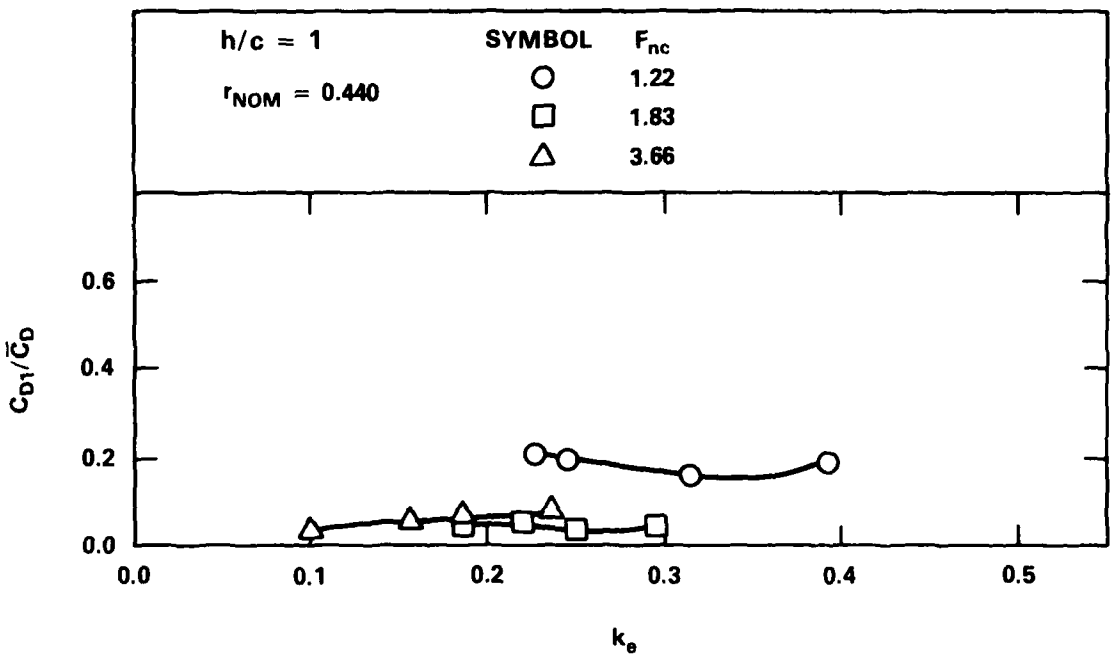

Figure 17D - Fundamental Frequency Drag Amplitude Response to Mean Drag Ratio; h/c = 1.0

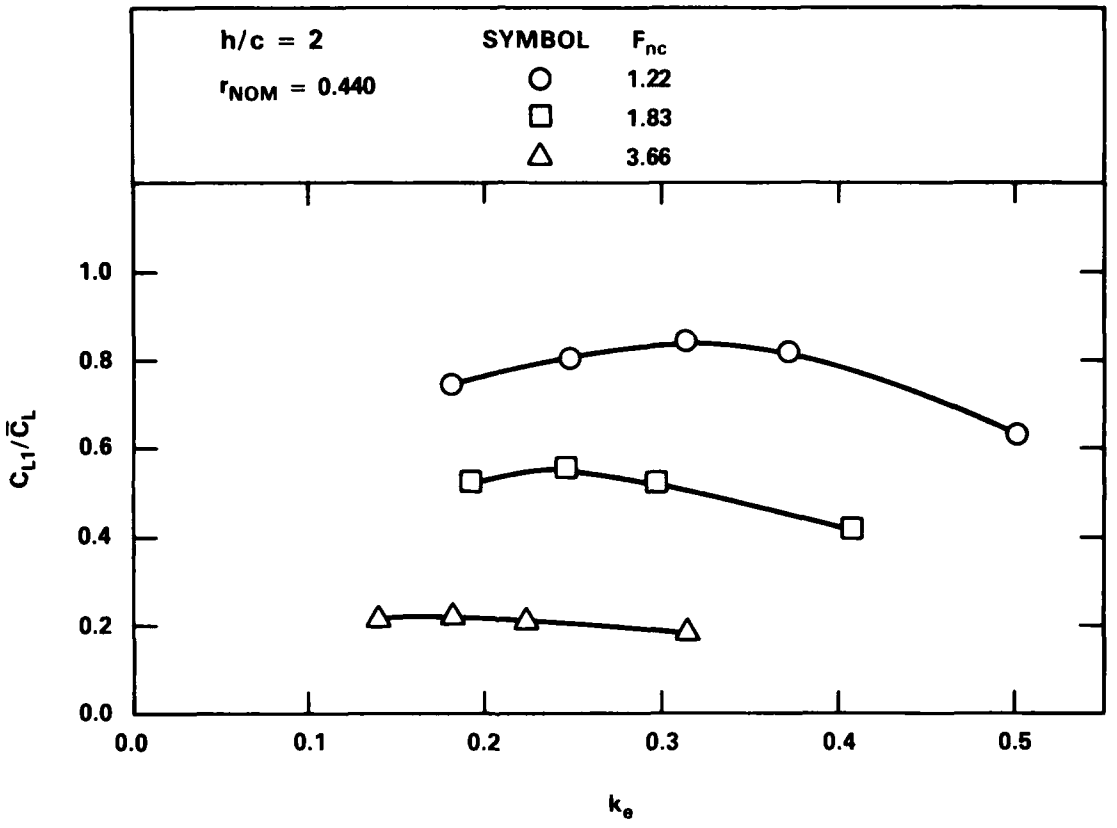

Figure 17E - Fundamental Frequency Lift Amplitude Response to Mean Lift Ratio; h/c = 2.0

AD-A096 506 DAVID W TAYLOR NAVAL SHIP RESEARCH AND DEVELOPMENT CE--ETC F/G 13/10
EXPERIMENTAL INVESTIGATION OF HYDROFOIL FORCE RESPONSE IN REGUL--ETC(U
FEB 81 G KARAFIATH
UNCLASSIFIED DTNSRDC/SPD-0956-01 NL

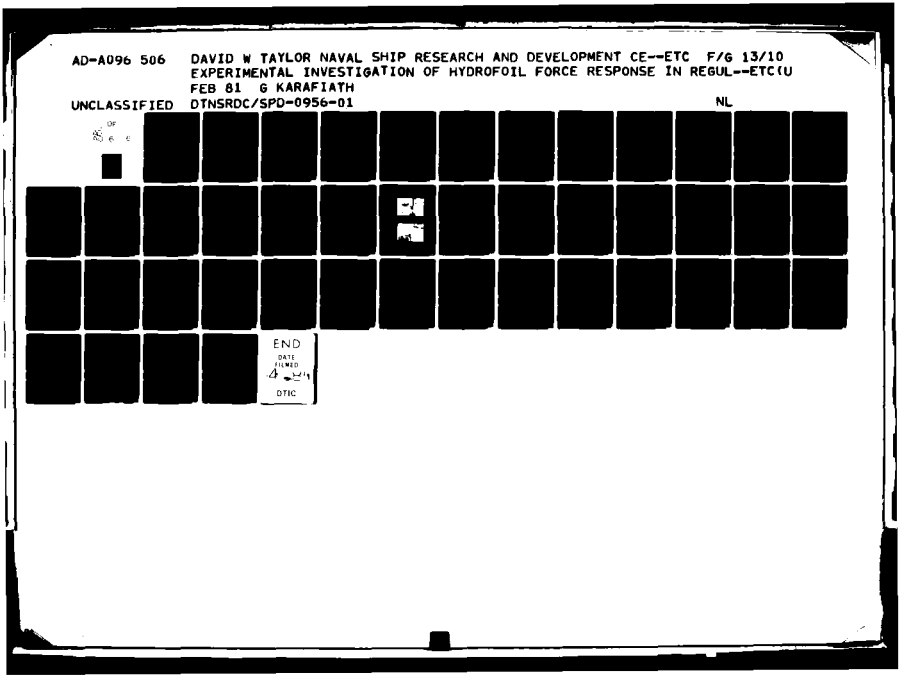

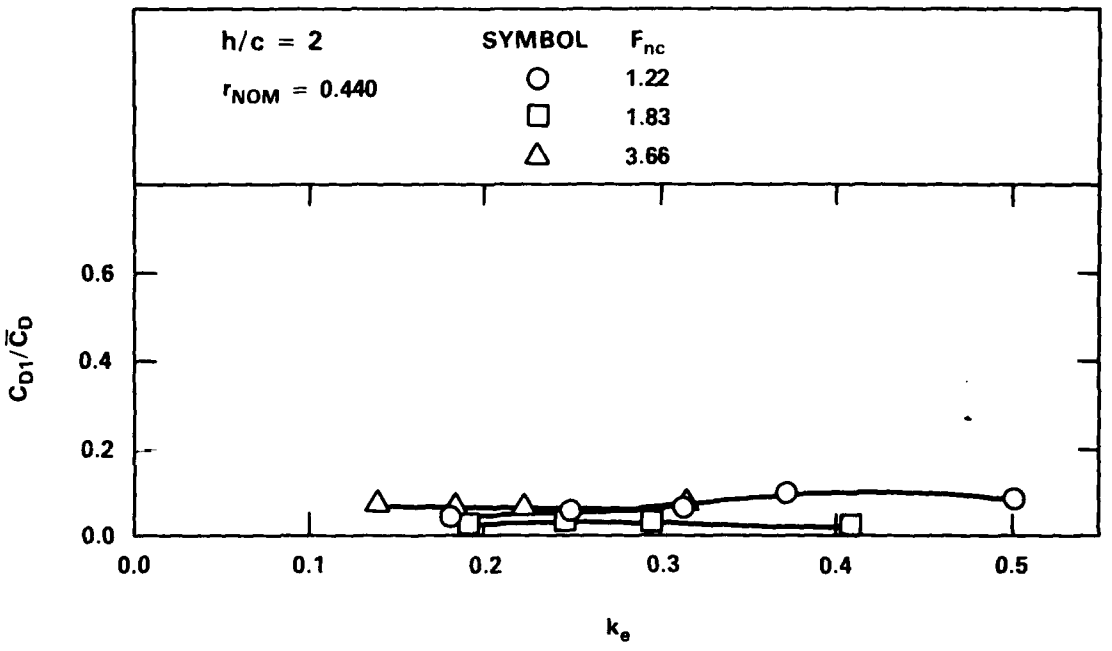

Figure 17F - Fundamental Frequency Drag Amplitude Response to Mean Drag Ratio; h/c = 2.0

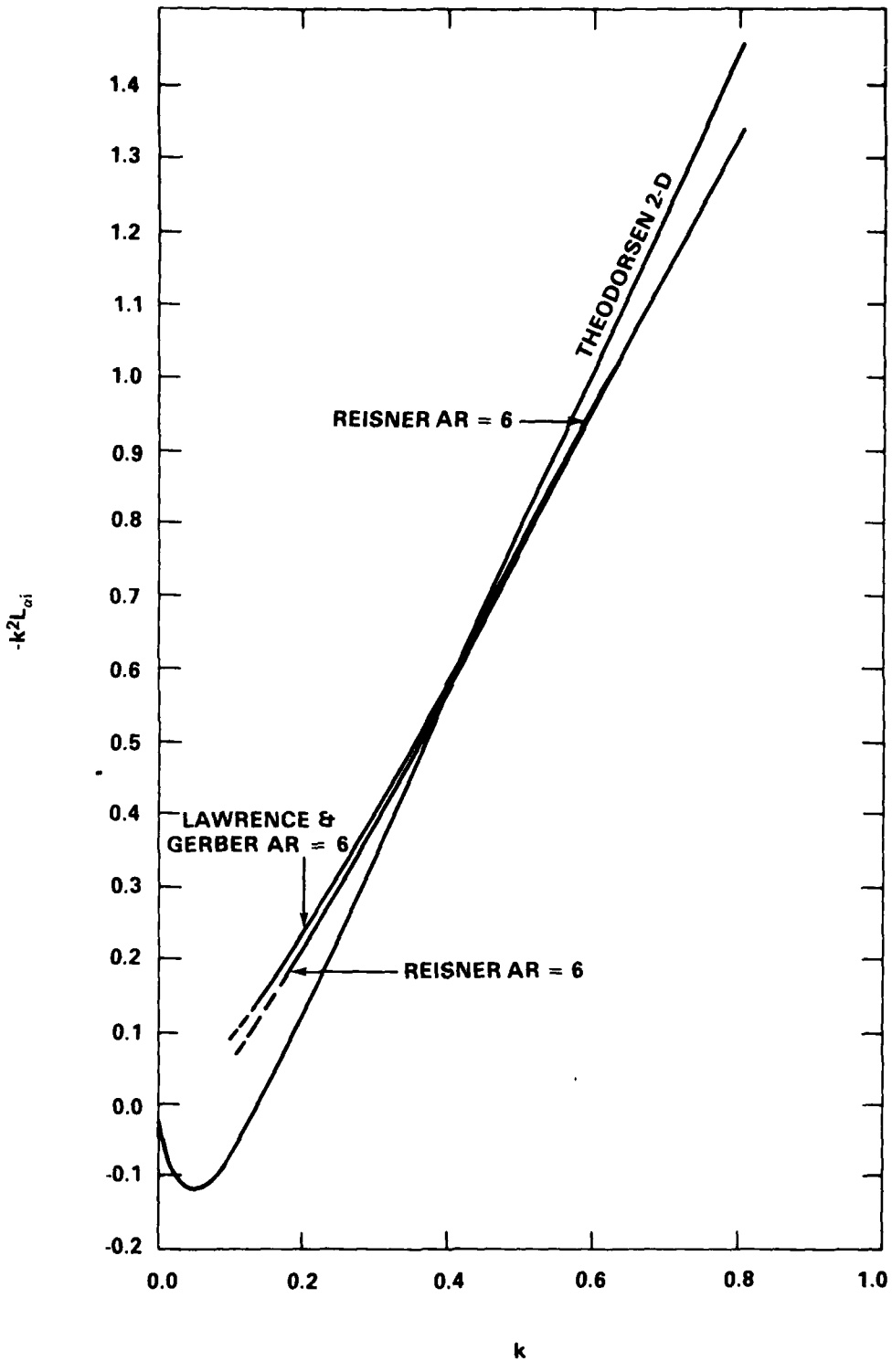

Figure 18A - Theoretical Prediction of $k^2L_{\alpha i}$

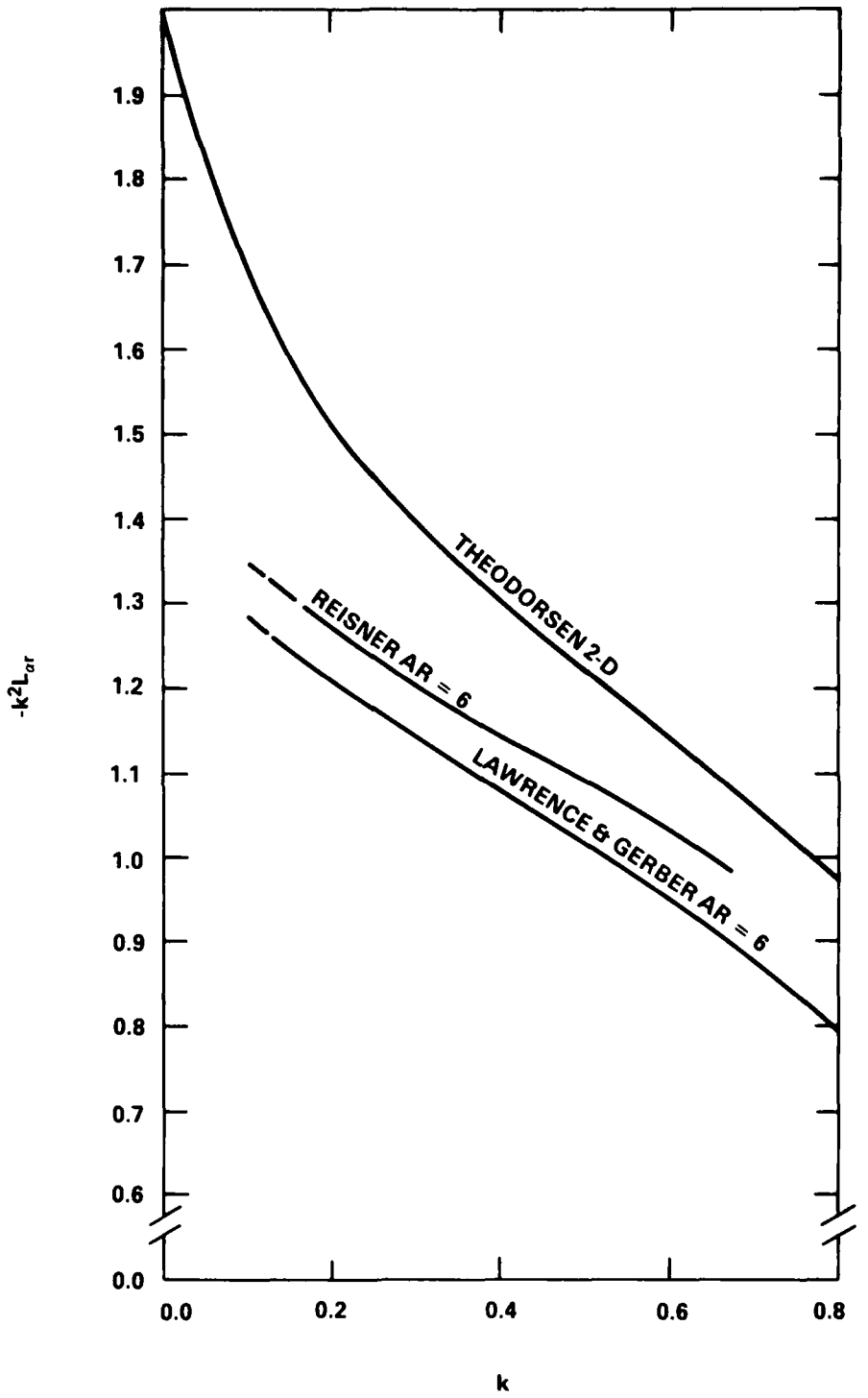

Figure 18B - Theoretical Prediction of $k^2L_{\alpha r}$

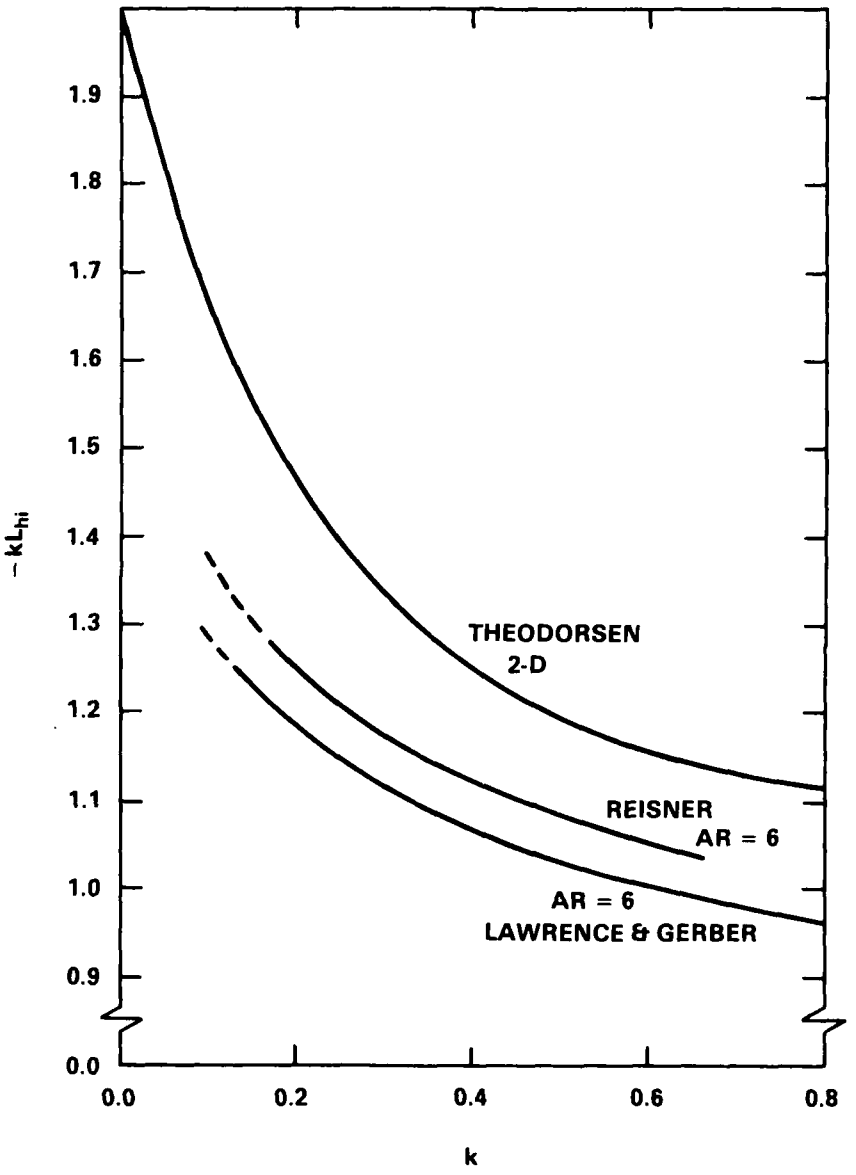

Figure 18C - Theoretical Prediction of k L_{hi}

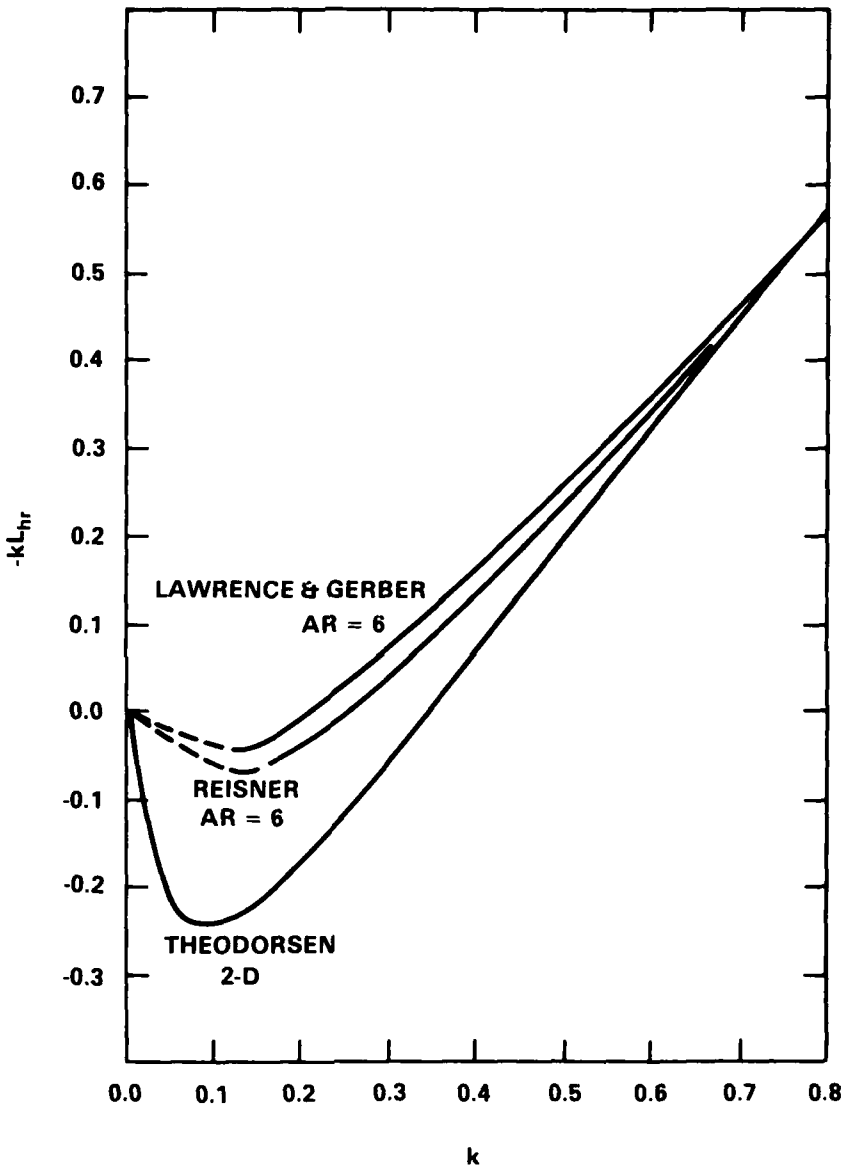

Figure 18D - Theoretical Prediction of k L_{hr}

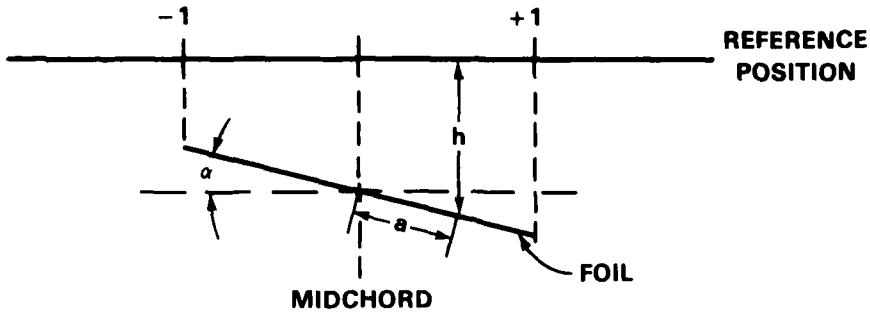

Figure 19 - Depth & Angle of Attack Definitions for the Idealized Foil Under Calm Water

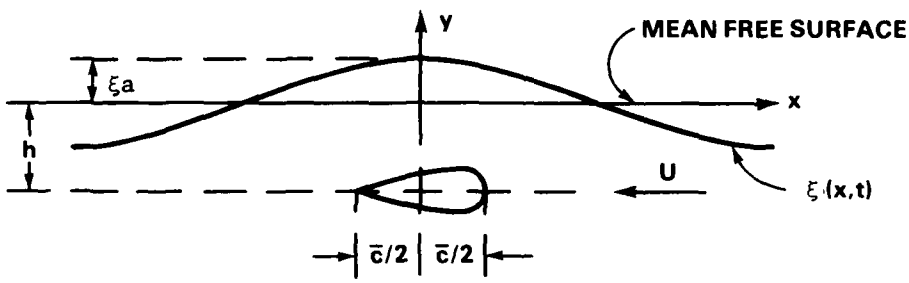

Figure 20 - Foil Operating Under Regular Waves

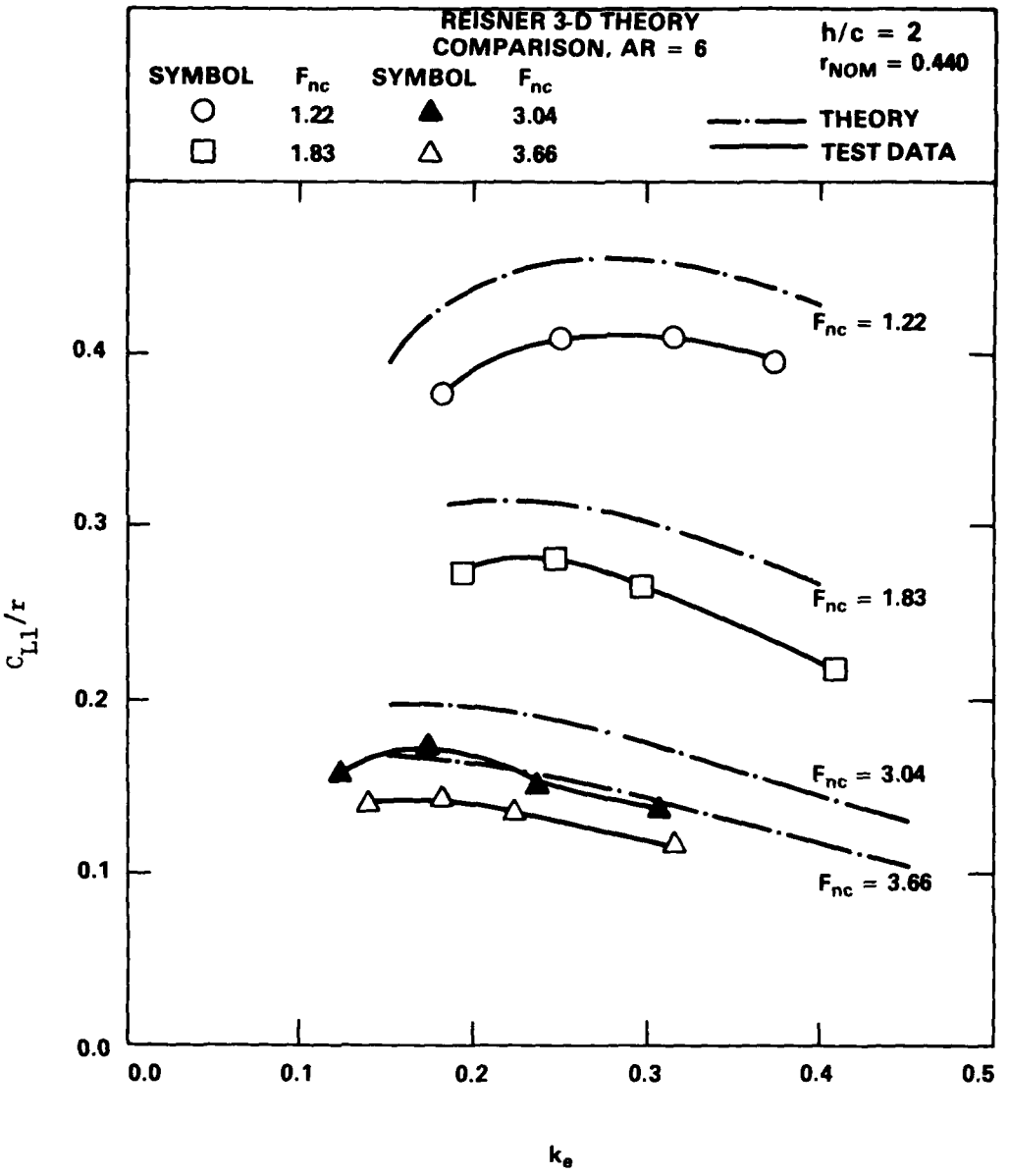

Figure 21 - Comparison of C_{L1}/r as Predicted by Reisner's Theory to the Present Experimental Results; h/c = 2.0

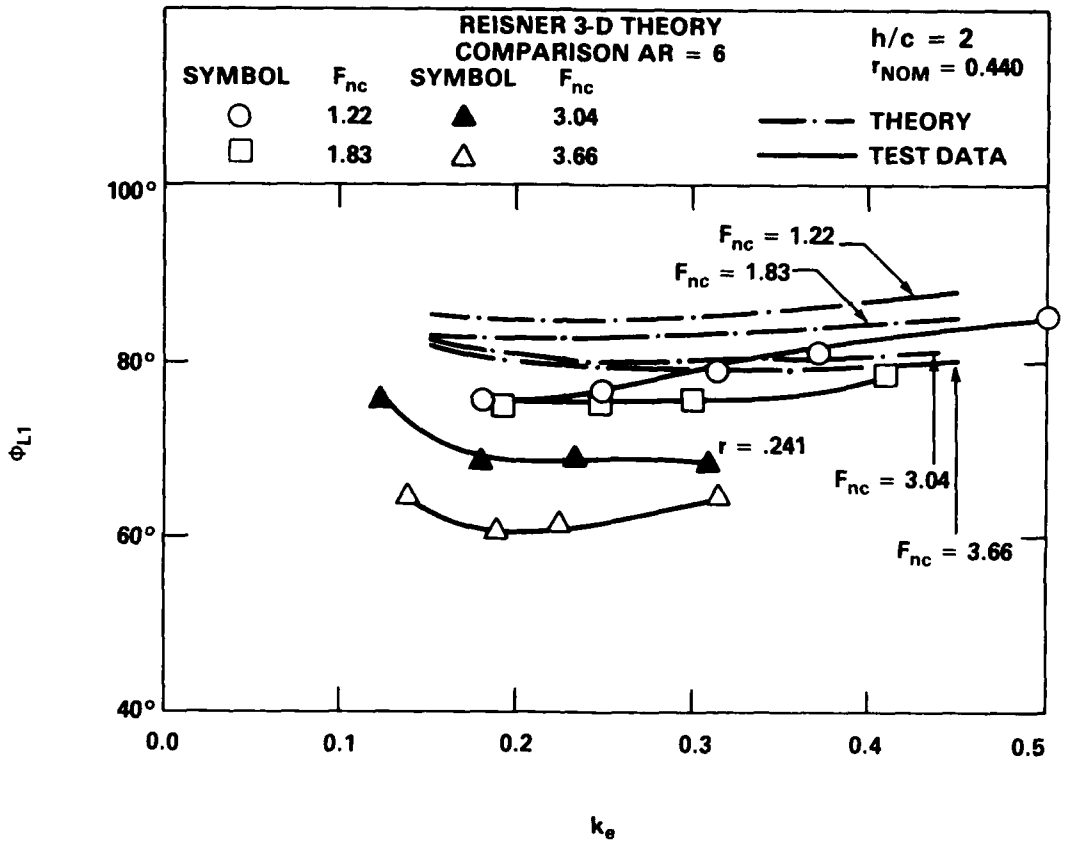

Figure 22 - Comparison of Φ_{L1} as Predicted by Reisner's Theory to the Present Experimental Results; h/c = 2.0

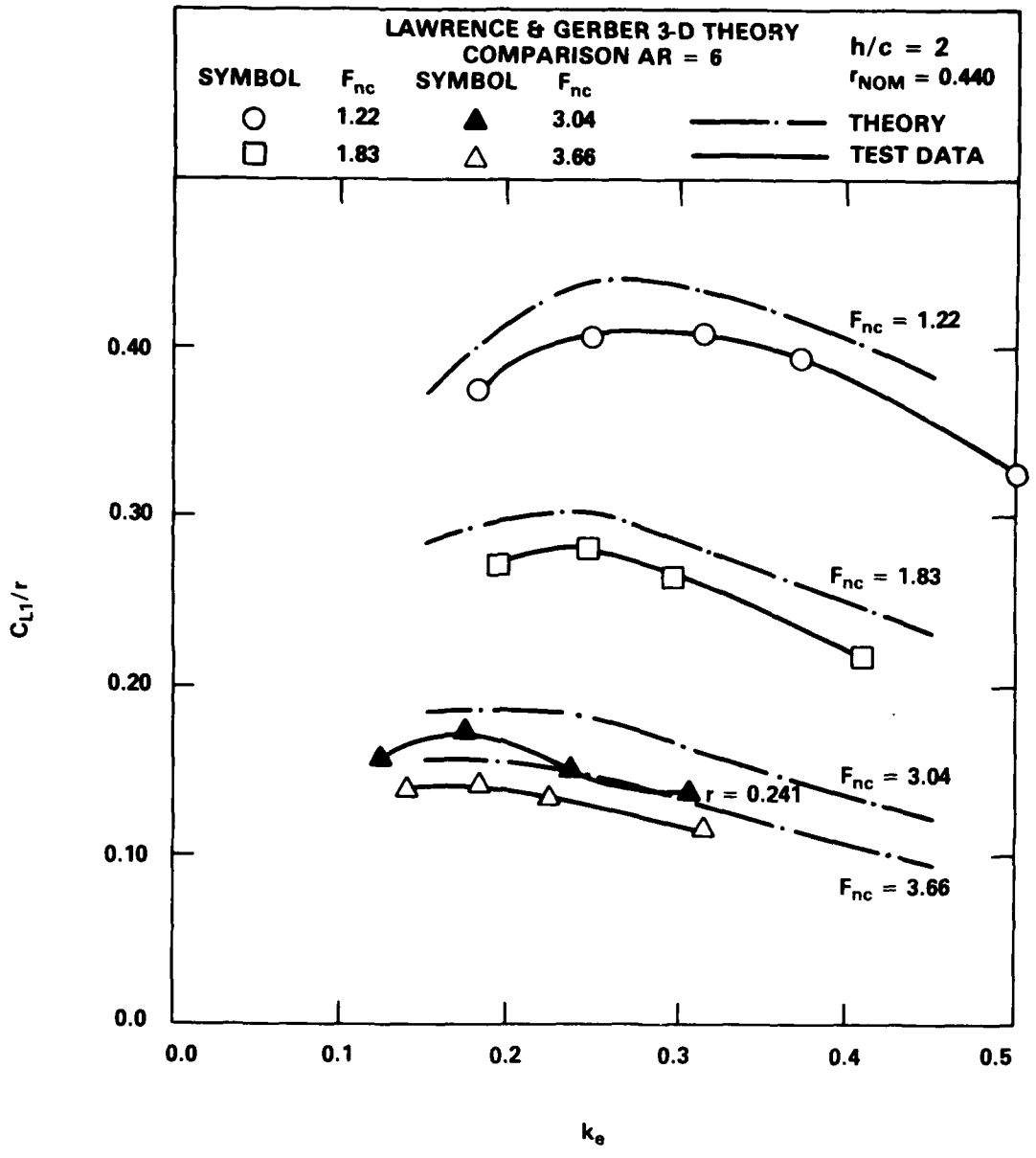

Figure 23 - Comparison of C_{L1}/r Predicted by the Lawrence and Gerber Theory to the Present Experimental Data; h/c = 2.0

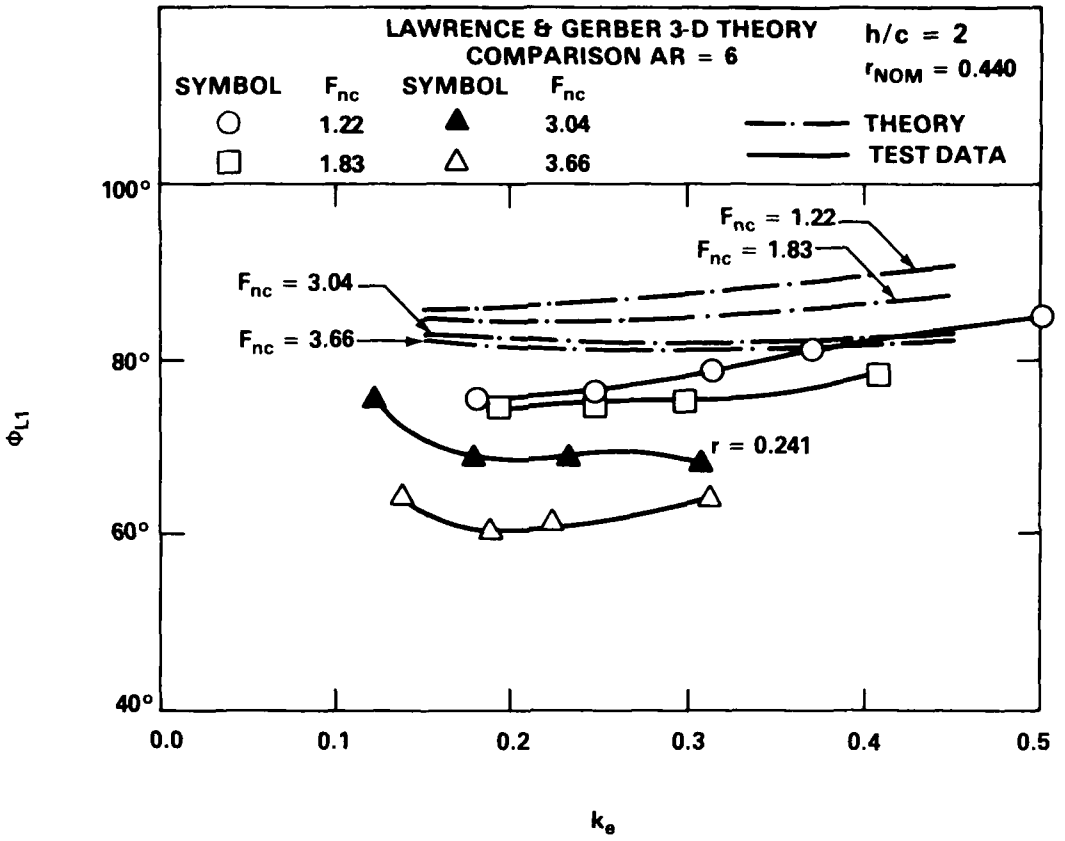

Figure 24 - Comparison of Φ_{L1} as Predicted by the Lawrence & Gerber Theory to the Present Experimental Data; h/c = 2.0

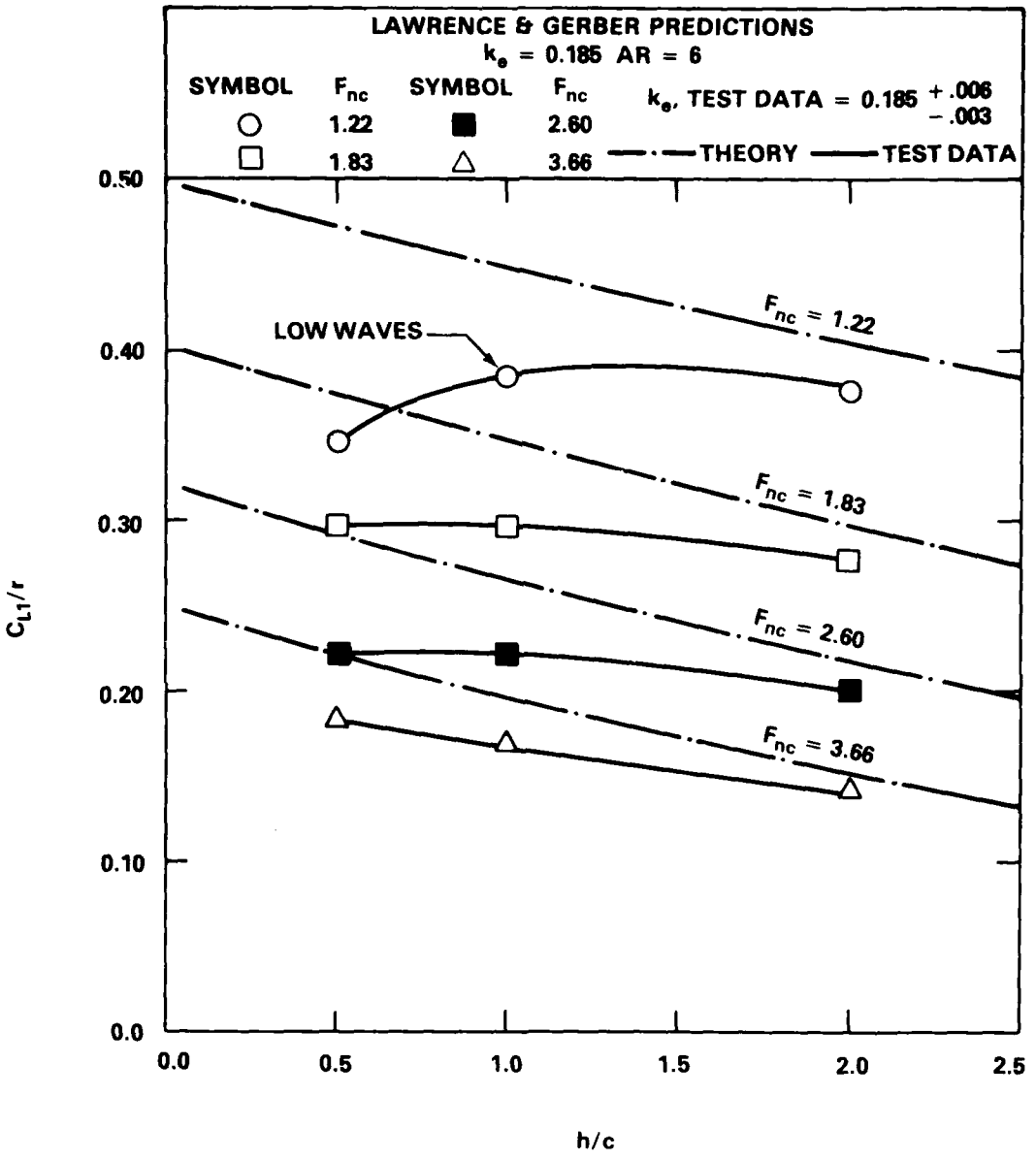

Figure 25A - Comparison of Lawrence & Gerber Theory Lift Amplitude Prediction to the Present Experimental Data at Varying h/c; k_e = 0.185; r_{nom} = 0.44

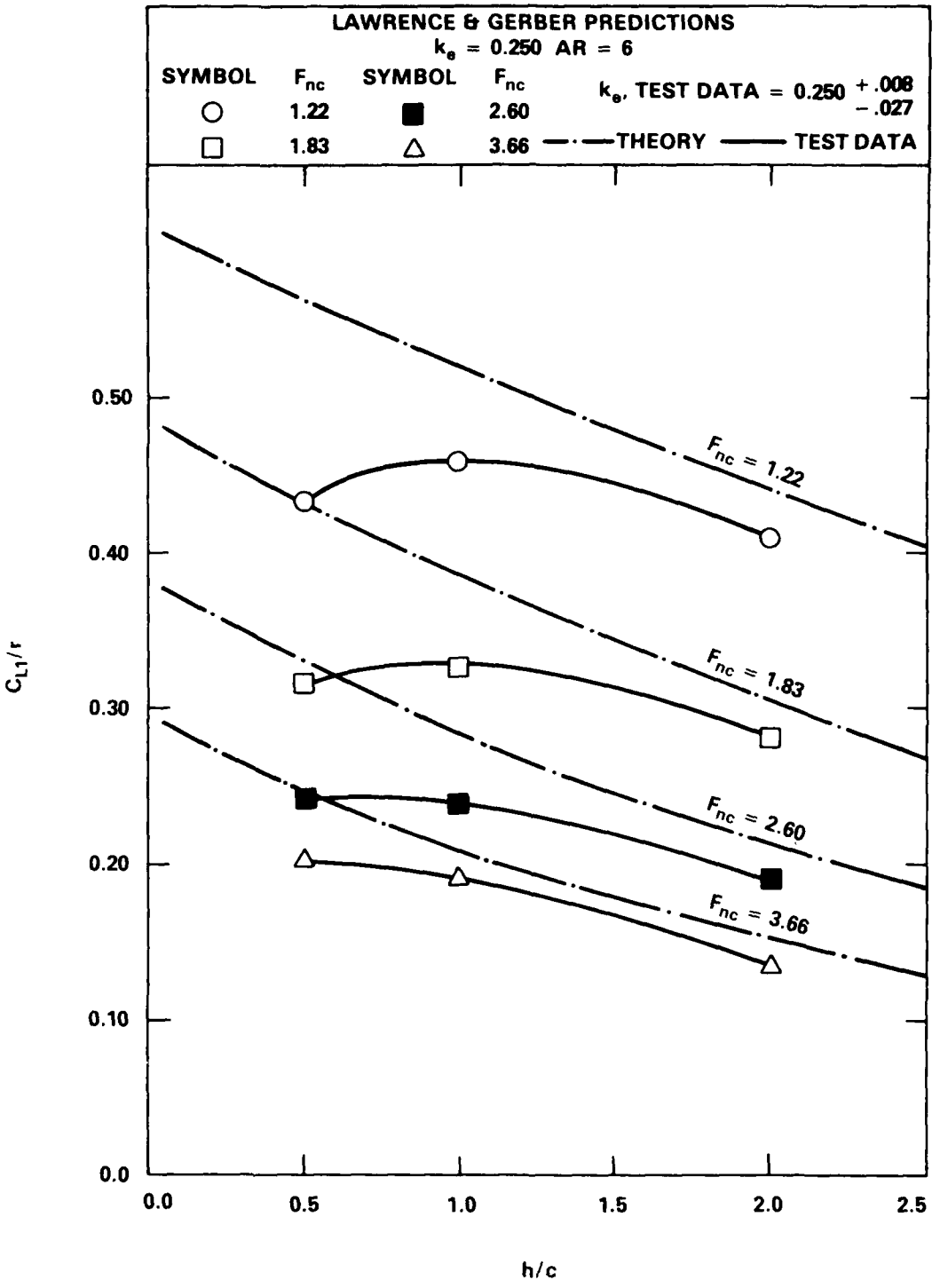

Figure 25B - Comparison of Lawrence & Gerber Theory Lift Amplitude Prediction to the Present Experimental Data at Varying h/c; k_e = 0.25; r_{nom} = 0.44

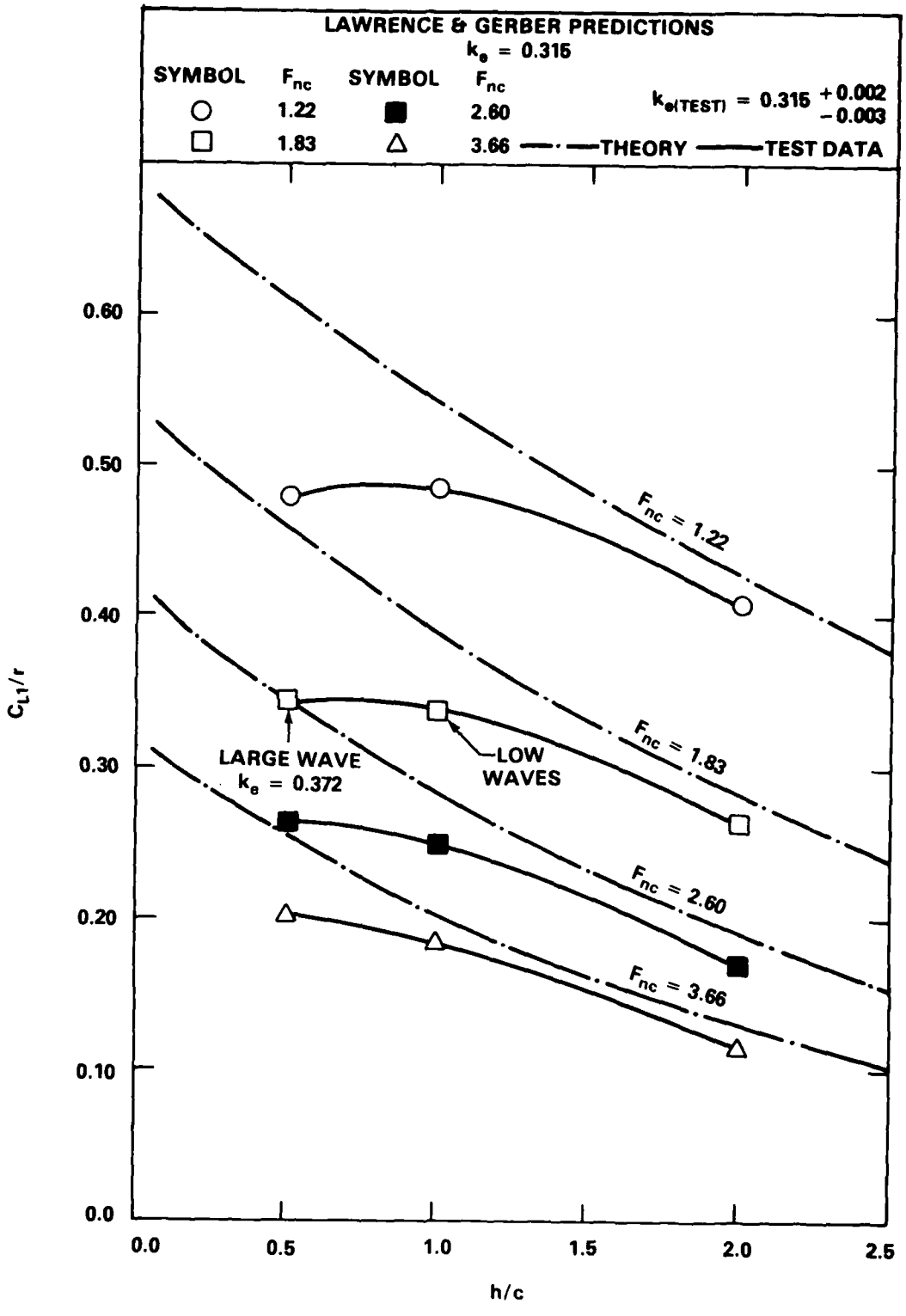

Figure 25C - Comparison of Lawrence & Gerber Theory Lift Amplitude Prediction to the Present Experimental Data at Varying h/c; k_e = 0.315; r_{nom} = 0.44

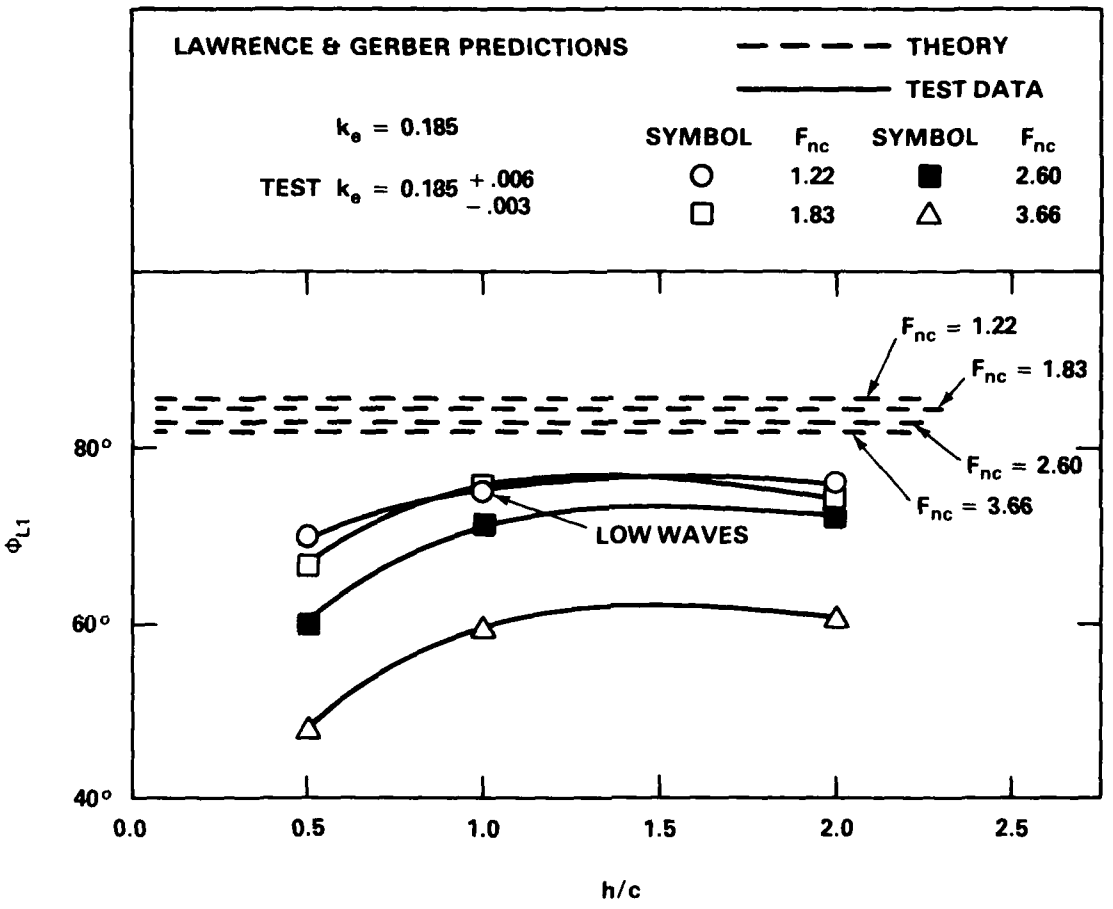

Figure 25D - Comparison of Lawrence & Gerber Theory Lift Phase Response Prediction to the Present Experimental Data for Varying h/c; k_e = 0.185, r_{nom} = 0.44

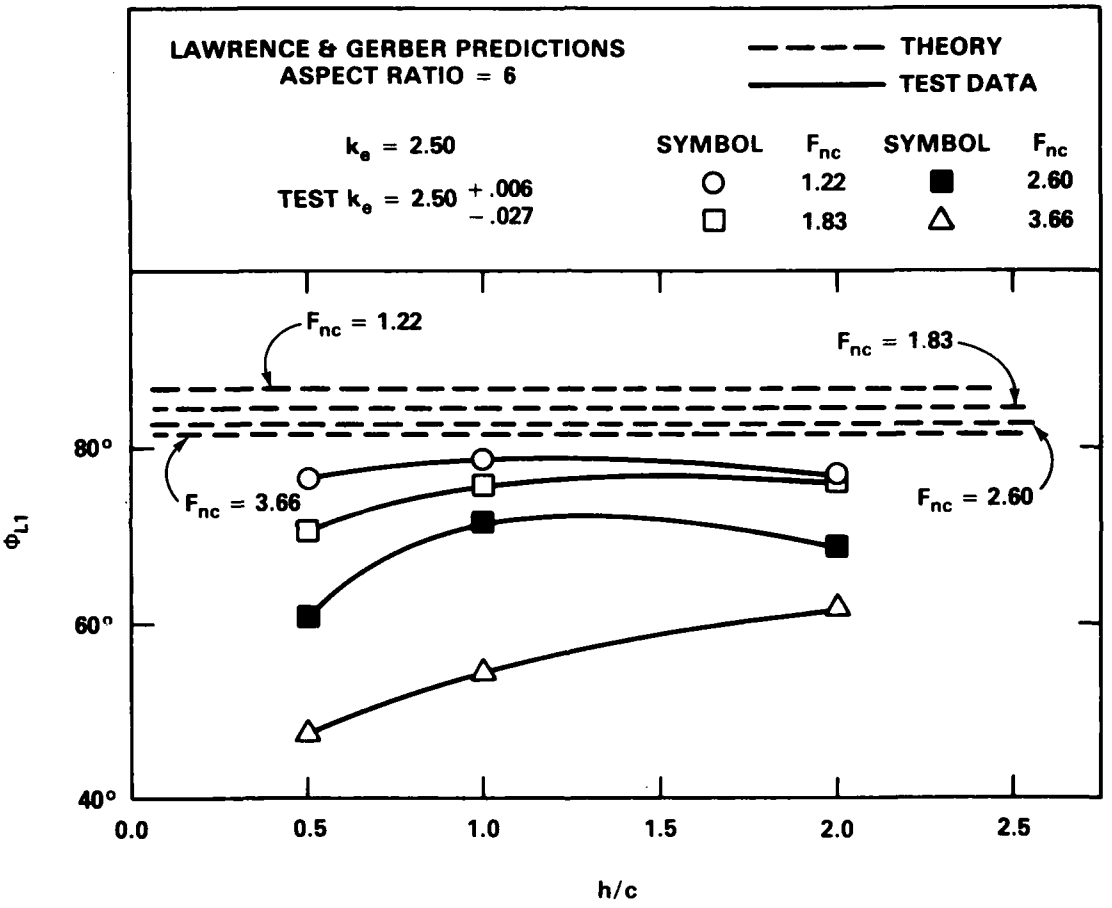

Figure 25E - Comparison of Lawrence & Gerber Theory Lift Phase Response Prediction to the Present Experimental Data for Varying h/c; k_e = 0.25; r_{nom} = 0.44

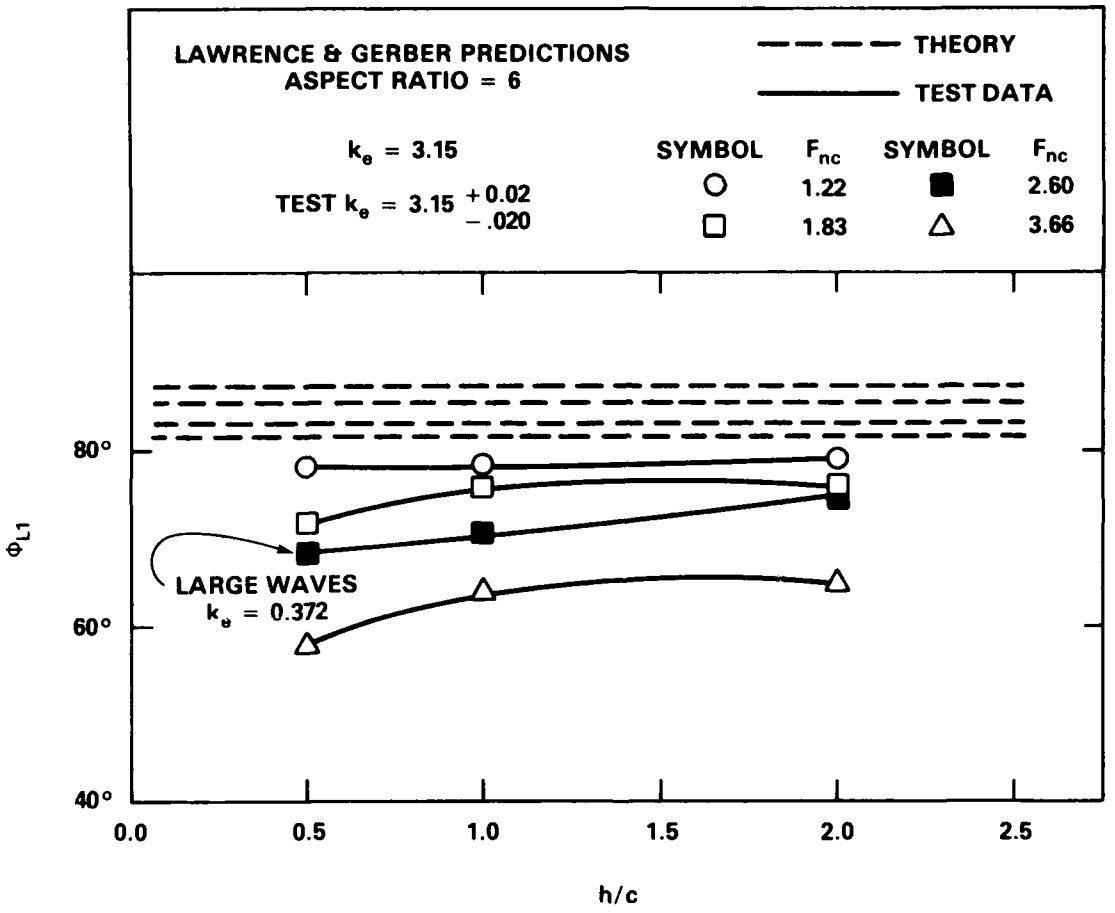

Figure 25F - Comparison of Lawrence & Gerber Theory Lift Phase Response Prediction to the Present Experimental Data for Varying h/c; k_e = 0.315; r_{nom} = 0.44

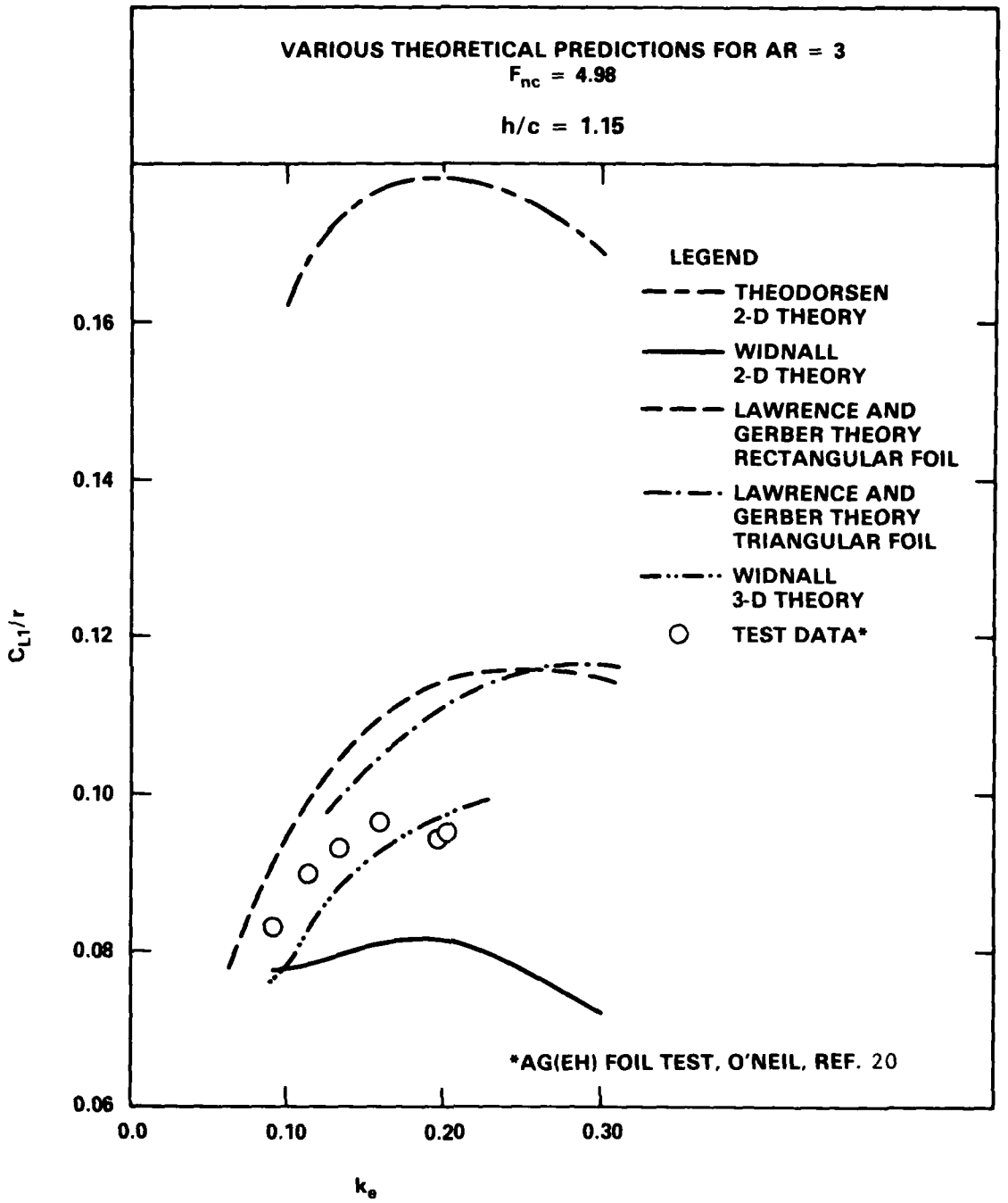

Figure 26 - Comparison of Several Theoretical Predictions of the AG(EH) Main Foil Lift Amplitude Response with Experimental Data; F_{nc} = 4.98; h/c = 1.15

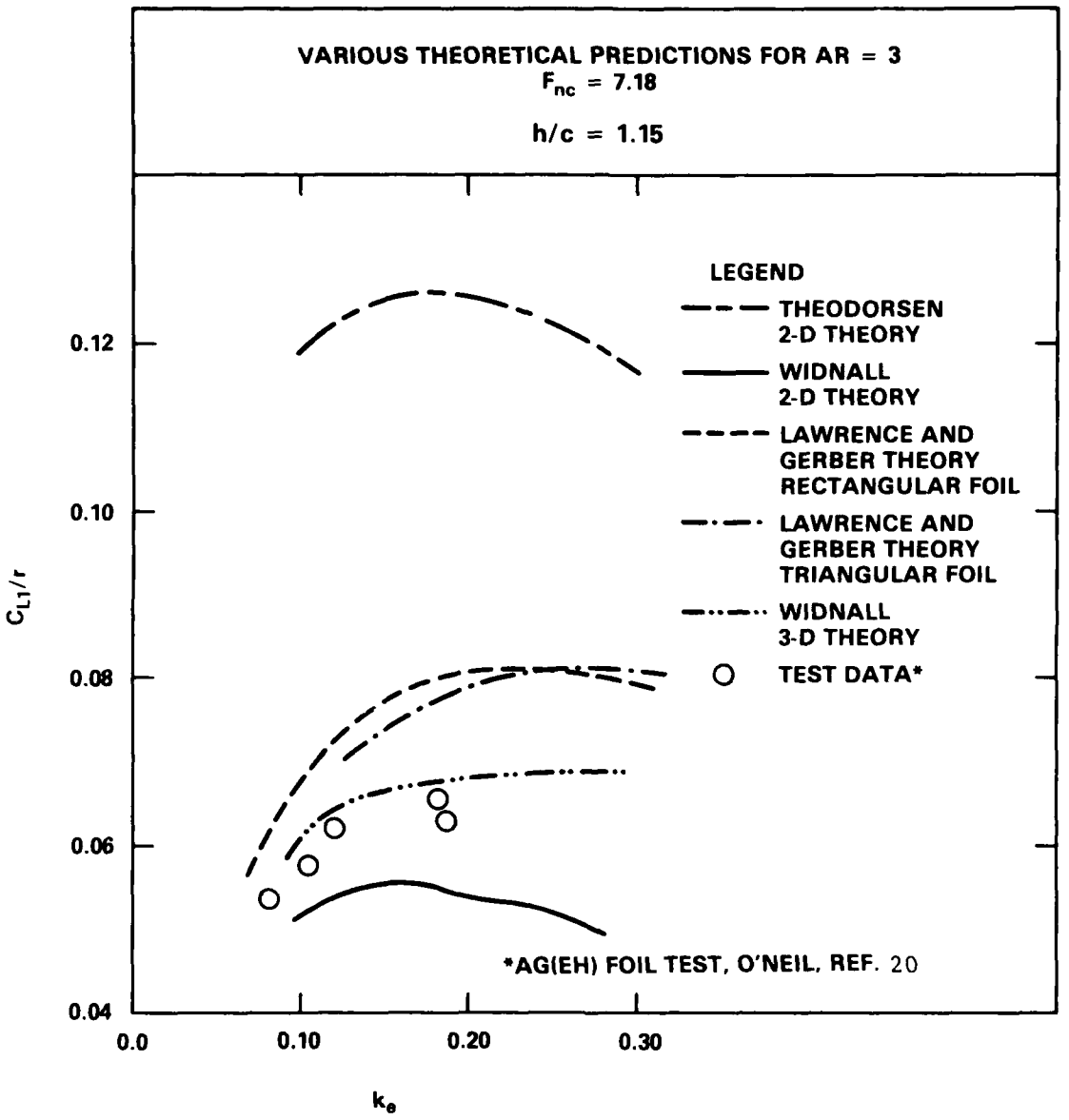

Figure 27 - Comparison of Several Theoretical Predictions of the AG(EH) Main Foil Lift Amplitude Response with Experimental Data; F_{nc} = 7.18; h/c = 1.15

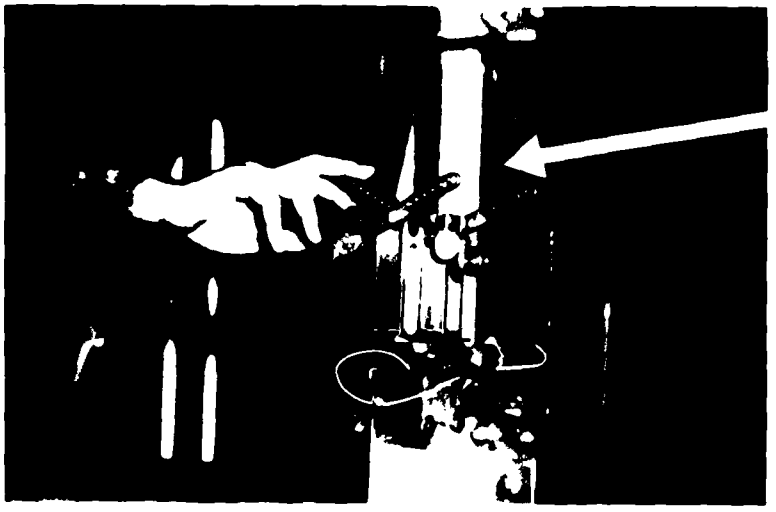

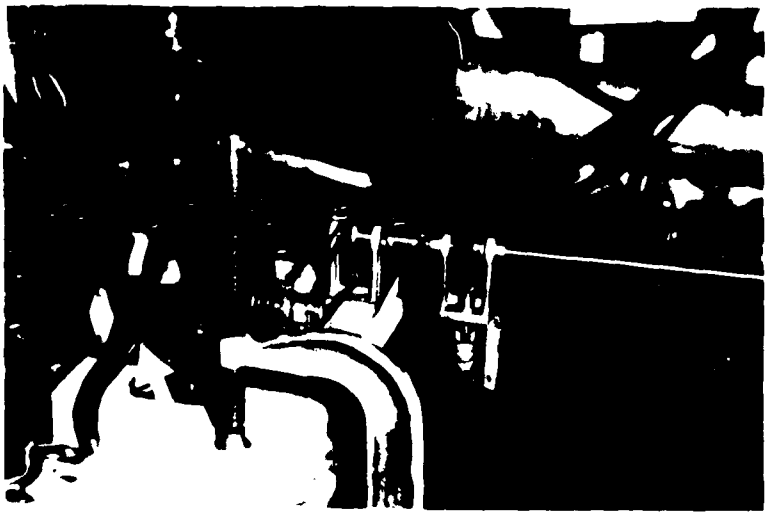

Figure 28 - Photograph of Shaker and Drive Motor

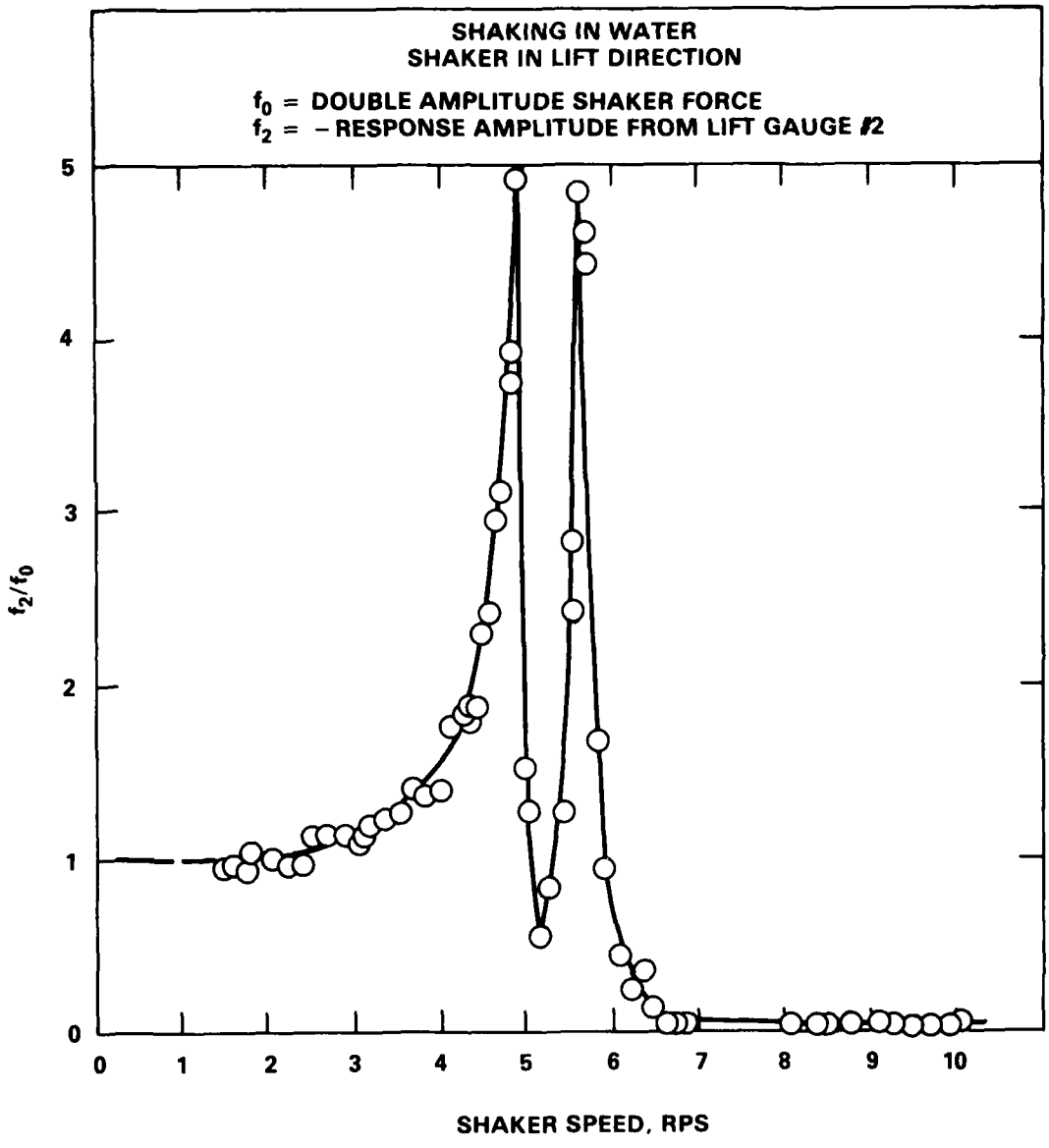

Figure 29 - Lift Response Amplification Factor
(in water, h/c = 0.5)

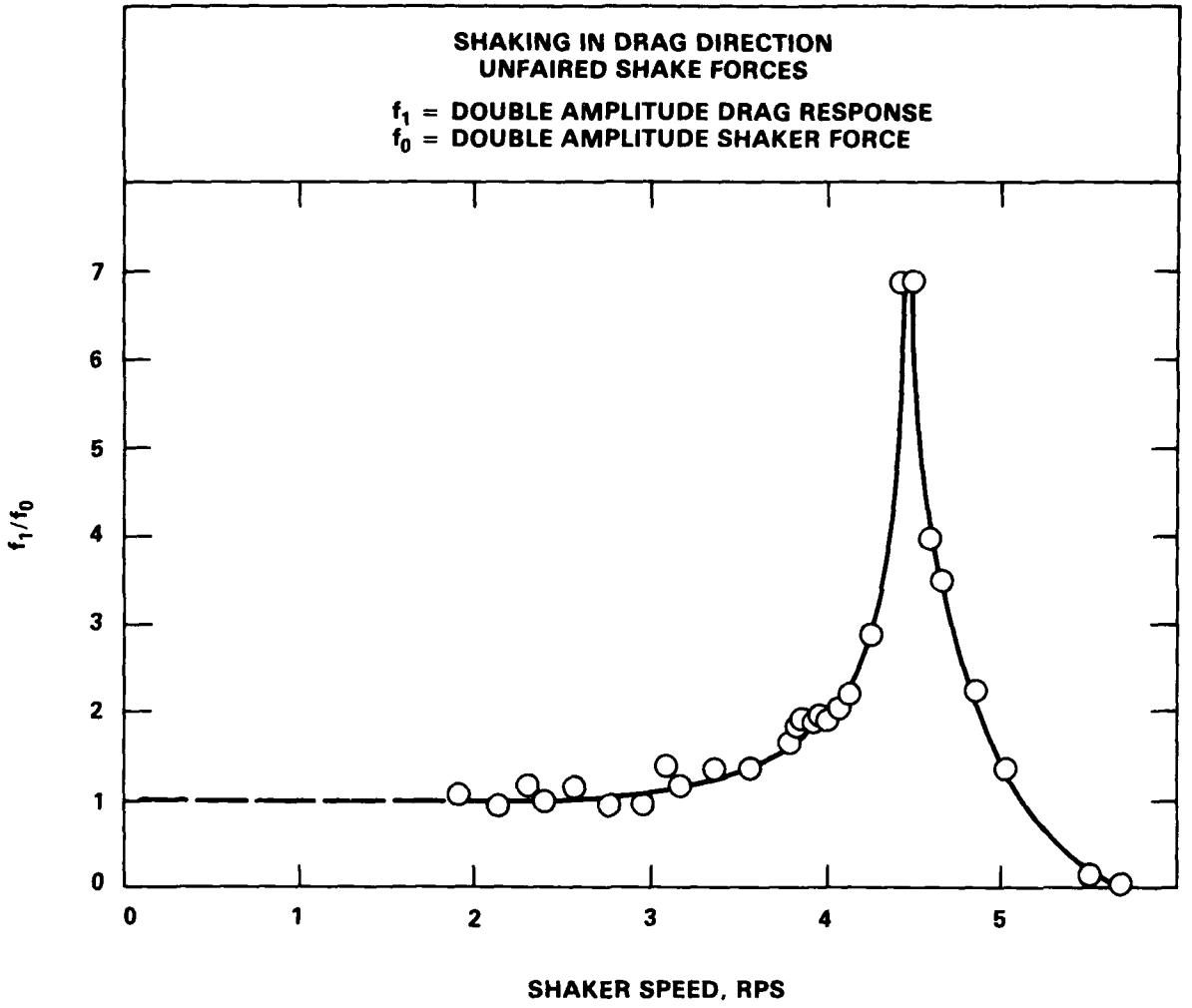

Figure 30 - Drag Response Amplification Factor
(in air)

APPENDIX A

TABULATED EXPERIMENTAL DATA

Tabulation of the experimentally determined lift and drag response on the aspect ratio 6 hydrofoil at depth chord ratio 0.5, 1.0 and 2.0

The lift and drag response listed in this appendix corresponds to the foil only condition. Dynamometer tares have been subtracted from the initial data.

Run #	k_e	F_{nc}	F_{nh}	ω_e	r	$\frac{C_{L1}}{r}$	ϕ_{L1}	$\frac{C_{D1}}{r}$	ϕ_{D1}	$\frac{C_{D2}}{r}$	ϕ_{D2}	C.
158	0.316	1.221	0.863	3.792	0.449	0.480	78.4	0.0206	72	0.00997	-25	
159	0.250	1.839	1.300	4.514	0.452	0.314	70.3	0.0055	50	0.00663	-35	
160	0.183	3.660	2.588	6.572	0.459	0.183	47.9	0.0061	- 2	0.00174	-87	
161	0.500	1.220	0.863	5.994	0.417	0.563	82.6	0.0235	89	0.01409	-27	
162	0.407	1.839	1.300	7.353	0.419	0.377	73.2	0.0044	81	0.00658	-40	
163	0.317	3.659	2.587	3.30	0.420	0.201	47.9	0.0025	69	0.00086	13	
164	0.572	1.220	1.725	6.850	0.291	0.516	-86.8					1
165	0.467	1.838	1.300	3.596	0.317	0.373	77.6					1
166	0.364	3.689	3.689	13.183	0.337	0.294	45.0					1
167	0.180	1.218	0.861	2.160	0.389	0.345	69.8	0.0169	63	0.00500	- 8	
168	0.139	1.832	1.295	2.509	0.398	0.252	62.1	0.0059	31	0.00135	-31	2
169	0.097	3.662	2.589	3.463	0.405	0.171	27.3	0.0059	-32			3,4
170	0.249	1.220	0.863	2.988	0.449	0.432	76.4	0.0213	71	0.00812	-22	
$h/c = \frac{1}{2}$												

Run #	k_e	F_{nc}	F_{nh}	ω_e	r	$\frac{C_{L1}}{r}$	Φ_{L1}	$\frac{C_{D1}}{r}$	Φ_{D1}	$\frac{C_{D2}}{r}$	Φ_{D2}	C.
171	0.192	1.839	1.300	3.464	0.444	0.296	66.6	0.0048	-32	0.00360	-18	
172	0.138	3.660	2.588	4.947	0.448	0.160	44.3	0.0043	-56	0.00154	-35	
173	0.371	1.220	0.863	4.445	0.453	0.529	80.6	0.0224	76	0.01230	-28	
174	0.295	1.839	1.300	5.336	0.453	0.344	70.5	0.0070	29	0.06685	-44	
175	0.222	3.662	2.589	8.004	0.466	0.190	48.4	0.0018	-84	0.00169	-85	
176	0.465	1.229	0.869	5.574	0.474	0.538	81.0	0.0221	82	0.01498	-27	
177	0.374	1.839	1.300	6.795	0.484	0.370	77.6	0.0031	59	0.00546	-30	
178	0.372	2.598	1.837	8.361	0.487	0.269	68.4	0.0006	66			
179	0.422	1.201	0.849	4.982	0.499	0.544	79.6	0.0240	76	0.01322	-27	
180	0.338	1.838	1.300	6.112	0.493	0.349	72.2	0.0037	49	0.00741	-40	
181	0.258	3.659	2.587	9.284	0.474	0.201	47.4	0.0015	84	0.00246	80	
300	0.371	1.219	0.862	4.445	0.273	0.519	80.2	0.0190	31	0.00607	-24	
301	0.296	1.837	1.300	5.345	0.271	0.349	71.8	0.0022	-59	0.00334	-37	
h/c = ½												

Run #	k_e	F_{nc}	F_{nh}	ω_e	r	$\frac{C_{L1}}{r}$	ϕ_{L1}	$\frac{C_{D1}}{r}$	ϕ_{D1}	$\frac{C_{D2}}{r}$	ϕ_{D2}	C.
302	0.222	3.661	2.589	7.979	0.279	0.198	49.9	0.0034	-79	0.00135	-84	
303	0.325	1.530	1.082	4.878	0.437	0.414	74.4	0.011	72	0.00709	-26	
304	0.252	2.598	1.837	6.443	0.443	0.241	60.8	0.0004	-35	0.00266	-44	
305	0.236	3.043	2.152	7.072	0.448	0.213	56.6	0.0012	-78	0.00075	-70	
306	0.224	1.531	1.083	3.673	0.448	0.373	71.8	0.0162	65	0.00718	-26	
307	0.184	2.597	1.834	4.703	0.448	0.220	59.9	0.0030	-11	0.00207	-38	
308	0.172	3.043	2.152	5.140	0.462	0.188	55.1	0.0013	66	0.00201	-61	
309	0.370	1.218	0.861	4.433	0.613	0.541	79.2	0.0067	53	0.01529	-24	
310	0.296	1.836	1.298	5.345	0.627	0.339	68.3	0.0079	35	0.00892	-39	
311	0.223	3.659	2.587	8.006	0.632	0.191	50.9	0.0195	76	0.00173	-40	4
330	0.567	1.219	0.862	6.794	0.240	0.567	87.8	0.0256	82			
331	0.463	1.838	1.300	8.366	0.206	0.383	74.0	0.0203	43			
332	0.364	3.663	2.590	13.105	0.226	0.204	47.1	0.0235	9			
333	0.464	1.217	0.861	5.515	0.249	0.539	78.7	0.0185	87	0.00870	-31	
$h/c = \frac{1}{2}$												

Run #	k_e	F_{nc}	F_{nh}	ω_e	r	$\frac{C_{L1}}{r}$	Φ_{L1}	$\frac{C_{D1}}{r}$	Φ_{D1}	$\frac{C_{D2}}{r}$	Φ_{D2}	C
334	0.377	1.837	1.299	6.806	0.247	0.372	13.7	0.0054	77	0.00335	-29	
335	0.290	3.659	2.587	10.412	0.254	0.0037	55.5	0.0016	89	0.00202	-44	
336	0.445	1.531	1.083	6.700	0.230	0.0153	64.7	0.0182	47			
337	0.355	2.597	1.836	9.072	0.245	0.0115	52.7	0.0207	26			
338	0.336	3.041	2.150	10.048	0.248	0.0064	45.7	0.0006	18			
$h/c = \frac{1}{2}$												

1. - Low Waves (Good data, but not desired wave height)
2. - Breaking Waves (Data follows trend)
3. - Short Run
4. - Trip Wire Broke

Run #	k_e	F_{nc}	F_{nh}	ω_e	r	$\frac{C_{L1}}{r}$	ϕ_{L1}	$\frac{C_{D1}}{r}$	ϕ_{D1}	$\frac{C_{D2}}{r}$	ϕ_{D2}	C.
130	0.409	1.835	1.835	7.376	0.483	0.343	82.4	0.0006	-65	0.00334	-17	3
131	0.317	3.656	3.656	11.383	0.476	0.177	63.9	0.0059	-73	0.00129	-61	3
132	0.314	1.218	1.218	3.756	0.230	0.479	78.9	0.0073	79	0.00507	-36	
133	0.247	1.836	1.836	4.456	0.220	0.329	71.8	0.0028	- 4	0.00222	-13	
134	0.183	3.657	3.657	6.575	0.228	0.165	64.9	0.0027	49	0.00070	48	
135	0.316	1.217	1.217	3.782	0.600	0.490	78.4	0.0089	67	0.01305	-28	
136	0.250	1.835	1.835	4.505	0.611	0.334	74.2	0.0026	25	0.00524	-29	
137	0.183	3.655	3.655	6.584	0.623	0.170	61.0	0.0029	-74	0.00191	60	
312	0.295	1.835	1.835	5.326	0.430	0.338	74.7	0.0015	-75	0.00496	-21	
313	0.252	2.596	2.596	6.418	0.437	0.238	71.2	0.0019	-12	0.00130	-50	
314	0.237	3.040	3.040	7.066	0.440	0.212	63.3	0.0009	81	0.00042	-78	
315	0.218	1.836	1.836	3.932	0.435	0.315	74.8	0.0018	69	0.00413	-20	
316	0.181	2.595	2.595	4.625	0.439	0.221	71.0	0.0011	59	0.00122	-35	
317	0.171	3.040	3.040	5.116	0.445	0.191	68.4	0.0009	88	0.00070	-17	

h/c = 1

Run #	k_e	F_{nc}	F_{nh}	ω_e	r	$\frac{C_{L1}}{r}$	ϕ_{L1}	$\frac{C_{D1}}{r}$	ϕ_{D1}	$\frac{C_{D2}}{r}$	ϕ_{D2}	C.
114	0.116	3.038	3.038	3.460	0.188	0.163	78.2	0.0012	-11			1
118	0.394	1.210	1.210	4.680	0.435	0.503	79.7	0.0068	86	0.00961	-30	
119	0.291	2.150	2.150	6.138	0.441	0.286	73.7	0.0016	1	0.00150	-59	
120	0.237	3.658	3.658	8.524	0.437	0.188	54.4	0.0030	76	0.00111	27	
121	0.465	1.218	1.218	5.560	0.447	0.504	81.8	0.0091	-68	0.00934	-29	
122	0.367	1.900	1.900	6.860	0.512	0.319	74.5	0.0008	- 4			
123	0.305	3.041	3.041	9.128	0.530	0.205	71.5	0.0016	48	0.00057	-76	
124	0.316	1.218	1.218	3.785	0.389	0.485	78.4	0.0063	74	0.01019	-29	
125	0.250	1.833	1.833	4.497	0.395	0.326	74.3	0.0012	8	0.00377	-26	
126	0.183	3.650	3.650	6.581	0.400	0.167	59.2	0.0028	83	0.00173	-12	
127	0.110	3.037	3.037	3.275	0.391	0.168	67.8	0.0018	- 9			
128	0.099	3.653	3.653	3.567	0.393	0.148	60.8	0.0014	-47	0.00187	-69	2
129	0.448	1.217	1.217	5.959	0.475	0.478	86.1	0.0108	-63	0.01039	-17	3
h/c = 1												

Run #	k_e	F_{nc}	F_{nh}	ω_e	r	$\frac{C_{L1}}{r}$	Φ_{L1}	$\frac{C_{D1}}{r}$	Φ_{D1}	$\frac{C_{D2}}{r}$	Φ_{D2}	C.
100	0.247	1.460	1.46	3.558	0.431	0.400	75.9	0.0040	72	0.00664	-26	
101	0.246	1.467	1.467	3.551	0.433	0.393	76.5	0.0034	72	0.00664	-21	
102	0.187	2.445	2.445	4.488	0.435	0.243	72.4	0.0005	36	0.00128	-13	
103	0.277	1.217	1.217	3.313	0.445	0.469	77.5	0.0069	64	0.01040	-18	
104	0.157	3.654	3.654	5.646	0.456	0.166	62.9	0.0019	83	0.00085	-24	
105	0.264	1.769	1.769	4.587	0.531	0.152	74.5	0.0014	70	0.00456	39	
106	0.265	3.041	3.041	7.930	0.554			0.0027	89			3
107	0.323	1.768	1.768	5.603	0.436	0.352	74.9	0.0019	90	0.00419	-28	
108	0.254	3.040	3.040	7.590	0.452	0.208	65.0	0.0016	29	0.00091	-13	
109	0.246	1.217	1.217	2.941	0.434	0.459	75.5	0.0081	65	0.00844	-25	
110	0.188	1.930	1.930	3.561	0.452	0.285	75.1	0.0013	28	0.00321	4	
111	0.149	3.042	3.042	4.440	0.459	0.184	68.4	0.0013	-75	0.00109	-40	
112	0.187	1.216	1.216	2.231	0.332	0.370	75.0	0.0053	43	0.00460	- 9	
113	0.139	1.929	1.929	2.628	0.313	0.238	75.3	0.0008	-40			
$h/c = 1$												

Run #	k_e	F_{nc}	F_{nh}	ω_e	r	$\frac{C_{L1}}{r}$	Φ_{L1}	$\frac{C_{D1}}{r}$	Φ_{D1}	$\frac{C_{D2}}{r}$	Φ_{D2}	C
327	0.185	1.835	1.835	3.338	0.431	0.296	75.4	0.0019	72	0.00472	-16	
328	0.154	2.595	2.595	3.935	0.435	0.214	72.0	0.0010	-73	0.00085	27	
329	0.144	3.040	3.040	4.303	0.442	0.173	69.8	0.0016	80	0.00149	-37	
339	0.376	1.835	1.835	6.777	0.247	0.328	77.5	0.0022	- 4	0.00397	-27	
340	0.325	2.596	2.596	8.282	0.244	0.249	70.3	0.0011	-54	0.00125	-51	
341	0.307	3.038	3.038	9.163	0.242	0.194	60.5	0.0018	-88	0.00197	-60	
h/c = 1												

1 - Low Waves (Good data, but not desired wave height)

2 - Breaking Waves (Data follows trend)

3 - Short Run

4 - Trip Wire Broke

Run #	k_e	F_{nc}	F_{nh}	ω_e	r	$\frac{C_{L1}}{r}$	Φ_{L1}	$\frac{C_{D1}}{r}$	Φ_{D1}	$\frac{C_{D2}}{r}$	Φ_{D2}	' C.
138	0.314	1.218	0.861	3.75	0.447	0.408	79.0	0.0022	51	0.00738	-16	
139	0.247	1.835	1.298	4.45	0.444	0.281	76.1	0.0012	-76	0.00331	- 4	
140	0.182	3.65	2.580	6.52	0.447	0.140	60.2	0.0026	-71.	0.00082	23	
141	0.501	1.218	.861	5.99	0.418	0.326	85.0	0.0033	-52			
142	0.408	1.835	1.298	7.36	0.435	0.217	78.3	0.0006	84			
143	0.315	3.654	2.584	11.32	0.430	0.115	64.8	0.0030	37			
144	0.372	1.217	0.860	4.45	0.447	0.394	81.3	0.0034	-34	0.00610	-22	
145	0.297	1.835	1.297	5.35	0.468	0.264	75.8	0.0009	-67	0.00373	-18	
146	0.223	3.654	2.584	7.99	0.470	0.134	61.6	0.0027	-77	0.00080	-33	
147	0.180	1.224	0.865	2.16	0.3955	0.375	75.6	0.0015	16	0.00438	-28	
148	0.164	1.835	1.297	2.96	0.158	0.237	87.7	0.0028	29	0.00069	67	
149	0.248	1.22	0.862	2.98	0.434	0.407	76.5	0.0017	74	0.00707	-30	
150	0.192	1.836	1.298	3.46	0.438	0.271	74.8	0.0009	-31	0.00287	-26	
151	0.138	3.656	2.585	4.97	0.439	0.138	64.2	0.0025	-17	0.00134	6	
h/c = 2.0												

Run #	k_e	F_{nc}	F_{nh}	ω_e	r	$\frac{C_{L1}}{r}$	Φ_{L1}	$\frac{C_{D1}}{r}$	Φ_{D1}	$\frac{C_{D2}}{r}$	Φ_{D2}	C.
152	0.314	1.217	0.861	3.76	0.215	0.398	77.5	0.00170	-66	0.00312	- 1	
153	0.248	1.835	1.298	4.47	0.212	0.273	74.0	0.00165	-80	0.00253	-19	
154	0.183	3.655	2.584	6.58	0.220	0.138	64.8	0.00150	-43	0.00096	-70	
155	0.314	1.220	0.863	3.77	0.592	0.395	79.0	0.00167	-44	0.00881	-25	
156	0.248	1.834	1.297	4.09	0.602	0.278	77.0	0.00110	-63	0.00349	-13	
157	0.182	3.654	2.583	6.54	0.596	0.145	64.9	0.00178	78	0.00158	-16	
342	0.409	1.529	1.081	6.15	0.233	0.271	81.5					
343	0.325	2.595	1.835	8.27	0.246	0.170	74.5					
344	0.307	3.039	2.149	9.15	0.241	0.137	68.8					
318	0.325	1.53	1.082	4.88	0.403	0.314	76.5	0.00184	-44	0.00454	-23	
319	0.252	2.596	1.836	6.43	0.407	0.189	68.6	0.00060	-31	0.00071	22	
320	0.237	3.040	2.150	7.09	0.413	0.150	69.2	0.00317	86	0.00155	-37	
321	0.243	1.529	1.082	3.65	0.462	0.326	73.6	0.00047	2	0.00406	-27	
h/c = 2.0												

Run #,	k_e	F_{nc}	F_{nh}	ω_e	r	$\frac{C_{L1}}{r}$	ϕ_{L1}	$\frac{C_{D1}}{r}$	ϕ_{D1}	$\frac{C_{D2}}{r}$	ϕ_{D2}	C.
322	0.185	2.596	1.835	4.73	0.469	0.199	72.3	0.00025	-21	0.00161	-17	
323	0.173	3.040	2.149	5.15	0.474	0.173	68.9	0.00002	17	0.00173	-37	
324	0.180	1.529	1.081	2.71	0.436	0.320	74.6	0.00216	-22	0.00283	25	
325	0.133	2.595	1.835	3.38	0.432	0.187	75.7	0.00042	-75	0.00102	17	
326	0.123	3.039	2.149	3.68	0.441	0.157	72.4	0.00039	-36	0.00064	60	
h/c = 2.0												

1 - Low Waves (Good data, but not desired wave height)

2 - Breaking Waves (Data follows trend)

3 - Short Run

4 - Trip Wire Broke

APPENDIX B

SAMPLE EXPERIMENTAL OUTPUT

SAMPLE EXPERIMENTAL OUTPUT

A sample of the data output obtained for each test spot is shown in Figure 1B and 2B. The output consists of two pages. Page 1 lists steady-state type and mean value information and page 2 lists the harmonic analysis for unsteady measurements recorded in wave tests. Page 2 is deleted during calm water tests.

The experimental conditions, encounter frequencies, wave lengths and water properties are shown as header type information and are repeated on page 2 of the sample output.

The primary measurements, drag, lift forward, lift aft, wave height (single amplitude), and carriage speed are shown as raw data in engineering units, on channels 1 through 6 of the output.

Channels 7 through 12 represent lift and drag corrections to the raw data which account for dynamometer interaction and unwanted lift effects due to slight pitch angle deflections of the sting dynamometer. The corrected lift and drag are shown in channels 10 and 12. Note that channels 5, 8, and 11 are not used.

LIFT AND DRAG CORRECTIONS SHOWN ON SAMPLE OUTPUT

In the ideal case with a perfectly rigid dynamometer there would be no need to correct the measured lift and drag. However, the sting support deflects slightly under the application of lift. As much as 2000 lbs (8896 m) lift was generated during some of the runs. The slight bending of the sting caused two problems:

1) A repeatable non-linear dynamometer interaction. The application of pure lift results in a small drag force.
2) A discrepancy between the totally rigid (no angular or other deflections) mode of operation of the foil as assumed by theory and the slight elasticity in the foil - dynamometer arrangement of the test set up. As a result of large lift forces, the angle of attack of the foil deflected from its 4^{o} static incidence angle to some higher mean angle of attack. During foil operation in waves the angle of attack oscillates slightly in response to the varying lift.

The problem of the non linear interaction drag produced by lift was solved by static calibration as discussed under the calibration section of this report. The amount of interaction drag is the difference between the channel 1 drag (which is the cal factor times the voltage difference of the drag gauge) and the channel 12 DRAG COR value. The channel 12 DRAG COR is the value of the drag corrected for dynamometer interaction. In the sample case of Figure 1B the MEAN drag was adjusted

CARRIAGE II LOW FROUDE NUMBER CONTROL FOIL 27 AUGUST 1979

FOIL WITH WIRE
IN WAVES

FOIL DEPTH RATIO	:	1.0000
KINEMATIC VISCOSITY(E5)	:	1.0414
MASS DENSITY OF WATER	:	1.9360
MEAN WATER DEPTH (FT)	:	19.5000

FE = 0.355 HZ WE = 2.231 RAD/SEC TE = 2.816 SEC

F0 = 0.250 HZ W0 = 1.570 RAD/SEC T0 = 4.001 SEC

LAMBDA = 75.762 FT WAVE SLOPE = 1.062 DEG CELERITY = 11.220 KTS
LAMBDA/L = 56.836 WAVE STEEP = 0.006 LAMBDA/H = 169.518

HEADING = 180.0 DEG

MEAS SPEED = 4.72 KNOTS
NOMN SPEED = 4.74 KNOTS

RUNS : 112.: 0.000 - 8.449

	CHAN		CALIB	GAIN	MEAN	STDDEV	ROOTDD
1	DPAG	LBS	6.593E+01	1.000E+00	1.667E+01	3.091E+00	2.944E+00
2	LIFT AFT	LBS	5.261E+02	1.000E+00	-6.31 E+01	3.115E+01	4.405E+01
3	LIFT FWD	LBS	3.742E+02	1.000E+00	1.803E+02	9.324E+01	1.304E+02
4	WAVE HT1	IN	5.000E+00	1.000E+00	2.613E 02	1.826E+00	2.682E+00
5	WAVE HT2	IN	0.000E+00	1.000E+00	0.000E 00	0.000E+00	0.000E+00
6	CARR SPD	KTS	2.962E+00	1.000E+00	4.719E+ 00	5.711E-03	7.086E-03
7	LIFT UNC	LBS	1.000E+00	1.000E+00	1.173E+ 2	6.111E+01	8.643E+01
8	PO UNCP	INLB	1.000E+00	1.000E+00	3.366E+01	2.478E+00	1.326E+01
9	DEL LIFT	LBS	1.245E-04	1.245E-04	-1.987E-06	8.265E-01	1.169E+00
10	LIFT COP	LBS	-3.500E-02	-3.500E-02	1.172E+02	5.024E+01	8.526E+01
11	PO COP	INLB	1.462E-03	1.462E-03	3.384E+01	9.383E+00	1.313E+01
12	DPAG COP	LBS	1.937E-05	1.937E-05	1.645E+01	1.992E+00	2.818E+00

FS = 0.187 FNC = 1.216 FNH = 1.216 RN = 1.02E+06

CF = 0.00439 CL = 0.17899 CM = 0.03877 CD = 0.02513

VFPS = 7.96428 DAS = 0.04383

Figure 1B - Sample Data Output - Page 1

FOIL DEPTH RATIO : 1.0000
[illegible] : 1.0414
[illegible] : 1.3360
[illegible] : 19.5000

FE = 0.355 HZ VE = 2.231 RAD/SEC TE = 2.816 SEC

F0 = 0.250 HZ W0 = 1.570 RAD/SEC T0 = 4.001 SEC

LAMBDA = 75.762 FT WAVE SLOPE = 1.062 DEG CELERITY = 11.220 KTS
LAMBDA/L = 56.836 WAVE STPN = 0.000 LAMBDA/H = 169.518

HEADING = 180.0 DEG

[illegible] SPEED = 4.72 KNOTS
[illegible] SPEED = 4.74 KNOTS

RUNS : 112.: 0.000 - 8.449

FREQ MULTIPLE			1.0		2.0	
FREQUENCY (RAD SEC)			2.231		4.462	
# OF CYCLES			5		6	
CHAN		FACTOR	AUTO/ROS	TRN FUN	AMP1 *	PHASE	AMP2	PHASE
1 DPAG	LBS	2.944E+00	7.86E-01	1.39E+01	3.314E+00	53.3	1.106E+00	-10.9
2 LIFT AFT	LBS	4.405E+01	9.74E-01	2.59E+02	4.291E+01	-107.4	2.347E+00	-117.3
3 LIFT FWD	LBS	1.304E+02	9.75E-01	7.66E+02	1.272E+02	75.5	7.181E+00	58.7
4 WAVE HT1	IN	2.682E+00	9.90E-01	1.00E+00	2.655E+00	0.0	8.257E-02	79.5
5 LIFT UNC	LBS	8.643E+01	9.75E-01	5.08E+02	8.426E+01	75.0	4.843E+00	56.8
6 PIT UNCP	INLB	1.326E+01	6.47E-01	3.13E+05	8.583E+00	125.6	1.109E+00	165.6
7 REL LIFT	LBS	1.169E+00	9.66E-01	8.96E+04	1.155E+00	-104.5	4.868E-02	-115.7
10 LIFT FOR	LBS	8.526E+01	9.79E-01	[illegible]	3.310E+01	75.0	4.795E+00	56.7
11 PIT COR	INLB	1.313E+01	6.30E-01	[illegible]	8.220E+00	138.5	1.339E+00	164.3
12 DPAG COR	LBS	2.818E+00	7.69E-01	1.70E+01	2.165E+00	[illegible]	1.110E+00	-11.5

KE = 0.187 FNC = 1.216 FNH = 1.216 RN = 1.02E+06

CF = 0.00439 CL = 0.17899 CM = 0.03877 CD = 0.02513

VEPS = 7.96428 DAS = 0.04383

CLR = 0.32035 CMP = 0.02837 CDR = 0.00996

ARMM	RO	DCL	DCD	DL	DD	CORL	CORD	CL	CD	CLR	CDR
1.	0.032	0.0017	0.0000	[illegible]	0.00027	83.12527	2.15432	0.17695	0.00331	0.38246	0.00996
2.	0.003	0.0001	0.0000	[illegible]	0.00000	4.77777	1.10997	0.00730	0.00170	0.02198	0.00511

Figure 2B - Sample Data Output - Page 2

from the 16.62 lb (73.92 N) channel 1 value to the corrected value 16.45 lbs (73.16 N) as shown in channel 12. Similarly the AMP1 and AMP2 values of the oscillating drag were adjusted as shown in Figure 2A.

The solution to the second problem, that of the foil incidence angle deflection along with the small spanwise bending of the foil and the small deflections in heave constitute a hydroelastic problem, the complete solution to which is outside the scope of this experimental effort. However, the problem was not ignored. It is assumed that the foil incidence angle deflection will have the largest effect on the lift response and a quasi-steady correction method was developed. Details of the method follow.

1) Calculate $\delta\alpha$, the change in angle of attack due to an increment in foil lift.

   By static calibration:

$$\delta\alpha = 3.74 \times 10^{-4} \times \delta L \qquad (1B)$$

where δL is in pounds (4.448 N)

$\delta\alpha$ is in degrees

Depending on the harmonic of the fundamental frequency under consideration, δL is obtained from the AMP1 or AMP2 lift response value found in channel 7.

2) From previous unpublished smooth water experiments on this foil obtain $\partial C_L/\partial\alpha$ and $\partial C_D/\partial\alpha^2$ as listed in Table 1B.

TABLE 1B

Variation of Lift Curve Slope and $\partial C_D/\partial\alpha^2$ with Depth Chord Ratio and Froude Number

h/c	$\frac{\partial C_L}{\partial\alpha}$	$\frac{\partial C_D}{\partial\alpha^2}$
2.0	$0.038775\ (F_{nc})^2 - 2.0347\ (F_{nc}) + 0.886$	0.00043
1.0	$0.001718\ (F_{nc}) + 0.0527$	0.00041
0.5	$0.004206\ (F_{nc}) + 0.03682$	0.00038

3) Calculate ΔC_L and ΔC_D - the lift and drag coefficient change due to a small change in angle of attack.

$$\Delta C_L = \frac{\partial CL}{\partial \alpha} \cdot \delta\alpha \tag{2B}$$

$$\Delta C_D = \frac{\partial C_D}{\partial \alpha^2} \cdot (\partial\alpha)^2 \tag{3B}$$

4) Calculate ΔL - the lift and drag due to a small change in angle of attack:

$$\Delta L = \Delta C_L \, (\tfrac{1}{2} \rho V^2 \, A_P) \tag{4B}$$

$$\Delta D = \Delta C_D \, (\tfrac{1}{2} \rho V^2 \, A_P) \tag{5B}$$

5) Calculate the corrected lift, CORL, and corrected drag, CORD, response.

$$\text{CORL} = \text{AMP1 (channel 7)} - \Delta L \tag{6B}$$

$$\text{CORD} = \text{AMP1 (channel 12)} - \Delta D \tag{7B}$$

The above procedure was repeated for the second harmonic and printed in a table on the last 3 lines of page 2 output (see Fig. 2B). The only significant correction to the data occurs to the lift response at the fundamental frequency and even that is very small, normally 2-3% but not more than 6%. All other corrections are too small, in the third significant digit, to be meaningful. Note that no correction is applied to the phase angle of the response.

The correction procedure outlined above was applied in two ways. First an average lift amplitude correction was applied to the uncorrected data representing the entire run. This lift correction appears in channel 9 on

page 2 and the corrected lift amplitudes are in channel 10. Next, a point by point correction was performed. Twenty data spots were taken each second, and each data spot was individually corrected. Both the lift and drag amplitudes were corrected in this manner and these corrections appear in the table on the last three lines of page 2. Throughout the test, only the fundamental frequency lift amplitude correction was at all significant, all other corrections being too small. The difference between the spot by spot correction method and average correction for the run method is infinitesimal and is due to computer round off error. For the sample case it was 83.10 pounds (369.6 N) AMP1 lift for the average run method vs 83.12 pounds (369.7 N) for the spot by spot method.

A line by line description of the output follows:

Page 1 - Fig. 1B

Line 1 Experiment title & date.

Line 2 & 3 Title identifying the run.

Line 4 - 7 Shows the foil depth-chord ratio measured to the ¼ chord location of the foil, the kinematic viscosity, mass density of water and the water depth.

Line 8 Lists encounter frequency FE in hertz, circular encounter frequency WE in radians/sec. and the encounter period TE in seconds.

Line 9 Lists the wave frequency FO in hertz, wave circular frequency WO in rad./sec. and wave period TO in seconds.

Line 10 Lists the wave length LAMDA in feet (0.3048 m), the wave slope in degrees and the wave celerity in knots.

Line 11 Lists the wave length to foil chord ratio LAMDA/L, the wave steepness and the wave length to wave height ratio, LAMDA/H

Line 12 Lists the heading (180^{o} indicates head seas)

Line 13 & 14 Lists the actual measured speed in knots and the nominal speed that was specified for the run.

Line 15 Lists the run number and the duration of the data collection time in seconds.

Line 16 - 28 Lists a table the heading of which is

CHAN - data channel
CALIB - calibration factor
GAIN - gain factor
MEAN - algebraic mean of the data

STDEN - standard deviation of the data
ROOTQO - standard deviation multiplied by $\sqrt{2.0}$

The individual channels of interests are:

Channel 1	Drag measured in pounds (4.448 N)
Channel 2	Lift aft measured in pounds (4.448 N)
Channel 3	Lift fwd measured in pounds (4.448 N)
Channel 4	Wave height measured in inches (2.54 cm) Wave height was taken 13.54 ft. (4.126 m) ahead of the mid-chord hydrofoil position on the centerline
Channel 5	Spare wave height channel - not used
Channel 6	Carriage speed - knots
Channel 7	Uncorrected lift equal to the sum of channels 2 and 3
Channel 8	Not used
Channel 9	Lift correction due to sting deflection
Channel 10	Corrected lift equal to channel 7 minus channel 9
Channel 11	Not used
Channel 12	Drag corrected for dynamometer interaction

Line 29 — Lists KE - the reduced frequency of encounter, FNC - the chord Froude Number, FNH - the foil depth Froude number, RN - the Reynold's number based on foil chord.

Line 30 — Lists CF - the Schoernerr friction coefficient, CL (script symbol $\overline{C}_L$) - the lift coefficient based on the mean value of channel 10, and CD - (script symbol $\overline{C}_D$) the drag coefficient based on the mean value of channel 12

Line 31 — Lists VFPS, - the carriage speed in feet/seconds (0.3048 m/s) and DAS in degrees. DAS is the calculated incremental mean angle of attack due to the angular deflection of the dynamometer nose piece resulting from the applied mean lift as recorded in channel 10.

Page 2 - Figure 2B - Unsteady output for runs in waves only

Line 1- 15 — Repeat the output on page 1

Line 16 - 18 — Lists the harmonic frequency multiple that was analyzed, the harmonic frequencies in rad./sec. and the number of cycles of data which were analyzed.

Line 19 - 29 — Consists of a table. The table headings are:

ROOTQO - equal to the standard deviation multiplied by $\sqrt{2.0}$
AMP1/RQO - is the quotient of the amplitude of the fundamental frequency response and ROOTQO

TRN FUN - Truncation Function, disregard this quantity

AMP1 & PHASE - amplitude and phase at the fundamental frequency as determined by harmonic analysis for each channel of data

AMP2 & PHASE - amplitude and phase at twice the fundamental frequency as determined by harmonic analysis for each data channel.

The data channels are the same as on page 1 lines 17 - 28.

Line 30 - 32 Starting with KE these are the same as on page 1 lines 29 - 31.

Line 33 CLR - fundamental frequency lift response operator script symbol; $\frac{C_{L1}}{r} = (L_1/\frac{1}{2}\rho A_p V^2) \cdot (1.0/r)$ where L_1 is the channel 10 AMP1 value as it appears on line 27.

CDR - fundamental frequency drag response operator script symbol; $\frac{C_{D1}}{r} = (D_1/\frac{1}{2} V^2 A_p) \cdot (1.0/r)$ where D_1 is the channel 12 AMP1 value as it appears on line 29

Line 34 - 36 Consists of a short table of additional reduced data at the fundamental and second harmonic frequency. Quantities in the lift and drag response correction due to foil incidence angle deflections are printed. All the quantities in this table were obtained on a point basis as opposed to the average lift and drag corrections shown on channels 9, 10 & 12.

The table headings are:

HARM - harmonic of the fundamental frequency

DA - the calculated amplitude of the angular deflection of the nose piece (in degrees) due to the oscillating lift forces imposed on the foil. It is calculated by taking static angular deflection calibration of the nose piece under lift and multiplying by the oscillating lift force (AMP1 channel 10 for the fundamental frequency or AMP2 for the second harmonic)

DCL - the change in lift coefficient calculated by multiplying DA with the foil lift curve slope obtained from previously unpublished smooth water experiments on this foil

DCD - the change in drag coefficient calculated by multiplying $(DA)^2$ by the $\frac{\partial C_D}{\partial \alpha^2}$ obtained from previously unpublihsed smooth water experiments.

DL - oscillating lift amplitude correction based on DCL

DD - oscillating drag amplitude correction based on DCD

CORL - Corrected value of the oscillating lift amplitude obtained by subtracting DL from the channel 7 amplitude - the CORL value should be almost identical to the channel 10 value of the corrected lift.

CORD - Corrected value of the oscillating drag amplitude

CL - Amplitude of the oscillating lift in coefficient form based on CORL

D - Amplitude of the oscillating drag in coefficient form based on CORD

CLR - Lift response operator - lift based on CL line 34

CDR - Drag response operator - drag based on CD line 34

DTNSRDC ISSUES THREE TYPES OF REPORTS

1. DTNSRDC REPORTS, A FORMAL SERIES, CONTAIN INFORMATION OF PERMANENT TECHNICAL VALUE. THEY CARRY A CONSECUTIVE NUMERICAL IDENTIFICATION REGARDLESS OF THEIR CLASSIFICATION OR THE ORIGINATING DEPARTMENT.

2. DEPARTMENTAL REPORTS, A SEMIFORMAL SERIES, CONTAIN INFORMATION OF A PRELIMINARY, TEMPORARY, OR PROPRIETARY NATURE OR OF LIMITED INTEREST OR SIGNIFICANCE. THEY CARRY A DEPARTMENTAL ALPHANUMERICAL IDENTIFICATION.

3. TECHNICAL MEMORANDA, AN INFORMAL SERIES, CONTAIN TECHNICAL DOCUMENTATION OF LIMITED USE AND INTEREST. THEY ARE PRIMARILY WORKING PAPERS INTENDED FOR INTERNAL USE. THEY CARRY AN IDENTIFYING NUMBER WHICH INDICATES THEIR TYPE AND THE NUMERICAL CODE OF THE ORIGINATING DEPARTMENT. ANY DISTRIBUTION OUTSIDE DTNSRDC MUST BE APPROVED BY THE HEAD OF THE ORIGINATING DEPARTMENT ON A CASE-BY-CASE BASIS.